

SELF & SOLUTE DIFFUSION IN
ZIRCONIUM & DILUTE ZR-CO ALLOYS

G.V. KIDSON

A STUDY OF SELF AND SOLUTE DIFFUSION
IN
PURE ZIRCONIUM AND DILUTE ZR-CO ALLOYS

by

GEOFFREY VICTOR KIDSON, B.A., M.SC.

A Thesis
Submitted to the Faculty of Graduate Studies
in Partial Fulfilment of the Requirements
for the Degree
Doctor of Philosophy

McMaster University

(May) 1968

DOCTOR OF PHILOSOPHY (1968)
(Metallurgy)

McMASTER UNIVERSITY
Hamilton, Ontario

TITLE: A Study of Self and Solute Diffusion in Pure
Zirconium and Dilute Zirconium-Cobalt Alloys

AUTHOR: Geoffrey Victor Kidson, B.A. (University of B.C.)
M.Sc. (University of B.C.)

SUPERVISOR: Professor J.S. Kirkaldy

NUMBER OF PAGES: 202

SCOPE AND CONTENTS:

The diffusion coefficient of ^{60}Co has been measured as a function of temperature in the body-centered-cubic phase of 99.99% zirconium. The diffusion rates are extraordinarily large, and follow the relation

$$D = [3.26 \pm 2.77] \times 10^{-3} \exp -(21,820 \pm 960/RT) \text{ cm}^2/\text{sec}$$

over the range 900 to 1600°C.

The Arrhenius plot has a positive curvature above 1600°C. The influence of cobalt additions on the diffusion of ^{95}Zr and ^{60}Co in dilute Zr-Co alloys was studied from 0 - 2 at.% cobalt at 933°C. A theoretical model was developed to relate the effect to the solute correlation factor. It is established that diffusion in these systems cannot be accounted for in terms of a vacancy mechanism alone. Other models are discussed.

PREFACE

This thesis is primarily concerned with an experimental study of self and solute diffusion in zirconium and some dilute zirconium-cobalt alloys. It was motivated by several unusual features of the diffusion behaviour in the body-centered-cubic phase of these and other closely related systems.

A general review of some of the well established aspects of both macro- and microscopic theories of diffusion in crystalline solids is given in Chapter I. This is intended to serve as both an introduction and a framework within which the results of the present investigation are discussed.

In Chapter II previous work, both experimental and theoretical, of direct relevance to the present study, is reviewed and the nature of the problem to be investigated is defined in Chapter III. The experimental methods are outlined and the results are tabulated in Chapter IV. Chapter V is concerned with a discussion of these in relation to some proposed models.

A theoretical treatment of the effect of solute additions on the diffusion of solvent atoms in a dilute b.c.c. alloy is developed in Chapter V and related to the impurity correlation factor. It is shown that the observations cannot be accounted for on the basis of a single mechanism of diffusion related to lattice vacancies alone.

Acknowledgements

I wish to thank my supervisor, Dr. J.S. Kirkaldy, for his encouragement and help during the course of this study. I am grateful to the Chalk River Nuclear Laboratories for support in the experimental work and for a leave of absence during January-April, 1967. Drs. O.J.C. Runnalls and G.R. Piercy have been especially kind in their interest and encouragement. I thank Dr. B. Wilkins of WNRE for supplying the zirconium-cobalt alloys, Dr. R. Ashley of CRNL for providing me with analyses of them, and Mr. D. Walker, also of CRNL, for his provision of counting facilities. Mr. Gary Young has given me a very great deal of careful and skilful help in many of the experiments for which I am particularly grateful. Dr. D. Graham of NASA, Cleveland, Ohio, with whom I have enjoyed stimulating discussions, has kindly permitted me to quote unpublished results. The manuscript was typed with skill and remarkable patience by Mrs. D. Moss, to whom I give special thanks.

Finally, I thank my wife and my children for their good humour and support throughout this work. They never asked why, but only, when?

TABLE OF CONTENTS

	PAGE
CHAPTER I	INTRODUCTION
I-1.	Macroscopic Diffusion Equations 1
I-2.	The Statistical Basis of the Macroscopic Diffusion Equations 5
I-3.	The Microscopic Basis of Diffusion 9
I-4.	Correlation Effects 14
I-5.	Solute Diffusion 19
I-6.	Isotope Effects in Diffusion 23
I-7.	The Influence of Solutes on Solvent Diffusion 28
I-8.	Summary 30
CHAPTER II	PREVIOUS WORK
II-1.	Self and Solute Diffusion in "Normal" Metals 32
II-2.	Self and Solute Diffusion in Anomalous Body- Centered-Cubic Metals 38
II-3.	The Single-Mechanism Hypothesis 47
II-4.	The Two-Mechanism Hypothesis 51
CHAPTER III	AIMS OF THE PRESENT INVESTIGATION 55
CHAPTER IV	EXPERIMENTAL TECHNIQUES AND RESULTS
IV-1.	Summary of Techniques 57
IV-2.	Materials and Specimen Preparation 58
IV-3.	Vacuum Annealing Furnaces 65
IV-4.	Specimen Sectioning 74
IV-5.	Radioactivity Measurements 77

IV-6.	The Diffusion of ^{60}Co in β Zr	82
IV-7.	The Diffusion of ^{95}Zr in Dilute Zr-Co Alloys	99
IV-8.	The Diffusion of ^{60}Co in Dilute Zr-Co Alloys	109
IV-9.	The Diffusion of ^{64}Cu in β Zr	114
IV-10.	The Time and Temperature Dependence of the Quality of Laue X-ray Diffraction Spots from Martensitically Transformed β Zr	116
IV-11.	The Diffusion of ^{60}Co in α Zr	127
CHAPTER V	DISCUSSION	
V-1.	The Shape of the Concentration Profiles	136
V-2.	An Outline of the Argument to Follow	144
V-3.	The Equilibrium Distribution of Free and Associated Vacancies in a Dilute B.C.C. Alloy	146
V-4.	The Average Solvent Jump Frequency in Dilute B.C.C. Alloys	154
V-5.	The Solute Correlation Factor in a Dilute B.C.C. Alloy	163
V-6.	The Mechanism of Diffusion in β Zr	167
V-7.	Cobalt Segregation in α and β Zr	181
CHAPTER VI	CONCLUSIONS	184
APPENDIX I	The Equilibrium Number of Single Vacancies in a Pure Metal	186
APPENDIX II	The Effect of a Finite Specimen Length	189
APPENDIX III	Errors	191
	References	197

I-1. MACROSCOPIC DIFFUSION EQUATIONS

The study of diffusion may be divided into two broad areas, that which is concerned with the development of a general system of differential equations governing the macroscopic features of the phenomenon and that concerned with the microscopic processes involved in the migrations of the atoms.

The most straightforward approach to the former is due to Fick⁽¹⁾ and is based on the postulate of a linear relation between the vector current \vec{J} of the diffusing atoms and their concentration gradient ∇C . In isotropic crystals and under simple conditions to be discussed below, this relation takes the form

$$\vec{J} = -D \nabla C \quad \text{I-1.1}$$

The proportionality constant, D , is called the diffusion coefficient and is a parameter that is characteristic of the specific system and annealing temperature. Equation I-1.1, which is called Fick's first law, can be transformed to a more useful form by application of the condition of continuity,

$$\frac{\partial C}{\partial t} + \nabla \cdot \vec{J} = 0 \quad \text{I-1.2}$$

If D is independent of position this becomes

$$\frac{\partial C}{\partial t} = D \nabla^2 C \quad \text{I-1.3}$$

and is known as Fick's second law of diffusion. In the more general case of anisotropic crystals, the diffusion coefficient must be replaced by a second rank tensor, so that the diffusion current, in terms of the flux components J_α , J_β , J_γ along arbitrarily chosen axes α , β , γ , are given by

$$\begin{bmatrix} J_\alpha \\ J_\beta \\ J_\gamma \end{bmatrix} = - \begin{bmatrix} D_{\alpha\alpha} & D_{\alpha\beta} & D_{\alpha\gamma} \\ D_{\beta\alpha} & D_{\beta\beta} & D_{\beta\gamma} \\ D_{\gamma\alpha} & D_{\gamma\beta} & D_{\gamma\gamma} \end{bmatrix} \begin{bmatrix} \partial C / \partial \alpha \\ \partial C / \partial \beta \\ \partial C / \partial \gamma \end{bmatrix} \quad \text{I-1.4}$$

Here the coefficient $D_{\alpha\beta}$, for example, is a measure of the contribution to the flux component J_α along the α axis, from the gradient $\partial C / \partial \beta$ along the β axis.

The equation, analogous to I-1.3, becomes:

$$\begin{aligned} \frac{\partial C}{\partial t} = & D_{\alpha\alpha} \frac{\partial^2 C}{\partial \alpha^2} + D_{\beta\beta} \frac{\partial^2 C}{\partial \beta^2} + D_{\gamma\gamma} \frac{\partial^2 C}{\partial \gamma^2} + (D_{\alpha\beta} + D_{\beta\alpha}) \frac{\partial^2 C}{\partial \alpha \partial \beta} + \\ & (D_{\alpha\gamma} + D_{\gamma\alpha}) \frac{\partial^2 C}{\partial \alpha \partial \gamma} + (D_{\beta\gamma} + D_{\gamma\beta}) \frac{\partial^2 C}{\partial \beta \partial \gamma} \end{aligned} \quad \text{I-1.5}$$

In a purely formal way, these equations can be simplified by a transformation to a new set of coordinates, x , y , z , chosen so as to diagonalize the diffusion tensor. Then I-1.4 becomes

$$\begin{bmatrix} J_x \\ J_y \\ J_z \end{bmatrix} = - \begin{bmatrix} D_{xx} & 0 & 0 \\ 0 & D_{yy} & 0 \\ 0 & 0 & D_{zz} \end{bmatrix} \begin{bmatrix} \partial C / \partial x \\ \partial C / \partial y \\ \partial C / \partial z \end{bmatrix} \quad \text{I-1.6}$$

Physically, equation I-1.6 reflects the fact that the symmetry properties of crystals guarantee that there exists a set of principle axes, x , y , z , such that the flux component along any one of them is due to the concentration gradient along that axis alone. Under these conditions, of course, equation I-1.5 reduces to

$$\frac{\partial C}{\partial t} = D_{xx} \frac{\partial^2 C}{\partial x^2} + D_{yy} \frac{\partial^2 C}{\partial y^2} + D_{zz} \frac{\partial^2 C}{\partial z^2} \quad \text{I-1.7}$$

The special case of isotropic crystals implies that

$$D_{xx} = D_{yy} = D_{zz} = D \quad \text{I-1.8}$$

from which we recover I-1.1.

Equations (I-1.1) to (I-1.6) form the required basis for a macroscopic description of the diffusion of a single species in the absence of any perturbing influences such as pressure, temperature, electrical or chemical concentration gradients. It does not provide any justification for the assumed relations, nor does it indicate how such complicating influences may be incorporated into the scheme of equations.

A more general description of diffusion, based on the Thermodynamics of Irreversible Processes, is possible. This does provide a systematic method for treating cases of arbitrary complexity. Like the foregoing, however, it does so in terms of phenomenological coefficients that cannot be related, on a purely thermodynamic approach, to the underlying atomic processes involved.

In part I-2, an alternative approach, known as the Method of Random Walks, is described. It will be shown that the diffusion coefficients defined by Fick for simple systems can be related, in a very direct way, to the statistical behaviour of the atoms. This then provides a bridge between the macroscopic descriptions and the more specific kinetic models. In principle, the formalism can be further extended to include the complex behaviour of multi-component systems in which diffusion is influenced by internal or external field gradients.

These several approaches to a theory of diffusion are, of course, complementary, each having certain advantages and disadvantages. In the following we will develop them only to the extent that they serve the primary aim of the experimental study.

I-2. THE STATISTICAL BASIS OF THE MACROSCOPIC DIFFUSION EQUATIONS

Figure I-2.1 shows the unidirectional concentration profile of radioactive ^{95}Zr in a matrix of pure natural zirconium after an anneal of 48 hours at 933°C . The tracer atoms were initially contained in a layer 60\AA thick at the plane $x = x_0$. It is clear that, while the range of displacements of the individual tracers is very wide, the overall distribution is symmetric about x_0 , smooth and highly reproducible. A more detailed examination of the shape of the curve shows it to be accurately Gaussian.

These observations provide the basis for developing a quantitative description of diffusion by the Method of Random Walks. Thus let $\Psi(\vec{\Delta R}, \Delta t)$ be a function that represents the probability that an atom undergoes a net displacement $\vec{\Delta R}$ during time Δt . The empirical value of Ψ for the unidirectional result of figure I-2.1, for example, is simply the ratio $n(x, \Delta t) dx / \int_{-\infty}^{\infty} n(x, \Delta t) dx$. In this case, of course, only the component $\Delta X = x - x_0$ of $\vec{\Delta R}$ is measured. For simple systems, involving negligible concentration gradients and no thermal, stress or electrical gradients, we can take Ψ to be independent of \vec{R} , and symmetric in $\vec{\Delta R}$; i.e. $\Psi(\vec{\Delta R}, \Delta t) = \Psi(-\vec{\Delta R}, \Delta t)$ I-2.1

If, then, the concentration at (\vec{R}, t) is $C(\vec{R}, t)$, we may write (2)

$$C(\vec{R}, t + \Delta t) = \int_{\mathcal{V}} C(\vec{R} + \vec{\Delta R}, t) \Psi(\vec{\Delta R}, \Delta t) d\vec{\Delta R} \quad \text{I-2.2}$$

Expressing \vec{R} in terms of the principle axes of the crystal and $\vec{\Delta R}$ in the component displacements, we may expand the L.H.S. of I-2.2 about t and the R.H.S. about \vec{R} , in Taylor

series, to obtain

$$\begin{aligned}
 & C(\vec{R}, t) + \Delta t \frac{\partial C}{\partial t} + O(\Delta t)^2 \frac{\partial^2 C}{\partial x^2} \\
 &= C(\vec{R}, t) \int_V \Psi(\Delta \vec{R}, \Delta t) d\Delta \vec{R} + \frac{\partial C}{\partial x} \int_V X \Psi(\Delta \vec{R}, \Delta t) d\Delta \vec{R} + \dots \\
 &+ \frac{1}{2} \frac{\partial^2 C}{\partial x^2} \int_V X^2 \Psi(\Delta \vec{R}, \Delta t) d\Delta \vec{R} + \dots \\
 &+ \frac{\partial^2 C}{\partial x \partial y} \int_V XY \Psi(\Delta \vec{R}, \Delta t) d\Delta \vec{R} + O \frac{\partial^3 C}{\partial x \partial y \partial z}
 \end{aligned} \tag{I-2.3}$$

Then, defining the moments of the component displacements by

$$\int_V X^n \Psi d\Delta \vec{R} = \langle X^n \rangle \tag{I-2.4}$$

$$\int_V X^n Y^m \Psi d\Delta \vec{R} = \langle X^n Y^m \rangle \tag{I-2.5}$$

while noting that

$$\int_V \Psi d\Delta \vec{R} = 1 \tag{I-2.6}$$

and that I-2.1 implies all odd moments are zero, we obtain

$$\begin{aligned}
 \frac{\partial C}{\partial t} \approx & \frac{\langle X^2 \rangle}{2\Delta t} \frac{\partial^2 C}{\partial x^2} + \frac{\langle Y^2 \rangle}{2\Delta t} \frac{\partial^2 C}{\partial y^2} + \frac{\langle Z^2 \rangle}{2\Delta t} \frac{\partial^2 C}{\partial z^2} \\
 & + \frac{\langle XY \rangle}{\partial x \partial y} \frac{\partial^2 C}{\partial x \partial y} + \frac{\langle XZ \rangle}{\partial x \partial z} \frac{\partial^2 C}{\partial x \partial z} + \frac{\langle YZ \rangle}{\partial y \partial z} \frac{\partial^2 C}{\partial y \partial z}
 \end{aligned} \tag{I-2.7}$$

Finally, since the component displacements along the principle axes are statistically independent we have $\langle XY \rangle = \langle X \rangle \langle Y \rangle = 0$ etc.

I-2.7 then reduces to

$$\frac{\partial C}{\partial t} \approx \frac{\langle X^2 \rangle}{2\Delta t} \frac{\partial^2 C}{\partial x^2} + \frac{\langle Y^2 \rangle}{2\Delta t} \frac{\partial^2 C}{\partial y^2} + \frac{\langle Z^2 \rangle}{2\Delta t} \frac{\partial^2 C}{\partial z^2} \tag{I-2.8}$$

Comparison of I-2.8 with I-1.7 indicates that we may identify the components of the diffusion tensor with

$$D_{xx} = \frac{\langle X^2 \rangle}{2\Delta t} ; \quad D_{yy} = \frac{\langle Y^2 \rangle}{2\Delta t} ; \quad D_{zz} = \frac{\langle Z^2 \rangle}{2\Delta t} \quad \text{I-2.9}$$

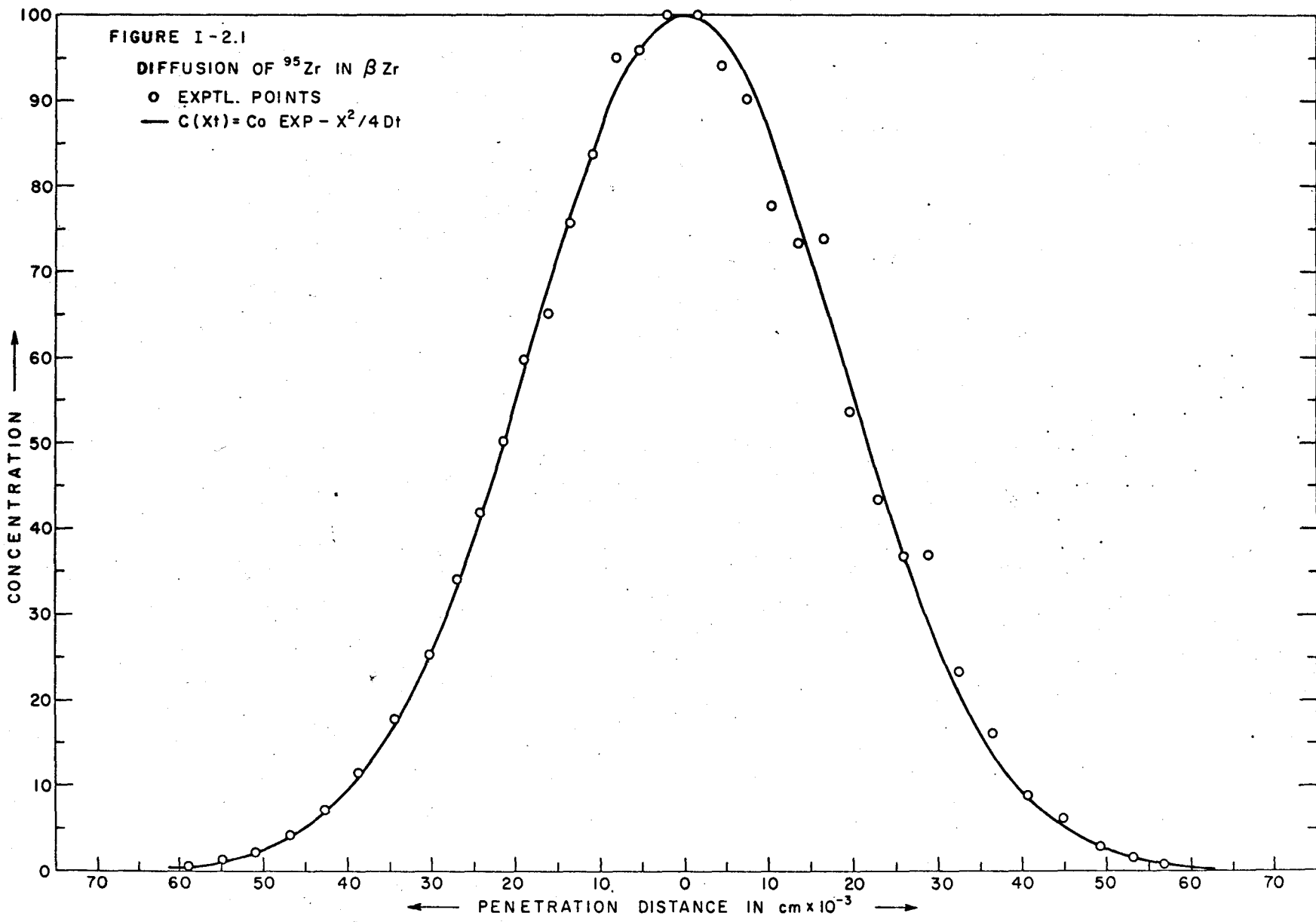
For isotropic crystals

$$\langle X^2 \rangle = \langle Y^2 \rangle = \langle Z^2 \rangle \quad \text{I-2.10}$$

so that the single diffusion coefficient of equation I-1.1 may be written as

$$D = \frac{\langle \Delta R^2 \rangle}{6\Delta t} ; \quad \text{I-2.11}$$

where we have used $\langle R^2 \rangle = \langle X^2 \rangle + \langle Y^2 \rangle + \langle Z^2 \rangle$. Henceforth, we confine our attention to such simple systems.



I-3. THE MICROSCOPIC BASIS OF DIFFUSION

The preceding established a formal junction between the equations of Fick and the statistical properties of the atoms in terms of the postulated probability function Ψ . In the following the theory will be developed further on the basis of more detailed assumptions about the diffusion process. Several mechanisms have been proposed to account for the mobility of the atoms in crystalline solids and, of course, a primary aim of fundamental studies is to establish the specific mechanism or mechanisms operative in a given system.

Table I-3.1 lists most of those that have been proposed.

The various possibilities are illustrated schematically in figure I-3.1. We note that in all of them it is assumed that the total displacement of an atom is the result of a series of many small jumps. We note also that with the exception of the first two, all mechanisms involve point or line defects of the lattice. A further possible mechanism is diffusion along the grain boundaries of polycrystalline specimens. While it has been established experimentally that this does occur, we defer further consideration here because such a process does not conform to the behaviour predicted by the probability function Ψ , whereas the others do.

We begin, then, by assuming that the net displacement $\vec{\Delta R}_k$ of the k^{th} atom can be written as

$$\vec{\Delta R}_k = \sum_{i=1}^{n_k} \vec{r}_{ik} \quad , \quad (k = 1, 2, \dots, n) \quad \text{I-3.1}$$

$$\text{Then } \Delta R_k^2 = \left(\sum_{i=1}^{n_k} \vec{r}_{ik} \right) \cdot \left(\sum_{i=1}^{n_k} \vec{r}_{ik} \right)$$

$$= \begin{bmatrix} r_1 \cdot r_1 + r_1 \cdot r_2 + \dots + r_1 \cdot r_n \\ + r_2 \cdot r_1 + r_2 \cdot r_2 + \dots + r_2 \cdot r_n \\ + \dots \\ + r_n \cdot r_1 + r_n \cdot r_2 + \dots + r_n \cdot r_n \end{bmatrix}_k \quad \text{I-3.2}$$

This may be written as

$$\Delta R_k^2 = \sum_{i=1}^{n_k} r_{ik}^2 + 2 \left(\sum_{j=1}^{n-1} \sum_{i=1}^{n-j} \vec{r}_i \cdot \vec{r}_{i+j} \right)_k \quad \text{I-3.3}$$

The mean square displacement is then

$$\overline{\Delta R^2} = \sum_{i=1}^{n_k} r_{ik}^2 + 2 \left(\sum_{j=1}^{n-1} \sum_{i=1}^{n-j} \vec{r}_i \cdot \vec{r}_{i+j} \right)_k \quad \text{I-3.4}$$

where the average is taken over the N atoms of the ensemble.

With the possible exception of diffusion along dislocations, all the mechanisms proposed imply that the length of the jump vectors in isotropic crystals are all equal to the near neighbor spacing a . Thus I-3.4 becomes:

$$\overline{\Delta R^2} = \frac{a^2}{N} \sum_{k=1}^N n_k + \frac{2a^2}{N} \sum_{k=1}^N \left(\sum_{j=1}^{n-1} \sum_{i=1}^{n-j} \cos \theta_{i,i+j} \right)_k \quad \text{I-3.5}$$

Now if the mechanism is such that the direction of any jump is always at random and independent of the previous or earlier jumps, then all the $\cos \theta$'s in I-3.5 average out to zero, and we are left with

$$\overline{\Delta R^2} = a^2 \bar{n} \quad \text{I-3.6}$$

where \bar{n} is the average number of jumps made by the N atoms

during the time Δt . We may then substitute $\overline{\Delta R^2}$ for the continuum result in equation I-2.11 by taking the limit $n, \Delta t \rightarrow \infty$:

$$\text{i.e. } D = \frac{\langle \Delta R^2 \rangle}{6\Delta t} = \lim_{n, \Delta t \rightarrow \infty} \frac{a^2}{6} \frac{\bar{n}}{\Delta t} \quad \text{I-3.7}$$

$$= \frac{a^2}{6} \Gamma \quad \text{I-3.8}$$

where Γ is the average jump frequency of the N atoms. Equation I-3.8 may be expected to hold for those cases in which the coordination shell of the diffusant is symmetric, since this justifies the assumption that the probability of a jump occurring to any one of the Z near neighbour sites is just $\left(\frac{1}{Z}\right)$.

This condition is met for self-diffusion by the mechanisms of (i) and (ii) and for both self and solute diffusion by the interstitial mechanism. Figure I-3.1. indicates that the coordination shells of vacancies in pure metals are symmetric as well. Thus, if we associate a diffusion coefficient D_v with the movement of vacancies, we can write

$$D_v = \frac{a^2}{6} \Gamma_v \quad \text{I-3.9}$$

where Γ_v is the average vacancy jump frequency in a pure lattice.

TABLE I-3.1

- (i) direct interchange of a pair of neighbouring atoms.
- (ii) the ring mechanism, in which there is a coordinated interchange of several atoms moving synchronously.
- (iii) the interstitial mechanism, in which the diffusing atoms jump from one interstitial site to another.
- (iv) the interstitialcy mechanism, in which an interstitial exchanges with an atom on a normal lattice site.
- (v) the vacancy mechanism, in which the atoms move into vacant near neighbour lattice sites.
- (vi) multiple vacancy mechanisms, in which atoms peripheral to groups of two or more vacancies move into unoccupied sites.
- (vii) the dislocation mechanism, in which atoms move along a dislocation network.
- (viii) some combination of two or more of the foregoing.

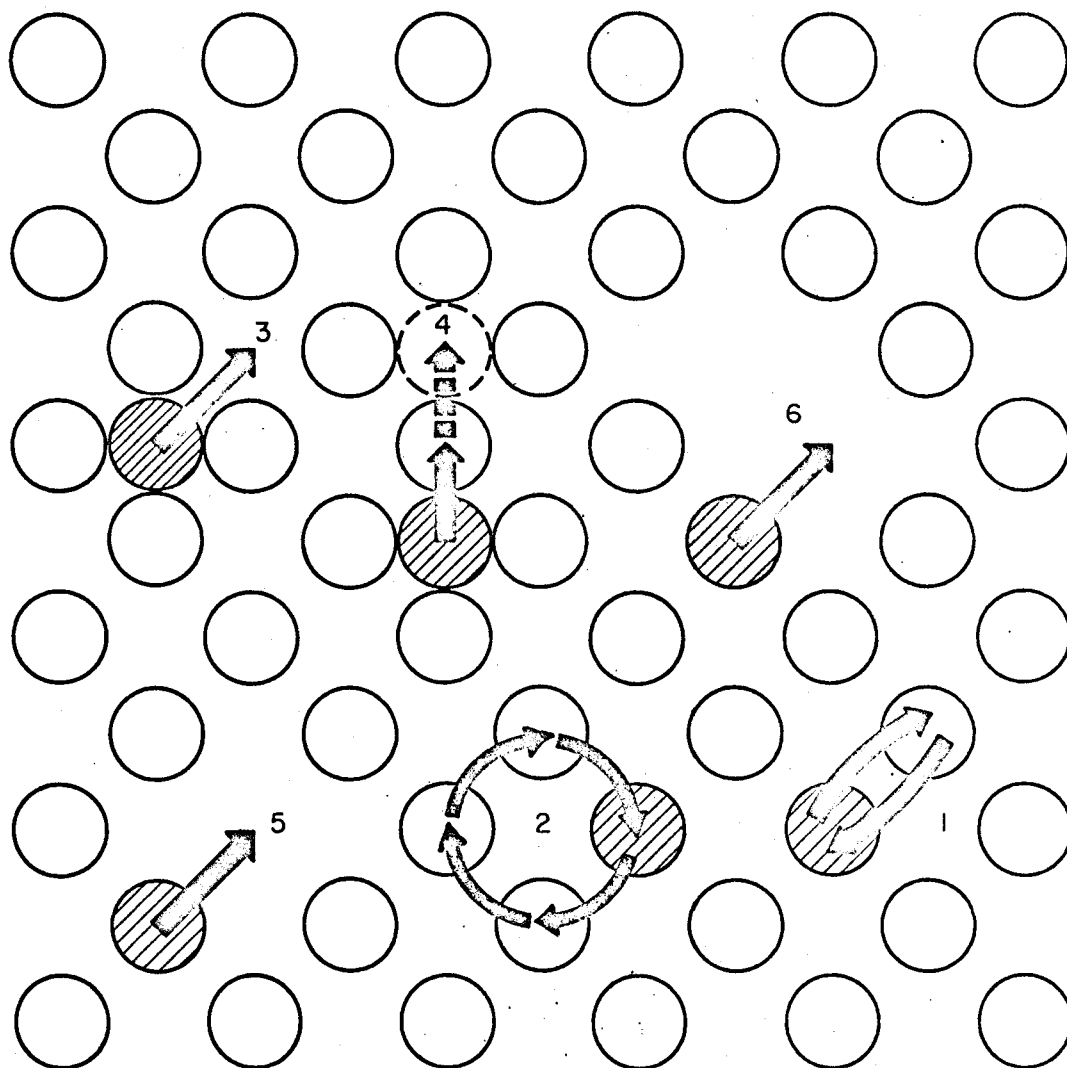


FIGURE I - 3.1 DIFFUSION MECHANISMS

(1) DIRECT INTERCHANGE

(2) RING

(3) INTERSTITIAL

(4) INTERSTITIALCY

(5) VACANCY

(6) DIVACANCY

I-4. THE MICROSCOPIC BASIS OF DIFFUSION: II

Correlation Effects

It is clear from figure I-3.1 that atoms diffusing by the vacancy mechanism do not have a symmetric coordination shell when a vacancy is in a near neighbour site. If an atom has just moved from site 0 to site 1 by exchange with a vacancy, it has a higher probability of returning to site 0 on its next jump than of going to any of the (Z-1) remaining sites. Thus the direction of its next jump is correlated with that of the previous jump and the $\overline{\cos \theta}$'s in equation I-3.5 do not average out to zero. For such cases equation I-3.5 is rewritten as

$$\overline{\Delta R^2} = a^2 \bar{n} \left\{ 1 + \frac{2}{\bar{n}} \cdot \frac{1}{N} \sum_{k=1}^N \sum_{j=1}^{\infty} \sum_{i=1}^{n_k - j} (\cos \theta_{i, i+j})_k \right\} \quad \text{I-4.1}$$

An examination of I-3.2 shows that the total number of vector pairs separated by j jumps is $\sum_{k=1}^N (n_k - j)$. In the vacancy mechanism, the cosine values are independent of the initial jump i⁽³⁾, so we can define an average $\overline{\cos \theta}_j$ such that

$$\begin{aligned} \sum_{k=1}^N \sum_{i=1}^{n_k - j} (\cos \theta_{i, i+j})_k &= \overline{\cos \theta}_j \sum_{k=1}^N (n_k - j) \\ &= N(\bar{n} - j) \overline{\cos \theta}_j \end{aligned} \quad \text{I-4.2}$$

Substituting in I-4.1,

$$\overline{\Delta R^2} = a^2 \bar{n} \left\{ 1 + 2 \sum_{j=1}^{\bar{n}-1} \left(1 - \frac{j}{\bar{n}}\right) \overline{\cos \theta}_j \right\} \quad \text{I-4.3}$$

Once again, $\langle \Delta R^2 \rangle$ in equation I-2.11 is replaced by $\overline{\Delta R^2}$ in the limit of $\bar{n}, \Delta t \rightarrow \infty$. Then

$$D = \frac{a^2}{6} \Gamma f \quad \text{I-4.4}$$

$$\text{where } f = \lim_{\bar{n} \rightarrow \infty} \left\{ 1 + 2 \sum_{j=1}^{\bar{n}-1} \left(1 - \frac{j}{\bar{n}}\right) \overline{\cos \theta_j} \right\}$$

$$= 1 + 2 \sum_{j=1}^{\infty} \langle \cos \theta_j \rangle \quad \text{I-4.5}$$

Since f contains the effect of the correlated jumps of the atoms it is called the correlation factor⁽⁴⁾. For lattices in which the jump vectors are axes of at least two-fold symmetry, as in the case of cubic crystals, it may be shown that⁽³⁾

$$\langle \cos \theta_j \rangle = \langle \cos \theta_1 \rangle \langle \cos \theta_{j-1} \rangle$$

$$= \langle \cos \theta_1 \rangle^j \quad \text{I-4.6}$$

This permits the reduction of I-4.5 to the simpler form

$$f = (1 + \langle \cos \theta_1 \rangle) / (1 - \langle \cos \theta_1 \rangle) \quad \text{I-4.7}$$

Atoms moving via the interstitialcy mechanism form an intermediate case between correlated and un-correlated motion. When such an atom is in an interstitial site, its next jump is un-correlated with the previous one because its coordination shell is symmetric. However, if it has just jumped from an interstitial to a substitutional site the direction of its next jump is influenced by the presence of the neighbouring interstitial atom. Thus only alternate jumps are correlated. Referring to equation I-4.5 we see that $\langle \cos \theta_j \rangle$ for $j \geq 2$ is zero, and for half the number of consecutive pairs $\langle \cos \theta_1 \rangle$ is zero. Thus we get

$$f = 1 + \langle \cos \theta_1 \rangle \quad \text{I-4.8}$$

It is clear that the explicit calculation of correlation factors depends upon a knowledge of the details of the jump mechanism and the geometry of the lattice. For the first 3 mechanisms in Table I-3.1, the jumps are uncorrelated and $f \equiv 1$. For the next two the calculation depends only upon a determination of $\langle \cos \theta_1 \rangle$. For the remaining 3, the geometries of the jumps are not yet well enough defined to permit detailed calculations.

The principle of evaluating $\langle \cos \theta_1 \rangle$ is straightforward⁽⁵⁾. We noted previously that in a pure crystal the probability of a vacancy taking a specific path in n jumps is $\left(\frac{1}{Z}\right)^n$. If there are α possible paths by which the vacancy can reach site i in n jumps, the probability of it doing so is $p_n(i) = \alpha_n \left(\frac{1}{Z}\right)^n$. Thus the total probability of the vacancy reaching site i is

$$P(i) = \sum_{n=0}^{\infty} p_n(i). \quad \text{I-4.9}$$

The probability that a vacancy, having just moved from site 0 to site 1 by exchange with an atom, then moves around to site j to effect the next jump is $P(j)$ and the contribution of this to $\langle \cos \theta_1 \rangle$ is $P(j) \cos \theta_{0 \rightarrow j}$. For all Z possible jump directions, then

$$\langle \cos \theta_1 \rangle = \sum_{j=1}^Z P(j) \cos \theta_{0 \rightarrow j} \quad \text{I-4.10}$$

Several methods have been devised to calculate $P(j)$. The most accurate values have been obtained by Compaan and Haven⁽⁶⁾ using an electrical analogue technique. Table I-4.1 lists f for self diffusion by several mechanisms and in various structures. Since the values are well separated,

an experimental determination of the correlation factor can, under favourable circumstances, provide positive identification of the jump mechanism⁽⁷⁾. Before discussing the methods available, we shall consider dilute impurity diffusion by the vacancy mechanism.

TABLE I-4.1CORRELATION FACTORS FOR SELF DIFFUSION

Structure	Vacancy Mechanism f_o	Interstitialcy
Diamond	0.5000	
Cubic	0.6531	
B.C.C.	0.7272	
F.C.C.	0.7815	0.8000
H.C.P.	0.7812 0.7815	
Silver Chloride		0.6666

I-5.

SOLUTE DIFFUSION

Equation I-4.4 is valid for both self and solute diffusion. If, in the former case, the atoms jump only by exchanging with vacancies, their average jump frequency Γ_o is related to that of the vacancies by

$$N_o \Gamma_o = n_v \Gamma_v \quad \text{I-5.1}$$

where N_o is the number of atoms per unit volume and n_v the number of vacancies. Thus I-4.4 can be written as

$$D = \frac{a^2}{6} \left(\frac{n_v}{N_o} \right) \Gamma_v f_o \quad \text{I-5.2}$$

This may be considered as follows: since the vacancies are distributed at random in the pure crystal, the probability that any one of the Z sites in the coordination shell of an atom is vacant, is $P_v = Z (n_v/N_o + n_v) \approx Z n_v/N_o$ for $n_v \ll N_o$. Moreover, the probability of the vacancy exchanging with the same atom is $W_o = (1/Z) \Gamma_v$. Thus I-5.2 becomes

$$D = \frac{a^2}{6} W_o P_v f_o \quad \text{I-5.2(a)}$$

In the same way, we may write for the diffusion coefficient of a dilute solute

$$\begin{aligned} D_i &= \frac{a^2}{6} \Gamma_i f_i \\ &= \frac{a^2}{6} W_2 P_i f_i \end{aligned} \quad \text{I-5.3}$$

Γ_i is the average jump frequency of the impurity and f_i its correlation factor. W_2 is the probability of a

vacancy-impurity exchange and P_i the probability that a vacancy is associated with an impurity. P_i will reflect any chemical interactions between the vacancy and impurity and W_2 will depend upon both chemical and physical, i.e. mass, effects. The form of the correlation factor remains unchanged. Now, however, the calculation of the probability coefficients in I-4.9 are not as straightforward as in the case of self diffusion. This can be seen by reference to the schematic lattice in figure I-5.1. The various W 's indicated take into account the possible influence of the presence of the impurity on the solvent-vacancy exchange frequencies.

Thus W_1 is a jump that leaves a vacancy associated with an impurity in the near neighbour shell, and may be expected to differ from k_1 which would result in the dissociation of the vacancy and impurity. The probability of a specific path is now $\prod_{i=1}^n P_i$, where the P_i for each jump must be considered separately. For example, an associated vacancy in figure I-5.1 can jump into 6 possible sites. The probability that it moves from site 1 to site 2 is $W_1/W_2 + 2W_1 + 3k_1$, and so on. An analysis of f_i , then, can be as detailed as desired, taking more and more possible jump types into account. f_i is clearly a function of all the W 's involved. The systematic treatment can be pursued most effectively by matrix methods⁽³⁾ and several recent papers have considered the problem in detail^(8,9,10). In all such analyses, however, f_i can be expressed in the form⁽¹¹⁾

$$f_i = \frac{B}{W_2 + B} \quad \text{I-5.4}$$

where B is a function of the various solvent-vacancy

exchange frequencies.

Techniques for experimentally determining f_o and f_i in self and impurity diffusion will be considered in I-6 and I-7.

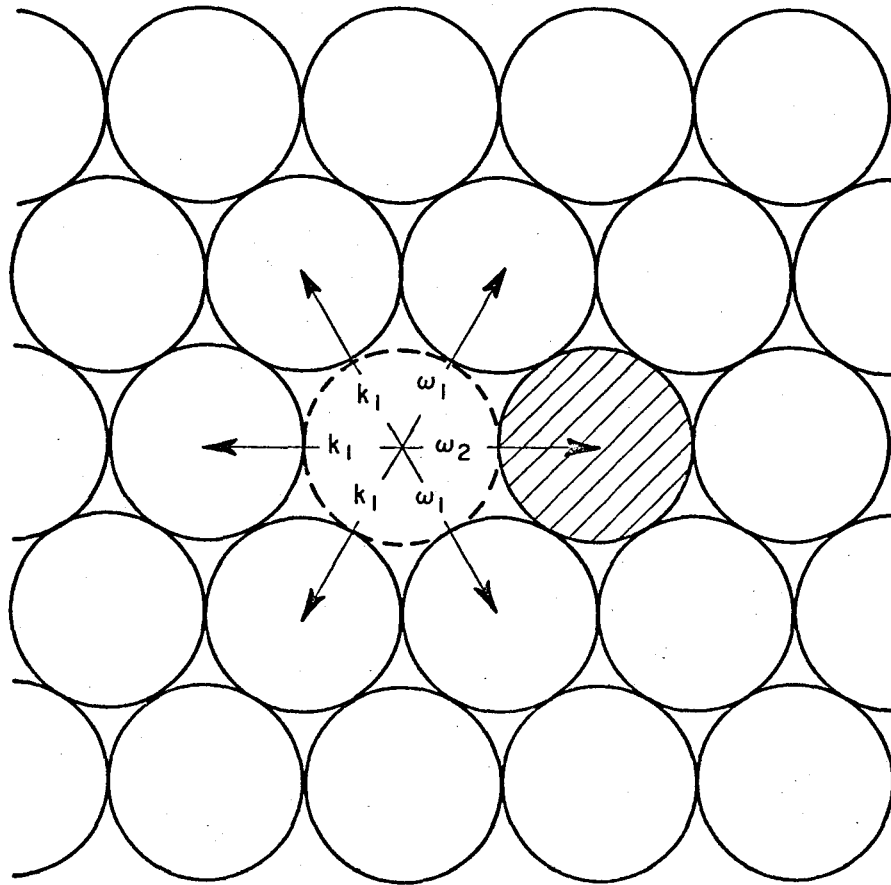


FIGURE I - 5.1

SCHEMATIC DIAGRAM TO SHOW DIFFERENT
 POSSIBLE JUMP PATHS OF A VACANCY ○ ,
 ASSOCIATED WITH AN IMPURITY ⊙ .

If two isotopes, α and β , of the same chemical species are used to measure diffusion under identical conditions in the same system, the only source of difference between the resultant coefficients lies in the mass difference of the two tracers. From I-5.3:

$$D^{\alpha} = \frac{a^2}{6} \omega_2^{\alpha} P^{\alpha} f^{\alpha}$$

$$D^{\beta} = \frac{a^2}{6} \omega_2^{\beta} P^{\beta} f^{\beta}$$

whence
$$\frac{D^{\alpha}}{D^{\beta}} = \frac{\omega_2^{\alpha}}{\omega_2^{\beta}} \frac{P^{\alpha}}{P^{\beta}} \frac{f^{\alpha}}{f^{\beta}}$$

$$\approx \frac{\omega_2^{\alpha}}{\omega_2^{\beta}} \frac{f^{\alpha}}{f^{\beta}}$$

I-6.1

provided we can ignore the possibility of small differences in P^{α} and P^{β} that could arise from mass differences alone⁽¹²⁾. It was first pointed out by Shoen⁽¹³⁾ and later more rigorously shown by Lidiard and Tharmalingham⁽¹⁴⁾, that a careful measurement of D^{α}/D^{β} can provide an experimental determination of f^{α} . Barr and LeClaire⁽¹¹⁾ obtained the same result in a simpler way by noting that the relation in I-5.4 implies we can write

$$f^{\alpha} = f^{\alpha} (\omega_2^{\alpha} / B); \quad f^{\beta} = f^{\beta} (\omega_2^{\beta} / B) \quad \text{I-6.2}$$

where we recall that B contains jump frequencies of the solvent only.

If ω_2^α and ω_2^β differ only slightly from one another, f^β may be expanded as a Taylor series about f^α in the form

$$\frac{1}{f^\beta} = \frac{1}{f^\alpha} \left[1 + \left(\frac{\partial \ln (1/f)}{\partial \ln (\omega_2/B)} \right)_\alpha \left(\frac{\omega_2^\beta}{\omega_2^\alpha} - 1 \right) + \frac{1}{2} f^\alpha \left(\frac{\partial^2 (1/f)}{\partial^2 (\omega_2/B)} \right)_\alpha \left(\frac{\omega_2^\beta}{B} - \frac{\omega_2^\alpha}{B} \right)^2 + \dots \right] \quad \text{I-6.3}$$

Then using I-6.1 to eliminate f^α/f^β Barr and LeClaire obtained

$$\left(1 - \frac{D^\alpha}{D^\beta} \right) = \left(1 - \frac{\omega_2^\alpha}{\omega_2^\beta} \right) \left(1 - \frac{\partial \ln (1/f)}{\partial \ln (\omega_2/B)} \right)_\alpha + 0 \left((\omega_2^\beta - \omega_2^\alpha)^2 \frac{\partial^2 (1/f)}{\partial (\omega_2/B)^2} \right) \quad \text{I-6.4}$$

Finally, using I-5.4, this reduces to

$$\left(1 - \frac{D^\alpha}{D^\beta} \right) = \left(1 - \frac{\omega_2^\alpha}{\omega_2^\beta} \right) f^\alpha \quad \text{I-6.5}$$

Thus if $\omega_2^\alpha/\omega_2^\beta$ is known, f^α can be measured for both self and impurity diffusion.

The treatment of the atom-vacancy exchange frequencies on the basis of absolute rate theory gives ω in the form⁽¹⁵⁾

$$\omega = \tilde{\nu} \exp (-\Delta g_m / kT) \quad \text{I-6.6}$$

where Δg_m is the difference in the Gibbs Free Energy between the atom in its equilibrium site next to a vacancy

and when it is at the saddle point between the two sites. $\tilde{\nu}$ is an effective vibration frequency of the atom in its normal site. If it is taken to be the Einstein frequency, which implies the vibrational modes of the atoms are completely decoupled, then

$$\tilde{\nu} \propto \sqrt{\frac{b}{m}} \quad \text{I-6.7}$$

in the harmonic approximation. b is the interatomic force constant and m the mass of the jumping atom. Since the Δg 's in I-6.6 will be the same for the two isotopes α and β , I-6.6 and I-6.7 lead to the result that

$$\frac{\omega_2^\alpha}{\omega_2^\beta} = \frac{\tilde{\nu}^\alpha}{\tilde{\nu}^\beta} = \left(\frac{m^\beta}{m^\alpha} \right)^{\frac{1}{2}} \quad \text{I-6.8}$$

Vineyard⁽¹²⁾ has reconsidered the evaluation of ω , again subject to the basic assumptions of absolute rate theory. In his treatment, however, the jump process is generalized to a many-body transition in phase space. In place of I-6.6, he obtains

$$\omega = \left\{ \frac{\prod_{j=1}^{3N} \nu_j}{\prod_{j=2}^{3N} \nu'_j} \right\} \exp - \left[\Phi(S) - \Phi(E) \right] / kT \quad \text{I-6.9}$$

for the jump probability. The ν_j are the $3N$ normal mode frequencies of the N atoms of the crystal when the jumping atom is in its equilibrium configuration and the total potential energy of the system is $\Phi(E)$. The ν'_j are $(3N-1)$ normal modes when the jumping atom is at the saddle point configuration and the potential energy of the system is $\Phi(S)$. I-6.9 may be compared with I-6.6 by writing

$$\begin{aligned}\omega &= \tilde{\nu} \exp - \Delta g_m / kT \\ &= \tilde{\nu} \exp S_m / k \cdot \exp - Q_m / kT\end{aligned}$$

and setting $Q_m = \Phi(S) - \Phi(E)$.

By expressing the ν_j and ν'_j s in terms of the determinant of the mass independent force constants Vineyard showed that ω could be given in the simpler form

$$\omega = \frac{C}{\sqrt{m^*}} \exp - [\Phi(S) - \Phi(E)] / kT \quad \text{I-6.10}$$

where C depends on the force constants, and m^* is the "effective mass" of the jumping atom. This now includes any movements of the neighbouring atoms in the saddle point configuration. Mullen⁽¹⁶⁾ and LeClaire⁽¹⁷⁾ have used this to show that the more rigorous treatment leads to

$$\left(1 - \frac{D^\alpha}{D^\beta}\right) / \left(1 - \left(\frac{m^\beta}{m^\alpha}\right)^{\frac{1}{2}}\right) = \Delta K f^\alpha \quad \text{I-6.11}$$

ΔK is the fraction of the total kinetic energy in the saddle point mode ν_1' that resides in the jumping atom. ν_1' in turn, is the mode that leads to the decomposition of the saddle point configuration.

We see then that an isotope measurement of diffusion provides the product $\Delta K f^\alpha$. While the foregoing has been expressed in terms of the vacancy mechanism, the results are not peculiar to it. Thus, for self diffusion, a comparison between f_0 and $\Delta K f^\alpha$ can, in favourable cases, provide unambiguous identification of the mechanism. For example, Peterson⁽⁷⁾ has found for palladium,

$$\Delta Kf^{\alpha} = (1.02 \pm 0.04) f_{\circ} \text{ (vacancy)}.$$

This can only be consistent with the vacancy mechanism.

Isotope measurements for impurity diffusion do not yield direct information about the mechanism. However, if the mechanism is well established, the impurity correlation factor can yield information about the jump frequency ratios. That f_i can have a range of values can be seen from equation I-5.4; if $\omega_2 \ll B$, $f_i \rightarrow 1$. This, of course, reflects the fact that the relatively large number of vacancy-solvent exchanges between the vacancy-solute exchanges effectively randomizes the directions of the latter and hence reduces the degree of correlation. The impurity diffusion coefficient is then dependent almost entirely upon ω_2 . In the other extreme, if $\omega_2 \gg B$, $f_i \rightarrow \frac{B}{\omega_2}$ and the diffusion coefficient becomes independent of ω_2 . In this case, the migrations of the impurity are dependent upon the solvent-vacancy exchange rates.

I-7. THE INFLUENCE OF SOLUTES ON SOLVENT DIFFUSION

Equation I-5.2 indicates that the self diffusion coefficient in a pure metal is a function of the atom fraction of vacancies n_v/N_0 and the atom-vacancy exchange frequency W_0 .

If impurity atoms are added to the crystal both the concentration and distribution of vacancies are altered. In addition, the solvent-vacancy exchange frequency will be different near the presence of an impurity than well removed from one, where it will remain close to W_0 . Thus the solvent tracer diffusion coefficient, which contains the average jump frequency of all the solvent atoms, will be influenced by the presence of the impurities, so that $D_s(C) = D(W_0, W_1, \dots)$ where the W 's are the various distinguishable solvent-vacancy exchange frequencies. This effect has been considered by Hoffman et al⁽¹⁹⁾, Reiss⁽²⁰⁾, Lidiard⁽¹⁸⁾ and more recently by Howard and Manning⁽²¹⁾, in all cases for the f.c.c. lattice.

As we have seen in I-5, the impurity correlation factor f_i is a function of W_2 , the impurity-vacancy exchange frequency, and the same solvent-vacancy exchange frequencies as appear in $D_s(C)$. Lidiard has considered the latter term, in a dilute f.c.c. alloy and obtained the relation

$$D_s(C) = D_s(0)[1 + bC] \quad \text{I-7.1}$$

where C is the atom fraction of impurity, $D_s(C)$ and $D_s(0)$ the diffusion coefficients of a solvent tracer in the alloy and in the pure solvent, respectively, and b is a factor that measures the enhancement ($b > 0$) or diminution ($b < 0$)

of the tracer diffusion coefficient. In Lidiard's model of "weak-perturbation" by the impurities, b can be expressed in terms of the impurity coefficient D_i , the solvent coefficient in the pure metal $D_s(0)$, the self diffusion correlation factor f_o and that of the impurity f_i . That is, he finds

$$b = -18 + \frac{4f_o}{(1-f_i)} \frac{D_i}{D_s(0)} \quad \text{I-7.2}$$

Thus a measure of $D_s(C)/D_s(0)$ provides b , and a knowledge of $D_i/D_s(0)$ then yields f_i , if the vacancy mechanism is operative.

Howard and Manning have considered the same problem in the same system, that is, a dilute ($C_i \leq 2$ atom %) f.c.c. alloy, with fewer simplifying assumptions. The results do not change the form of I-7.1 or I-7.2, but permit more detailed inferences to be drawn regarding the jump frequency ratios implicit in f_i .

In chapter I both the macro- and microscopic formalisms of diffusion in simple systems have been reviewed. Particular attention was given to the vacancy mechanism in developing the theory of correlation effects because this appears to be best established for self and substitutional solute diffusion in metals.

Within this framework the approximations used are well defined and the treatments quite general. Such a formalism is clearly required if quantitative calculations of the atom jump frequencies are to be compared with experiment. Certainly, detailed measurements of the type described can provide considerable information of fundamental interest.

A primary aim of the experimentalist is to establish the mechanism or mechanisms by which the atoms move. While the emphasis both here and in the literature has been placed on the vacancy mechanism, others do occur. For example, the contribution of diffusion along dislocations to the total observed flux is a subject of growing interest. It generally appears to be unimportant at temperatures greater than about half the absolute melting point, but at lower temperatures it can become the dominant mechanism. Several special techniques are available for such studies.

Other mechanisms are known to occur in ionic crystals and in the past decade interest has grown in both elemental and compound semiconductors. In these latter materials the diffusion processes are sometimes quite complex, with apparent departures from the simple laws of Fick frequently being reported.

Such characteristic differences in behaviour are generally rationalized in terms of the various classes of solids. Occasionally, however, uncharacteristic behaviour is found in a given type of solid, which provides a stimulus for more intensive study. In chapter II we shall review those aspects of diffusion in the body-centered-cubic phases of zirconium and titanium that are unusual and describe in subsequent chapters an experimental study designed to test some of the proposed interpretations of their behaviour.

II-1. SELF AND SOLUTE DIFFUSION IN "NORMAL" METALS

From the experimental evidence available it would appear that the body-centered-cubic metals can be classified into two quite distinct groups with regard to their diffusion behaviour; there are those that are normal in that they conform to expectations based on previous experience, and those that are anomalous in that they depart from this behaviour.

In the following, the features of diffusion that characterize normal behaviour will be established and related to the theory of chapter I. In II-2, the results of experiments on the anomalous class of b.c.c. metals are reviewed and in II-3 some of the proposed interpretations are outlined.

The solution of Fick's second law, appropriate to the experimental conditions for the results shown in figure I-2.1 is ⁽²²⁾

$$C(x,t) = (S_0/2\sqrt{\pi Dt}) \exp - x^2/4Dt \quad \text{II-1.1}$$

$C(x,t)$ is the concentration of the diffusant at a point x after an annealing time t , S_0 is the total quantity of tracer contained in the initial thin layer and D is the diffusion coefficient. Thus one characteristic of normal behaviour is that the concentration profile results in a linear relation between $\ln C$ and x^2 . The diffusion coefficient can, of course, be evaluated from the slope.

Measurements are generally made at a series of temperatures ranging from the melting point T_m down to about $0.6 T_m$.

A second characteristic of normalcy is that the diffusion coefficients so obtained follow a simple Arrhenius temperature dependence of the form

$$D(T) = D_0 \exp - Q/RT \quad \text{II-1.2}$$

where D_0 , the frequency factor, and Q , the activation energy, are temperature independent. That is to say, a plot of $\ln D$ vs $(1/T)$ is linear.

Some values of D_0 and Q for self diffusion in a variety of crystal structures are listed in table II-1.1. These results show a third characteristic of normal behaviour; that is, that the frequency factors fall into a rather narrow range, from about 0.05 to $5 \text{ cm}^2/\text{sec}$. A fourth characteristic is associated with the strong correlation between Q and T_m , as illustrated in figure II-1.1. If Q is expressed in calories per gram mole, it is related to the absolute melting point by

$$Q \approx 34 T_m \quad \text{II-1.3}$$

Several conclusions may be drawn from these observations. The adherence of the concentration profile to equation II-1.1 implies that the diffusant behaves in a way consistent with the theory of random walks. A fairly common source of departure from this occurs if diffusion along grain boundaries becomes important. In such cases the plot of $\ln C$ vs x^2 shows a positive curvature. The effect of grain boundaries can be taken into account in the differential equation for $C(x,t)$, and analysis shows that $\ln C$

varies as $x^{6/5}$ over that portion of the concentration profile in which grain boundary effects are dominant⁽³⁴⁾.

Such behaviour is most pronounced at relatively low temperatures, and in small grained specimens. In intermediate cases, grain boundary effects can go undetected unless the concentration profiles are measured over very large diffusion distances. This point has been emphasized by Shewmon⁽³⁵⁾.

The linearity of the Arrhenius curves are consistent with the assumption of one dominant mechanism of diffusion occurring over the temperature range covered by the measurements.

The frequency factor can be written in the form

$$D_0 = \gamma \alpha^2 f_0 \tilde{\nu} \exp \Delta S/RT \quad \text{II-1.4}$$

where α is the lattice parameter, γ a geometrical constant of the order of unity, f_0 the correlation factor and ΔS the thermal entropy associated with diffusion. For $\tilde{\nu} \approx 10^{13}$ /sec,

$$D_0 \approx 10^{-2} \exp \Delta S/RT \text{ cm}^2/\text{sec} \quad \text{II-1.5}$$

Zener⁽³⁶⁾ has given some theoretical justification for expecting $\Delta S > 0$, which provides a basis for the narrow range of D_0 values observed.

It is also apparent that if self diffusion occurs by the vacancy mechanism, the activation energy, defined by $-R \partial \ln D / \partial (1/T)$ can be identified with

$$Q = H_v^f + H_v^m \quad \text{II-1.6}$$

where H_v^f and H_v^m are the enthalpies of vacancy formation and movement respectively. There are techniques by which

these parameters can be measured separately^(37,38). In those cases for which this has been done, there is generally good agreement with the result indicated in equation II-1.6. This gives considerable support to the vacancy mechanism in these systems. It has also been noted that for f.c.c. structure $H_V^f \simeq H_V^m \simeq \frac{1}{2}Q$, whereas in b.c.c. metals $H_V^f \simeq \frac{2}{3}Q$.

There is, at present, no satisfactory theoretical understanding of the correlation between Q and T_m .

TABLE II-1.1

VALUES OF THE PARAMETERS D_0 AND Q FOR SELF
DIFFUSION IN "NORMAL" METALS*

Metal	D_0 cm ² /sec	Q kcal/g.atom	T_m °K	Q/T_m
Al	1.71	34	933	36.4
Cr	0.2	73.7	2148	34.3
Co	0.17	62.2	1768	35.2
Cu	0.33	48.2	1356	35.5
Au	0.091	41.7	1336	31.2
α Fe	1.9	57.2	1809	31.6
δ Fe	1.9	57.0		
γ Fe	2.5	67.7		
Pb	1.37	26.06	600	43.4
Mo	0.5	96.9	2883	33.6
Ni	1.9	68.0	1726	39.4
Nb	1.1	96.0	2741	35.0
Pd	0.2	63.6	1825	34.8
Pt	0.2	66.5	2042	32.6
Ag	0.34	43.5	1234	35.2

* Taken from a recent compilation by J. Askill, O.R.N.L.-3795 (1965).

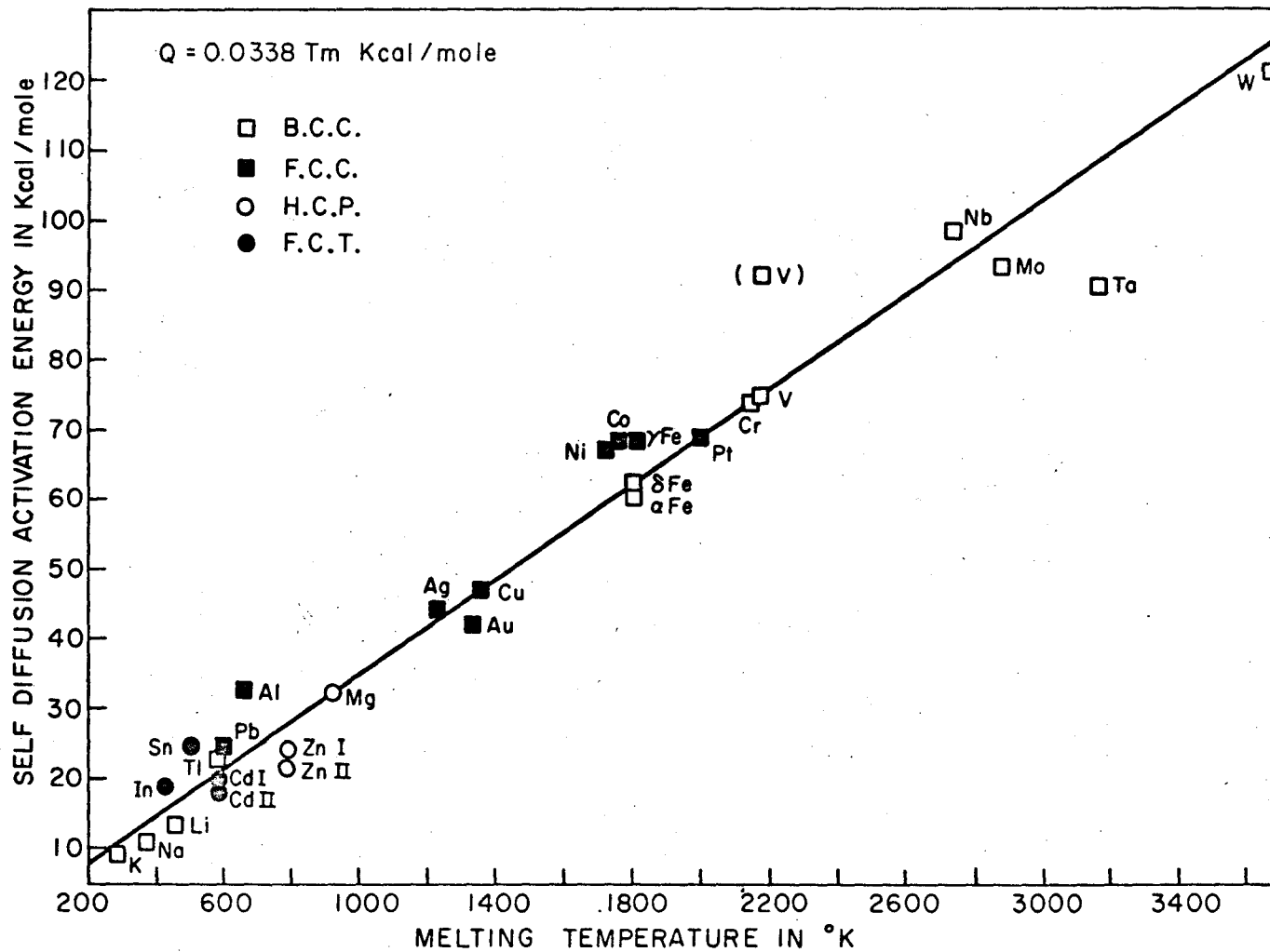


FIGURE II - 1.1 EMPIRICAL CORRELATION BETWEEN THE SELF DIFFUSION ACTIVATION ENERGY AND MELTING POINT OF METALS.

II-2. SELF AND SOLUTE DIFFUSION RESULTS IN
ANOMALOUS BODY-CENTERED-CUBIC METALS

The first suggestion of unusual behaviour in b.c.c. metals came during 1958 and 1959, when studies of solute diffusion in β -Ti and of self diffusion in Cr and γ -U indicated that the values of the diffusion parameters D_0 and Q were unusually small, as shown in Table II-2.1.

In view of the many similarities between Ti and Zr, a study of self diffusion in b.c.c. β Zr was undertaken at CRNL⁽⁴⁴⁾. In summary, the following points emerged:

- 1) The temperature dependence of the diffusion coefficients determined over the range of 1100 to 1500°C could be represented reasonably well by

$$D = 2.4 \times 10^{-4} \exp(-30,100/RT) \text{ cm}^2/\text{sec} \quad \text{II-2.1}$$

- 2) The concentration-penetration profiles appeared typical of bulk diffusion.
- 3) In most of the measurements, the radioactive tracer layer of ^{95}Zr was evaporated onto a specimen at room temperature. The specimen was then heated through the phase transition from the close packed hexagonal, α phase to the body-centered-cubic β phase, and thence to the annealing temperature. In some runs, however, by use of a specially designed apparatus, the specimens were pre-annealed at about 1200°C for 30 minutes, and the tracer layer then deposited while maintaining the specimen at temperature. This treatment did not produce a significant difference in the measured diffusion.

coefficients.

- 4) It was observed that rapid sintering occurred in a bundle of 0.010" diameter zirconium wires when annealed in the β phase. A diffusion coefficient, calculated on the assumption that the sintering took place by volume diffusion⁽⁴⁵⁾, was about fifty per cent lower than the value obtained from the conventional measurements.
- 5) Using techniques developed by Barnes⁽⁴⁶⁾ for copper and by Ells and Evans⁽⁴⁷⁾ for aluminum, zirconium specimens were bombarded with mono-energetic helium ions and subsequently annealed in the β phase. This treatment resulted in the formation of microscopic pores which have been attributed to the clustering of helium atoms, followed by a migration of vacancies to these clusters. The pore formation in the β Zr was very rapid. It was concluded at that time that most of the observations were consistent with the vacancy mechanism*. The low values of D_0 and Q were not accounted for.

Subsequent to the work described above, further studies were reported on self diffusion in β Zr⁽⁴⁸⁾, β Ti⁽⁴⁹⁾ and V⁽²⁴⁾, as well as on solute diffusion in β Zr⁽⁴⁸⁾, γ -U⁽⁵¹⁾ and β Ti⁽⁵²⁾. Hagel⁽⁵³⁾, using 99.997% chromium, measured self diffusion over a considerably broader temperature range than covered by the earlier work of Paxton and Gondalf⁽⁴³⁾ and found quite normal values for D_0 and Q , contrary to those previously reported.

Lundy and Federer⁽⁴⁸⁾ remeasured self diffusion in β Zr, using material of purity comparable to that used by

* This was also supported by the report of a Kirkendall Effect in β Zr- γ U diffusion couples⁽⁵⁰⁾.

Kidson and McGurn in the study outlined earlier. Again, however, the temperature range was extended, in this case from the $\alpha \rightarrow \beta$ phase transition at 863°C to the melting point at 1860°C. A comparison of their results with those of the earlier study is shown in figure II-2.1. There is good agreement over the temperature range covered by the latter. However, a marked departure from linearity in the Arrhenius plot is evident when taken over the complete temperature range. Similar effects were reported for solute diffusion in β Ti, when these studies were extended to higher temperatures⁽⁵⁴⁾.

The work on self and solute diffusion in the b.c.c. γ phase of uranium yielded low D_0 and Q values, although the temperature range available was not large enough to permit an unambiguous assessment of the evidence for curvature⁽⁵¹⁾. Peart⁽²⁴⁾ reported very careful measurements of self diffusion in vanadium, in which a sharp kink in the Arrhenius curve separates two linear regions at 1356°C. The D_0 and Q values associated with the curve below 1356°C are normal, while those above 1356°C are rather high.

A measurement of the isotope effect for iron in β Ti has been reported by Gibbs et al⁽⁵⁴⁾, using ^{55}Fe and ^{59}Fe . The results are shown in table II-2.2 where

$$\phi^{59} = \{1 - D^{59}/D^{55}\} / \{1 - \sqrt{55/59}\} \quad \text{II-2.2}$$

The effect of Nb additions to β Ti on the diffusion of niobium was investigated by Peart and Tomlin⁽⁵⁵⁾ and extended by Graham⁽⁵⁴⁾. These studies showed that both D_0 and Q were progressively decreased, as was the degree of curvature in the Arrhenius curve as the Nb content increased.

Peart and Tomlin also found a regular decrease in the diffusivity of ^{55}Fe in Ti-Fe alloys, and Ti-Nb alloys over the range of 0 to 15 atomic % solute additions, whereas that of ^{95}Nb increased with Fe additions in Ti-Fe alloys.

All of the preceding investigations have been described in the proceedings of a conference on Diffusion in Body-Centered-Cubic Metals, held at Gatlinberg, Tenn. in 1964⁽⁵⁷⁾.

Since then several new experiments in the β phases of Ti and Zr have been reported. Askill⁽⁵⁸⁾ studied the diffusion of ^{182}Ta in β Ti, using various combinations of pre-anneal and diffusion anneal conditions. These included high purity argon anneals, high (10^{-8} torr), medium (10^{-5} torr), and low (10^{-2} to 10^{-3} torr) vacuum anneals. None of these variations produced any measurable effect on the diffusion rates.

Peart⁽⁵⁹⁾ has reported a study of the influence of hydrostatic pressures up to 4000 atmospheres on the diffusion of Fe in β Ti and a Ti + 10% Fe alloy. He found that the diffusion coefficient of ^{59}Fe at 808°C in the alloy decreased as pressure increased such as to give a linear relation between $\ln D$ and pressure P . The activation volume for the diffusion process is related to the slope of this curve by⁽⁶⁰⁾

$$\Delta V = RT \left(\frac{\partial \ln D}{\partial P} \right)_T - RT \left(\frac{\partial \ln \gamma \alpha^2 \tilde{v}}{\partial P} \right)_T \approx RT \left(\frac{\partial \ln D}{\partial P} \right)_T$$

II-2.3

If the diffusion mechanism involves both the formation and movement of point defects, ΔV is the sum of ΔV^f , the change in crystal volume per defect formed and ΔV^m , the

change due to the lattice dilation during the diffusive jump. The ratio $\Delta V/V$, where V is the atomic molar volume, was found to be 0.6 for ^{59}Fe in the alloy. This can be compared with $\Delta V/V \approx 0.8$ for f.c.c. systems in which the vacancy mechanism is well established.

The effect of pressure on the diffusion of ^{59}Fe in Ti was unexpected, and is shown in figure II-2.2. The large negative value of ΔV is inconsistent with both vacancy and interstitial mechanisms.

Finally, Graham⁽⁶¹⁾ has measured the isotope effect for self diffusion of ^{95}Zr and ^{89}Zr in βZr in order to determine the correlation factor over a temperature range. Again the results are unexpected in that $^{95}\phi \approx 0$. Graham had earlier tested his technique on self diffusion in γ iron⁽⁶²⁾, for which he found $f \approx 0.72$, consistent with the vacancy mechanism at temperatures of the order of 1450°C . At 1121°C , grain boundary diffusion was observed and the diffusion was independent of the mass of the diffusing atom.

TABLE II-2.1SELF DIFFUSION IN BODY-CENTERED CUBIC METALS

<u>REFERENCE</u>	<u>METAL</u>	D_0 (cm^2/sec)	<u>Q OBSERVED</u> (kcal/mole)	<u>Q CALCULATED</u> (kcal/mole)
39	γ Uranium	1.81×10^{-3}	27.5	49
40	γ Uranium	1.17×10^{-3}	26.6	49
41	γ Uranium	2.33×10^{-3}	28.5	49
42	Tracer Cr^{51} in β Titanium	5×10^{-3}	35.3	73
43	Chromium	10^{-4}	52.0	76

TABLE II-2.2THE ISOTOPE EFFECT FOR ^{55}Fe , ^{59}Fe IN β Ti*

<u>Temp (°C)</u>	<u>D(^{59}Fe)</u>	<u>ϕ(^{59}Fe)</u>
1082	6.92×10^{-8}	0.025 ± 0.025
1228	2.00×10^{-7}	0.095 ± 0.032
1369	6.14×10^{-7}	0.095 ± 0.024

* As reported by Gibbs et al⁽⁵⁴⁾

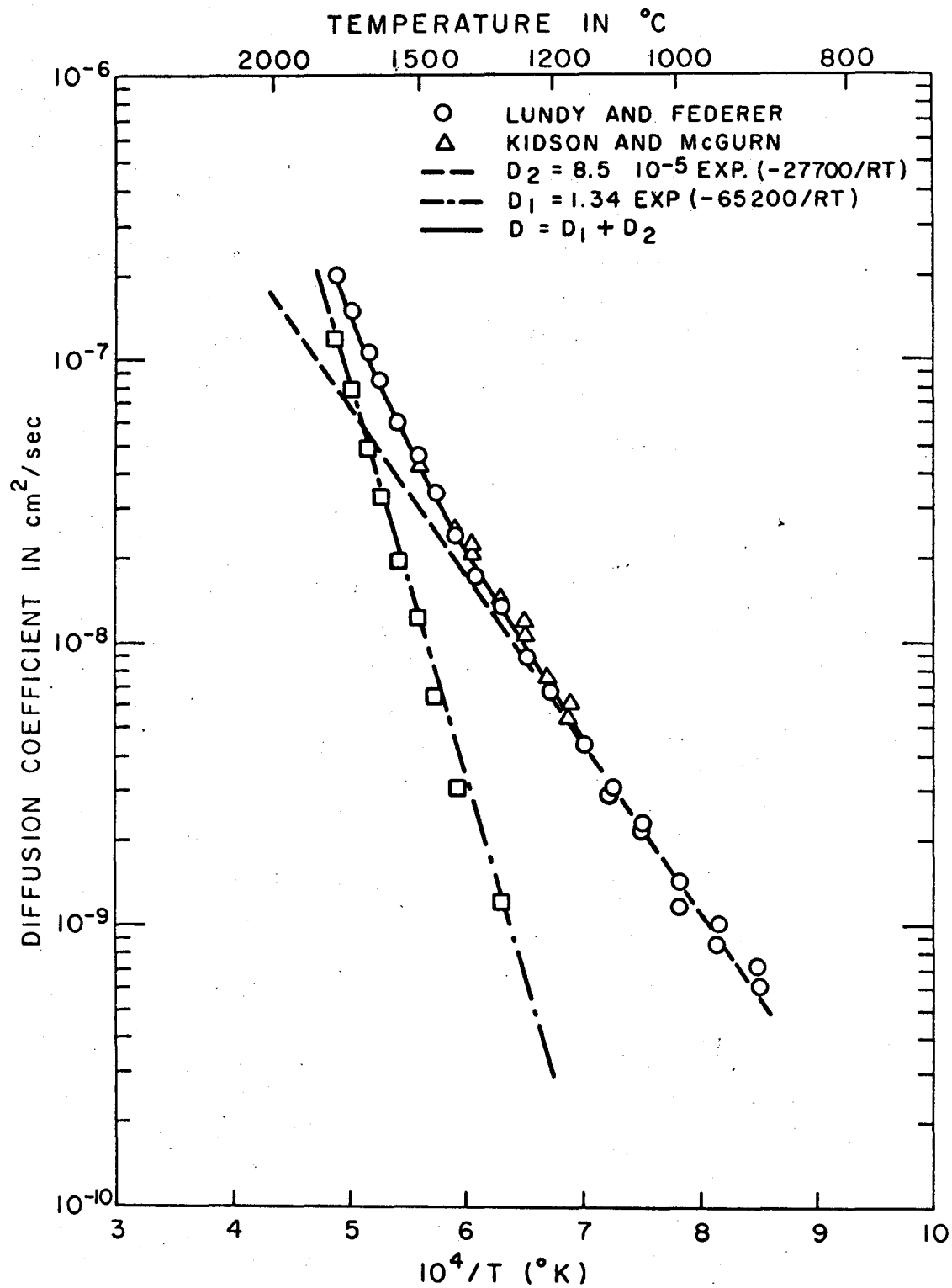


FIGURE II - 2.1 ARRHENIUS CURVE FOR SELF DIFFUSION IN β Zr

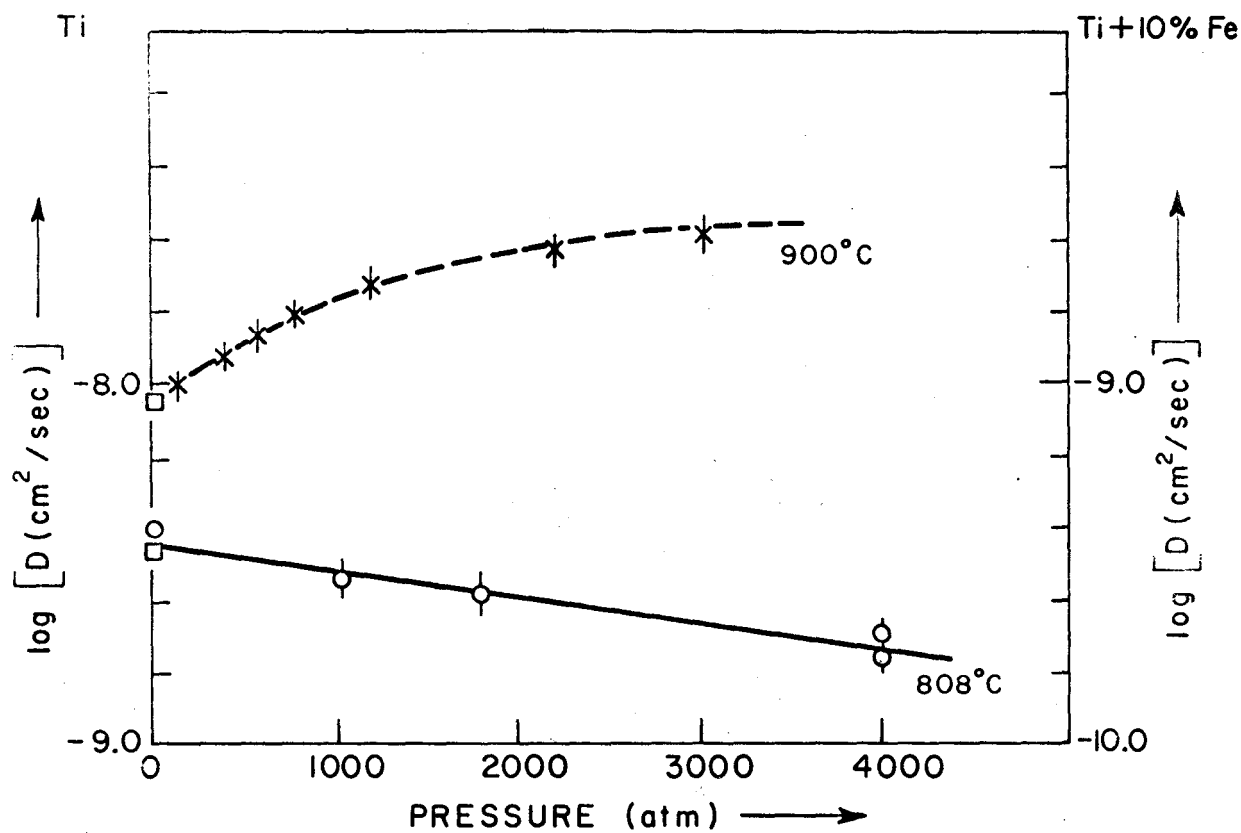


FIGURE II - 2.2

PRESSURE DEPENDENCE OF THE DIFFUSION COEFFICIENT OF ^{59}Fe IN Ti AND Ti + 10% Fe*.

- x ^{59}Fe IN IODIDE Ti
- o ^{59}Fe IN Ti + 10% Fe
- * AS REPORTED BY R. PEART⁽⁵⁹⁾

II-3. THE SINGLE MECHANISM HYPOTHESIS

The unusual diffusion behaviour of the anomalous b.c.c. metals β Zr, β Ti and γ -U has stimulated a number of speculative interpretations. Some of the more recent experiments have been designed specifically either to refute a particular proposal, or to test another. In several cases these have led to further unexpected results. Nevertheless the most prominent features that characterize these systems remain as (i) the non-linear Arrhenius curves, (ii) the low D_0 and Q values and (iii) the high diffusion rates. It is remarkable that some solutes in β Ti and γ -U have diffusion coefficients usually associated with the liquid state.

The various attempts to interpret these results in terms of specific models fall into two general classes; in the first are those that assume a single mechanism is operative, but in which D_0 and Q are temperature dependent, while in the second are those that assume two or more mechanisms contribute, each having different, but temperature independent, parameters.

Lundy and Federer⁽⁴⁸⁾ noted that the activation energies for self diffusion in β Zr, as defined by

$$Q = - R \partial \ln D / \partial (1/T) \quad \text{II-3.1}$$

appeared to follow the relation

$$Q = A + BT \quad \text{II-3.2}$$

where $A = -15,500$ cal/mole, $B = 30.9$ cal/mole/°K. They stressed that thermodynamic arguments alone do not exclude the possibility of temperature dependent activation energies. Dienes^(63,64) questioned this premise, and gave arguments to show that a linear temperature dependence of the activation energy could not arise from equation II-3.1. This point, however, was subsequently refuted by Gibbs⁽⁶⁵⁾, thereby providing support for the point of view of Lundy and Federer*. Nevertheless, problems remain in the interpretation of the significance of the results.

If it is assumed that diffusion activation enthalpies in general are linearly dependent on temperature, then it may be argued that failure to observe nonlinear Arrhenius curves in metal systems other than β Zr, β Ti and γ -U is due either to the range of temperature being too restricted or to the value of the coefficient B in equation II-3.2 being too small. The first point would appear to be invalid, at least in the case of self diffusion in niobium⁽²⁵⁾, for which the Arrhenius curve is strictly linear over a range of almost nine orders of magnitude in D and 1500° in temperature.

The second point implies that the value of Q observed in other systems arises primarily from the coefficient A in equation II-3.2. A reasonable account must then be given for the negative value deduced for β Zr. No features specific to Zr, Ti and U were advanced by Lundy and Federer to account for the rapid diffusion rates in these systems.

* Gibbs, however, subscribes to the Two-Mechanism Hypothesis - see II-4.

A particularly interesting model that does provide an appealing rationale for the unusual diffusion behaviour of the anomalous metals has recently been proposed by Aaronson and Shewmon⁽⁶⁷⁾. They assume that the vacancy mechanism is dominant at all temperatures, so that the measured activation energy is the sum $H_V^f + H_V^m$. The progressive decrease in Q with temperature is attributed primarily to a decrease in H_V^m and to a lesser extent to H_V^f . The postulated decreases in these parameters, in turn, are based on the following points:

- (i) A rather successful model, proposed by Lazarus⁽⁶⁸⁾, for the calculation of H_V^m assumes that a major portion of it is associated with the elastic strain energy of the lattice when a jumping atom is at the saddle point. If the ratio of elastic shear coefficient $\frac{1}{2}(C_{11} - C_{12}) / C_{44} \ll 1$, then the main contribution to H_V^m comes from $\frac{1}{2}(C_{11} - C_{12})$ alone.
- (ii) Zener⁽⁶⁹⁾ has pointed out that the shear coefficient $\frac{1}{2}(C_{11} - C_{12})$ will be small in b.c.c. structures, particularly in those for which the interatomic forces between the ions can be approximated by a central force potential. If $\frac{1}{2}(C_{11} - C_{12}) \rightarrow 0$, the structure becomes mechanically unstable with respect to close packed structures. In some systems the b.c.c. structure may exist at high temperatures because of a large thermal vibrational entropy associated with the low $\frac{1}{2}(C_{11} - C_{12})$ values, but, Zener suggests, they will transform martensitically to a close packed structure as the temperature is lowered.

(iii) While the elastic shear constants of β Zr and β Ti have not been measured, those of α Zr and α Ti have⁽⁷⁰⁾. In both of these metals $\frac{1}{2}(C_{11} - C_{12}) \rightarrow 0$ as the $\alpha \rightarrow \beta$ transformation temperature is approached.

Aaronson and Shewmon suggest then that the $\frac{1}{2}(C_{11} - C_{12})$ of the β phase structure also decreases as the transformation temperature is approached, and that this in turn accounts for the decrease in Q . They advance further arguments to account for the low D_0 values, the rapid solute diffusion rates and the anomalous effects of applied pressure.

II-4.

THE TWO-MECHANISM HYPOTHESIS

An alternative view, adopted by a number of people, including the writer⁽⁷¹⁾, attributes the anomalous behaviour of β Zr, β Ti and γ -U to the simultaneous contribution of two mechanisms, each characterized by temperature independent D_0 and Q parameters. It is assumed that the measured diffusion coefficient can be written as

$$D = D_{01} \exp - Q_1/RT + D_{02} \exp - Q_2/RT \quad \text{II-4.1}$$

The effective activation energy, defined by equation II-3.1 becomes

$$\begin{aligned} Q &= - R \partial \ln D / \partial (1/T) \\ &= \frac{1}{D} \{ Q_1 D_1 + Q_2 D_2 \} \end{aligned} \quad \text{II-4.2}$$

That is, Q represents a weighted average of the two activation energies involved, and is clearly temperature dependent. The problem, then, is to separate the two components D_1 and D_2 from the observed data and identify the associated mechanisms.

Since no unique method of decomposition of the Arrhenius curve exists, the method adopted by the author was based on two assumptions. First, the supplementary observations described in II-2 imply that vacancies occur in β Zr and probably play an important role in diffusion. If the contribution of a single vacancy mechanism is represented by $D_1 = D_{01} \exp - Q_1/RT$, then the parameters D_{01} and Q_1 are probably of the order predicted by the normal systems.

This implies that $D_1 \ll D$ at the low temperatures. The curve, then, was decomposed by assuming that $D \simeq D_2$ in this region.

For self diffusion in β Zr, the results of Kidson and McGurn⁽⁴⁴⁾ and of Lundy and Federer⁽⁴⁸⁾, when considered together, can be fitted quite well for temperatures less than about 1400°C by

$$D_2 \simeq 8.5 \times 10^{-5} \exp(-27,700/RT) \text{ cm}^2/\text{sec} \quad \text{II-4.3}$$

Taking $D_1 = D - D_2$, it is found that a good fit is obtained from

$$D_1 = 1.34 \exp(-65,200/RT) \text{ cm}^2/\text{sec} \quad \text{II-4.4}$$

The full curve in figure II-2.1 is that calculated from $D = D_1 + D_2$, while the dotted curve is that for D_1 alone.

The values of D_{01} and Q_1 obtained in this way are certainly of the magnitude expected for normal systems, and lend support to the assumption of a vacancy mechanism for D_1 . Additional support comes from similar treatment of the data for self and solute diffusion in β Ti⁽⁵⁴⁾.

Any model proposed for D_2 must, of course, be consistent not only with the low values of D_{02} and Q_2 but also with the shape of the concentration profiles that appear, at least over most of the temperature range, to be characteristic of volume diffusion*.

* In fact, however, there is an indication of a departure from linearity in a few of the $\ln C$ vs x^2 plots, reported by Lundy and Federer at temperatures below about 1200°C. Similar effects were noted by Kidson and McGurn at temperatures below 1100°C, and these results were excluded from the reported Arrhenius curve.

Two proposals have been made to account for D_2 . The first, and most obvious, of these is that defects are introduced into the lattice by the $\alpha \rightarrow \beta$ transformation. In particular, excess vacancies⁽⁵⁶⁾, dense dislocation networks^(71,72) and "surfaces of internal division"⁽⁷³⁾ have been suggested.

The chief difficulties with these are (i) the large numbers required to account quantitatively for D_{O_2} and (ii) the lack of any effect on the diffusion coefficient by the pre-annealing experiments conducted by Kidson and McGurn on β Zr and by Rothman⁽⁵¹⁾ on γ -U.

On this basis, these models were initially rejected by the author and an alternative suggested in which D_2 arose from a relatively temperature independent concentration of vacancies that was associated with an impurity, probably interstitial oxygen⁽⁷¹⁾. Applying the model quantitatively to the results of self diffusion in β Zr, it was found that D_{O_2} could be accounted for by assuming an impurity concentration of only 10^{-4} . Q_2 was then identified with H_V^m alone. The immediate difficulty with this proposal was that it implied a binding energy of about 30 kcal/mole between the oxygen and the vacancies. Moreover, it predicted that the degree of enhancement due to D_2 should be directly proportional to the oxygen content. Graham⁽⁵⁴⁾ and Askill⁽⁵⁸⁾, however, found little effect on the solute diffusion rates in β Ti when specimens of differing purity and annealing conditions were used.

Subsequent to this proposal, Fisher and Renken⁽⁷⁰⁾ published a report that gave strong evidence to indicate that the $\alpha \rightarrow \beta$ transformations in Ti and Zr were, like

those of the $\beta \rightarrow \alpha$, martensitic in character and produced, at least momentarily, a large defect density in the β phase. In a review paper⁽⁷²⁾, the present writer emphasized that if these were dislocations, and if it could be assumed that they occurred in sufficient number (and, of course, were not removed by the pre-annealing treatment) then not only could one account for the self diffusion results in β Zr and β Ti, but for the solute diffusion results as well.

Gibbs⁽⁷⁴⁾ and Gibbs and Askill⁽⁷⁵⁾ have continued to reject the dislocation mechanism and have advanced the novel suggestion that the values of D_{02} and Q_2 associated with the low temperature portion of the Arrhenius curves are due to single vacancies, whereas those associated with D_1 are due to divacancies. They base this hypothesis on the unusually low elastic modulus associated with Ti, Zr and U.

CHAPTER III

III-1. AIMS OF THE PRESENT INVESTIGATION

None of the models described in chapter II have found full acceptance by workers in this field. However, the proponents of a single mechanism are generally concerned with accounting for low and temperature dependent D_0 and Q values associated with the vacancy mechanism whereas those favouring the two mechanism hypothesis generally attribute the higher temperature results to a normal vacancy component and attempt to relate the low temperature results to a different defect, notably dislocations. The primary aim of this work is to devise a means of establishing whether a single mechanism or a two mechanism hypothesis is valid.

Zirconium was chosen as the host metal for several reasons: it has a suitable radioactive isotope for self diffusion studies whereas titanium does not, less work has been done on solute diffusion in β Zr than in β Ti and, finally, the Chalk River Nuclear Laboratories have a considerable interest in this material.

In selecting a solute, note was taken of the extraordinarily rapid diffusion of the transition metals Fe, Co and Ni in β Ti and γ -U. The choice of one of these had several advantages: if the vacancy mechanism was operative, the effect of fast diffusing solute additions on solvent diffusion could be large, if dislocation effects were contributory, they could be enhanced by a tendency of the

solute to segregation arising from the relatively low solubility of these elements. Cobalt was chosen primarily for its convenient isotope.

The program was to include the following:

- (i) a measurement of the diffusion coefficients of ^{60}Co in β Zr over the complete temperature range of the β phase, using specimens in a variety of metallurgical conditions;
- (ii) a study of the effect of cobalt additions on the diffusion of ^{95}Zr in dilute Zr-Co alloys;
- (iii) a study of the effect of cobalt additions on the diffusion of ^{60}Co in dilute Zr-Co alloys;
- (iv) an attempt to assess the lattice perfection of β Zr as a function of temperature and time by observing the quality of Laue back reflection diffraction spots. This was to involve the design and construction of a high temperature, high vacuum Laue X-ray camera.

As it turned out, some rather interesting results were also obtained for the diffusion of ^{60}Co in the low temperature close packed hexagonal phase of Zr. One measurement was made of diffusion of ^{64}Cu in β Zr.

The experimental methods and results are described in chapter IV and their significance discussed in chapter V.

CHAPTER IV EXPERIMENTAL TECHNIQUES AND RESULTS

IV-1 SUMMARY OF TECHNIQUES

The methods of measuring diffusion coefficients in all of the experiments to be described below had the following in common: a thin layer of radioactive tracer was evaporated onto a carefully prepared flat surface of the specimen; the latter was annealed in a vacuum, and subsequently sectioned in a precision lathe, the slices being parallel to the initial surface. The specific activity in each slice was measured and from this a concentration profile established. In those cases for which it was appropriate, the diffusion coefficient was obtained from a least squares analysis of the $\ln C$ vs x^2 curve described in II-1. More detailed descriptions of the materials, methods and results are given below.

The zirconium used in this study came from three sources. Most of the measurements were made on specimens cut from a 3/8 inch diameter swaged rod supplied by the Wah Chang Corporation. The analysis for this material is given in table IV-2.1. The oxygen content was confirmed independently at CRNL.

Small buttons, 1/4 inch in length, were cut from the swaged rod on a cut-off wheel, using a special jig designed to ensure accurately flat and parallel faces. Identifying numbers were stamped on the side and one end of the specimens, which were then chemically cleaned in a solution of 45 parts by volume H₂O, 55 parts HNO₃ and 5 parts HF. They were mounted in bakelite in groups of 7, lightly polished on 6-0 emery paper followed by a final polish on a Syntron vibratory polisher, using an alumina slurry and a 5% chemical polishing solution. One group of specimens was annealed in a vacuum of 5×10^{-7} torr for 5 days at 840°C, another for 10 days under the same conditions, a third for 2 days at 900°C followed by 5 days at 840°C. The remainder were left in the as-swaged condition.

A few samples were prepared from a 3/8 inch diameter pseudo-single crystalline rod supplied by the Materials Research Corporation and some others from a similar rod provided by the Oak Ridge National Laboratories*. The specimens were cut into 3/8 inch length, using a spark

* Through the courtesy of Dr. M. Picklesimer

cutting machine, carefully mounted in a cold setting plastic, chemically polished to remove the worked layer and then attack polished on the Syntron vibratory polisher to produce a flat surface. X-ray diffraction patterns obtained with a standard back-reflection Laue camera indicated a pronounced substructure, as shown in figure IV-2.1, (a) and (b). That this structure was highly stable was shown by the lack of change after annealing at 840°C for 96 hours, as shown in figure IV-2.1 (c). For comparison, figure IV-2.1(d) shows the sharp spots produced from a large grained specimen obtained by annealing a sample cut from the swaged rod for 10 days at 840°C.

Dr. B. Wilkins of the Whiteshell Nuclear Research Establishment kindly provided a series of dilute zirconium-cobalt alloys. These were in the form of 3/8 inch diameter rods, swaged from buttons produced in a cold hearth, argon filled arc-melting unit. The nominal compositions of the rods were 0.4, 0.8, 1.2, 1.6 and 2.0 atomic % cobalt.

Diffusion specimens 1/4 inch in length were cut from the rods, numbered from 1 to 11 and numbers 1, 4 and 7 of each composition analysed for cobalt and oxygen content. The results are given in table IV-2.2. Following the standard surface preparation the remaining specimens were given a final homogenizing anneal at 940°C for 2 days.

Just prior to deposition of the radioactive tracer layer, the specimens were given a light chemical polish, washed in water, rinsed in methanol and dried in warm air. They were immediately transferred to the vacuum evaporation unit shown in figure IV-2.2.

The radioactive ^{60}Co was prepared by irradiating small rings of 0.010" diameter 99.999% pure cobalt wire in the NRU reactor for 4 hours in a flux of 10^{14} n/cm²/sec. One such ring was then removed from the storage flask and placed in the tungsten wire basket filament shown in figure IV-2.2. The unit was evacuated to about 5×10^{-6} torr and the tracer layer evaporated onto one surface of several specimens at a time by passing a current of about 25 amps through the filament for about 20 seconds. All parts except a central portion of 5/16 inch diameter on the specimen faces were masked from the tracer by the brass plate holder. Two small discs of aluminum foil set in the holder were used to determine the thickness of the evaporated layer by comparing their activity with that of a known weight of irradiated cobalt. The layer thicknesses ranged from 75 to 200Å.

Similar techniques were used for the experiments involving the use of ^{95}Zr and ^{64}Cu .

The specimens were generally annealed in pairs; those that were not to be used immediately were stored under a vacuum of 5×10^{-5} torr in a lead shielded dry box.

TABLE IV-2.1

ANALYSIS OF ZIRCONIUM CRYSTAL SUPPLIED BY THE
WAH CHANG CORPORATION

Zirconium

Heat No. 6-350306

Analysis in ppm

	<u>Top</u>	<u>Bottom</u>
Al	< 25	< 25
B	< 0.2	0.2
C	< 40	< 40
Cb	<100	<100
Cd	< 0.3	< 0.3
Co	< 5	< 5
Cr	24	28
Cu	< 25	< 25
Fe	260	235
H	4.1	3.4
Hf	200	155
Mg	< 10	< 10
Mn	< 10	< 10
Mo	< 10	< 10
N	5	8
Ni	34	30
O	100	170
Pb	< 5	< 5
Si	46	48
Sn	< 10	< 10
Ta	<200	<200
Ti	< 20	< 20
V	< 5	< 5
W	< 25	< 25
Zn	< 50	< 50

Hardness in BHN

Average 54.0
Range 50.3 - 56.8

TABLE IV-24ANALYSIS OF Zr-Co ALLOYS

<u>Sample #</u>	<u>Cobalt at.%</u>	<u>Average</u>
.4-1	0.39	
.4-4	0.40	
.4-7	0.40	0.40
.8-1	0.76	
.8-4	0.75	
.8-7	0.73	0.75
1.2-1	1.24	
1.2-4	1.22	
1.2-7	1.22	1.23
1.6-1	1.63	
1.6-4	1.63	
1.6-7	1.59	1.62
2.0-1	1.95	
2.0-4	2.01	
2.0-7	1.98	1.98

Fig. IV-2.1(a)
As received "crystal" from M.R.C.

Fig. IV-2.1(d)
Fine grained polycrystal

Fig. IV-2.1(b)
O.R.N.L. crystal, as received

Fig. IV-2.1(c)
O.R.N.L. crystal, as annealed

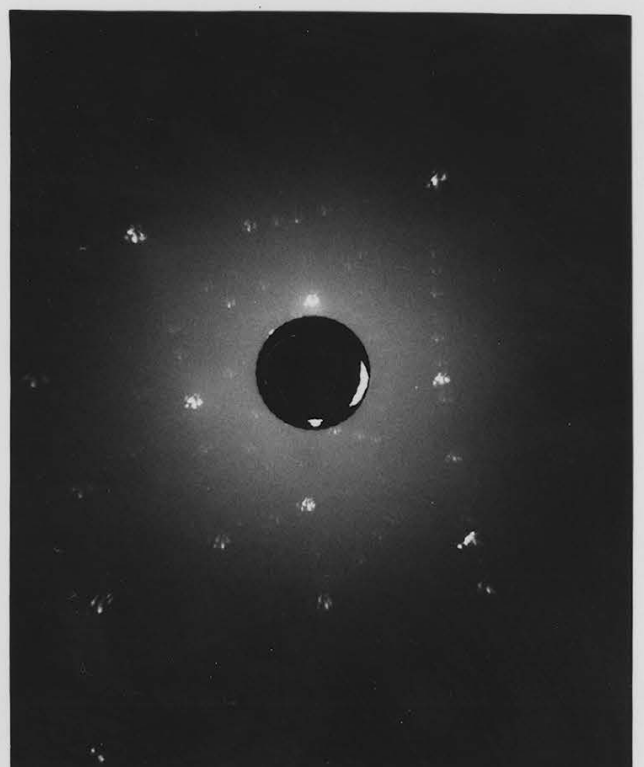
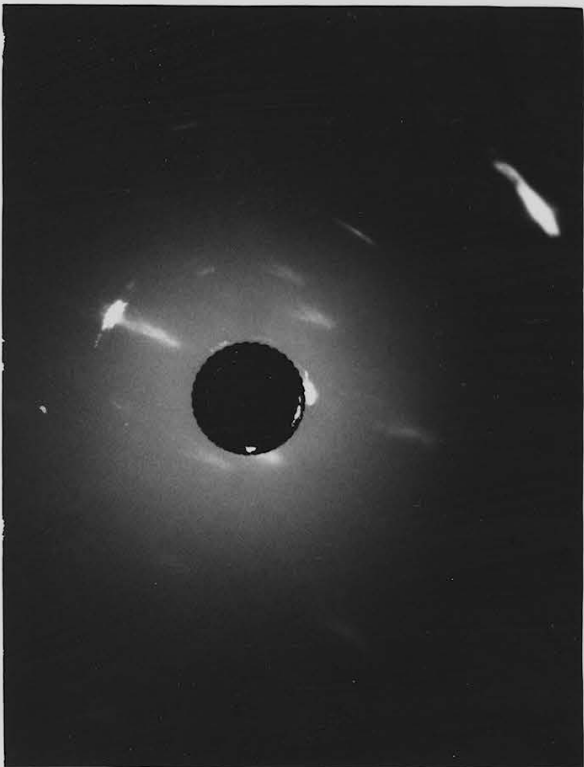
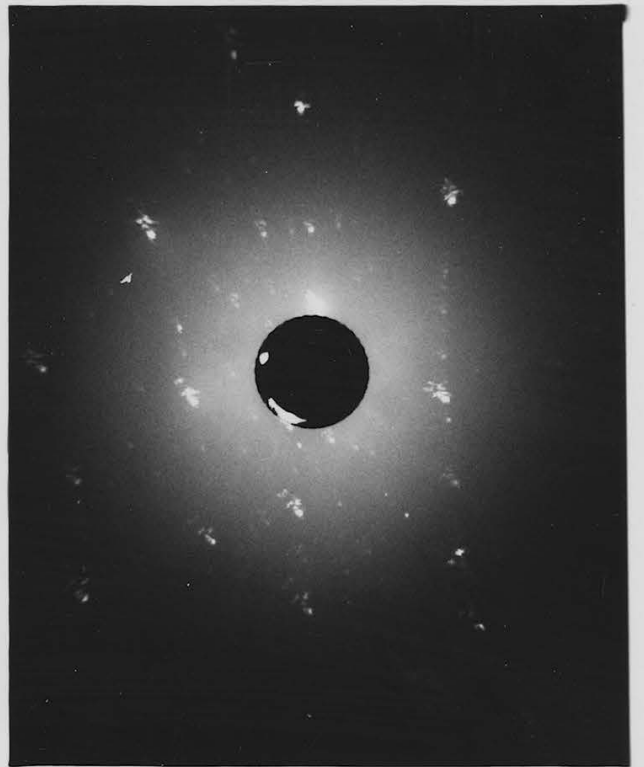
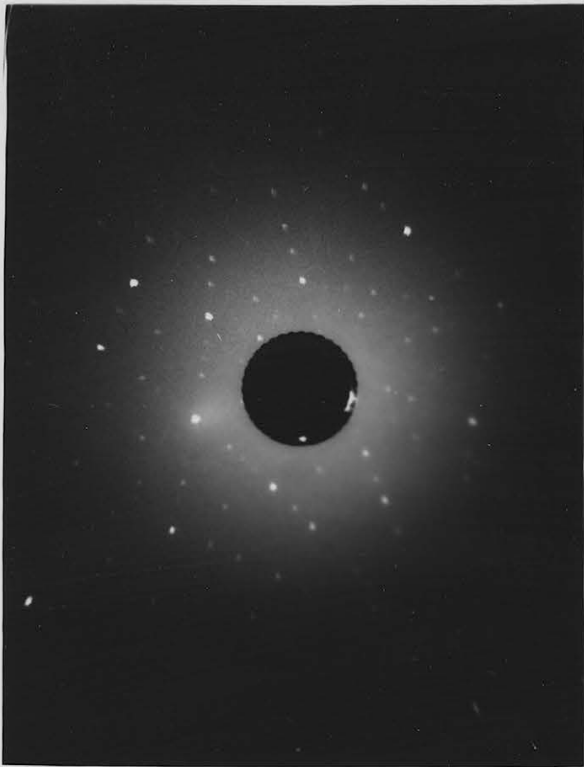
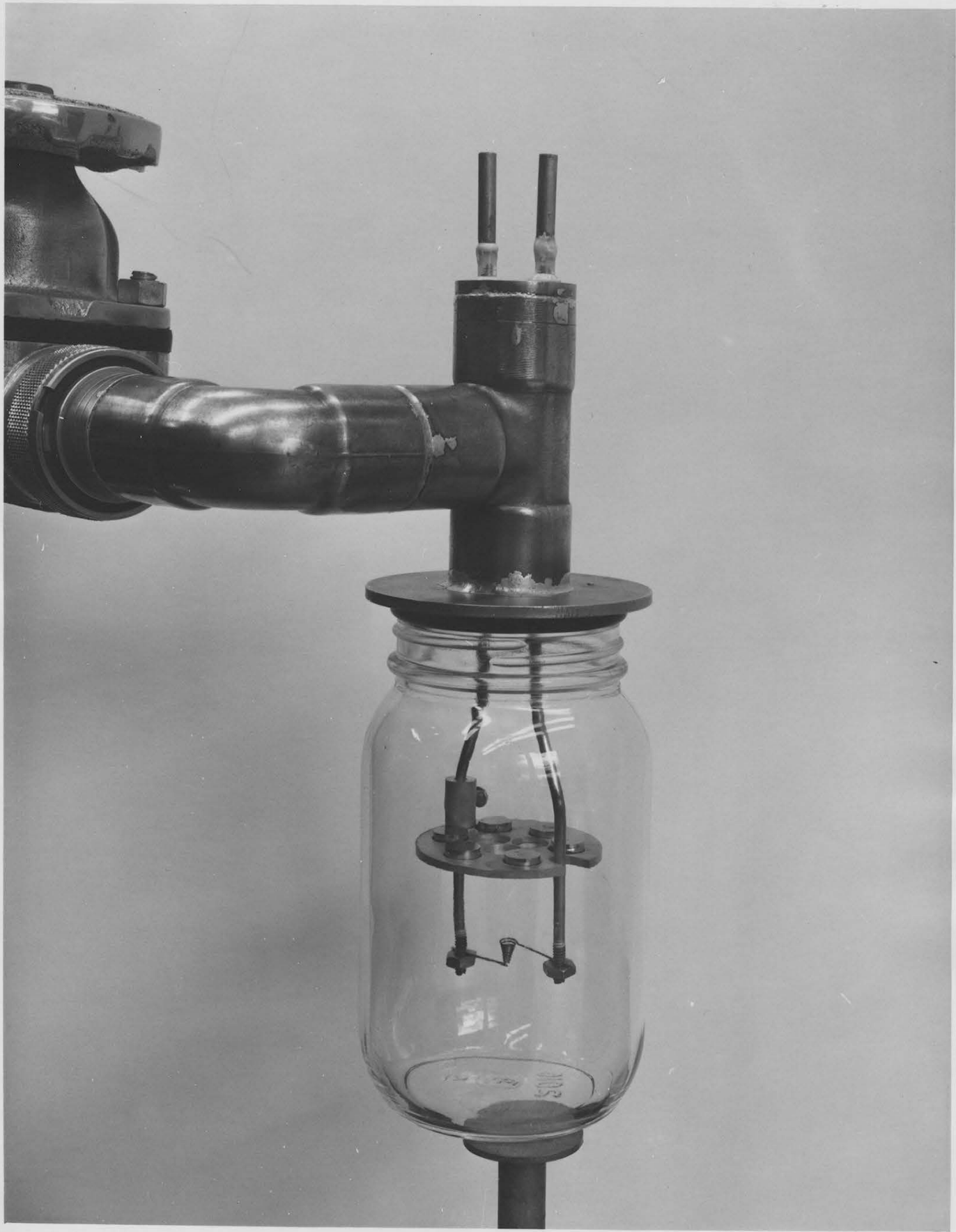


Fig. II-2.2

Vacuum evaporation unit.



Two vacuum furnaces were constructed for the diffusion anneals. One of these, consisting of a dynamically pumped quartz tube and a roll-on furnace, is shown in figure IV-3.1. The specimens were held in a zirconium capsule, in pairs, with active surfaces face to face. They were prevented from welding together or to the container by means of small, degassed, tungsten wire rings. The capsule was held in the center of the quartz tube on an alumina thermocouple insulator as shown in figure IV-3.2. Two calibrated Pt - Pt + 10% Rh thermocouples were separated from the specimens by a thin walled tantalum tube in the zirconium capsule. The latter was found necessary to avoid alloying between the specimens and the thermocouple.

The system was evacuated to about 5×10^{-7} torr, using an oil diffusion pump, a cold trap and a baffle valve. Pressures were measured with an Ionization Gauge. The furnace was heated by three Kanthal windings, one central winding that was controlled with a Honey-well Brown Pyrovane Controller, and two end windings, connected in parallel and powered from a Variac Autotransformer. Figure IV-3.3 shows a temperature profile of the furnace at 959°C in the center.

In preparation for a diffusion anneal, the required furnace temperature was established, using a dummy specimen in the zirconium capsule. The furnace was rolled off, the quartz tube cooled, the specimens mounted in place, the system re-evacuated and the furnace rolled back on. The specimen temperature was continuously monitored on a

Honeywell Speedomax recorder, and checks made between the two Pt - Pt + 10% Rh thermocouples using a Rubicon potentiometer. Temperatures were controlled to $\pm 3^{\circ}\text{C}$ and measured to $\pm 1^{\circ}\text{C}$.

Annealing times were measured with a stop clock. Following an anneal, the furnace was rolled off and the specimen cooling curve recorded. Total effective annealing times were corrected for heating and cooling by the method described in appendix II. The use of this system was limited by the quartz tube to temperatures below about 1100°C .

For the anneals, between 1100 and 1700°C , a special high vacuum high temperature furnace was constructed as shown in figures IV-3.4 and 3.5. In this unit single diffusion specimens were held in a zirconium cup, that sat on a thoria thermocouple insulator. This in turn was held by a stainless steel clamp that permitted vertical, longitudinal, lateral and tilt adjustment of the specimen holder. Two Pt - Pt + 10% Rh thermocouples were used for temperature measurements below 1400°C , and were replaced by W + 5% Re - W + 26% Re thermocouples at the higher temperatures.

The heating element consisted of a $3/4$ inch I.D. by 5 inch long tantalum tube arc welded at the top to a concentric 1 inch I.D. by 4 inch long tantalum tube, so as to form a continuous piece. Power was supplied via heavy molybdenum electrodes clamped to water cooled feed-throughs. These in turn were supplied via a Sola constant voltage regulator, through a Variac Autotransformer and thence to a step down transformer. The radiation shields were made from two inner cylinders of tantalum sheet and one outer cylinder of zirconium sheet, supported in place by a polished stainless steel plate. The system was enclosed in

a water cooled stainless steel cylinder, whose inside surfaces were electropolished. All permanent joints were arc-welded, demountable joints were sealed with standard copper gaskets and flanges obtained from Varian Corporation.

The vacuum pumping system consisted of a bakeable ultra-high vacuum valve, a Varian VacIon pump, backed up by a cryogenic pump. The latter was used to reduce the pressure to 10^{-4} torr, after which the vacuum valve was closed and the VacIon pump switched on. If the system was pre-baked, the ultimate vacuum attainable was better than 1×10^{-9} torr.

It was found in operation, however, that the extensive degassing of the specimen could not be handled by the 15 l/sec VacIon pump alone and it became necessary to back this up with the conventional system used on the other furnace. The usual vacuum during an anneal was of the order of 10^{-6} torr.

The very short annealing times required made it reasonable to control the temperatures manually by adjusting the Variac voltage output. The approximate voltages required to attain a range of steady state temperatures were measured and used as a guide. Very rapid initial heating for a diffusion run was achieved by using a large voltage during the heat-up, subsequently cutting it back as the desired temperature was approached. At the end of an anneal the power was shut off and the cooling curve recorded. Typical heating and cooling curves are shown in fig. IV-3.7. As can be seen, the thermal arrest, due to the β - α phase transformation, serves as a rough check on the thermocouple behaviour. While this was highly accurate in different experiments to be described later, the present geometry

resulted in an apparent span of about $\pm 10^{\circ}\text{C}$ around the known transformation temperature of 863°C .

Fig. IV-3.1
"Roll-on" Annealing Furnace

Fig. IV-3.2
Specimen Capsule on T.C. Insulator

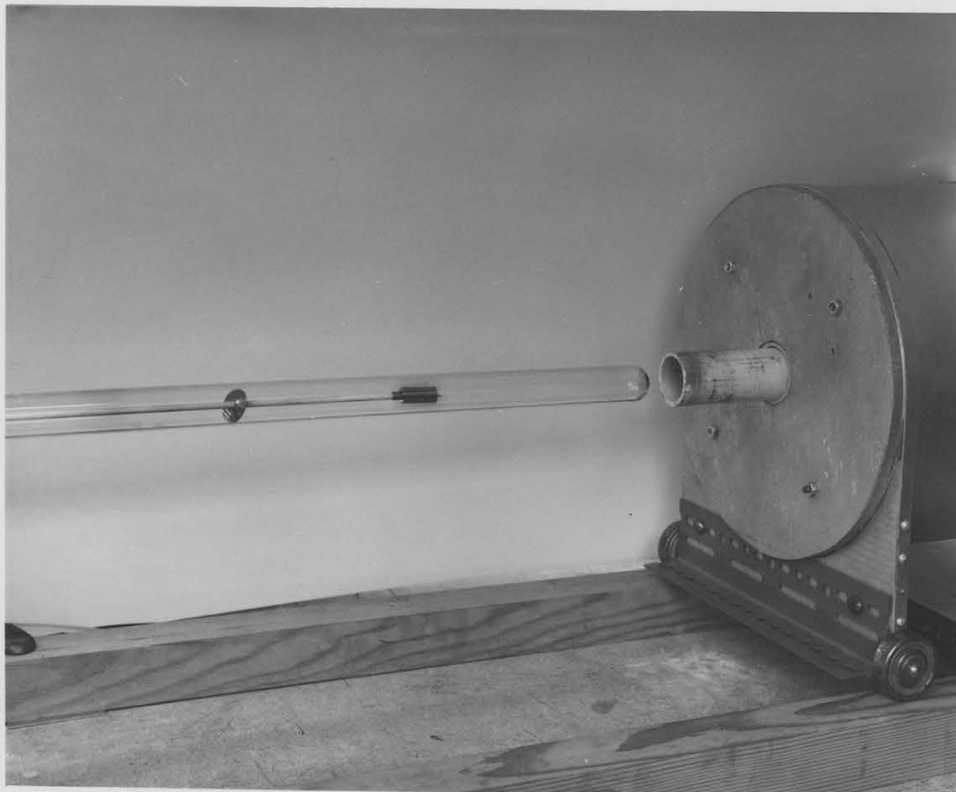
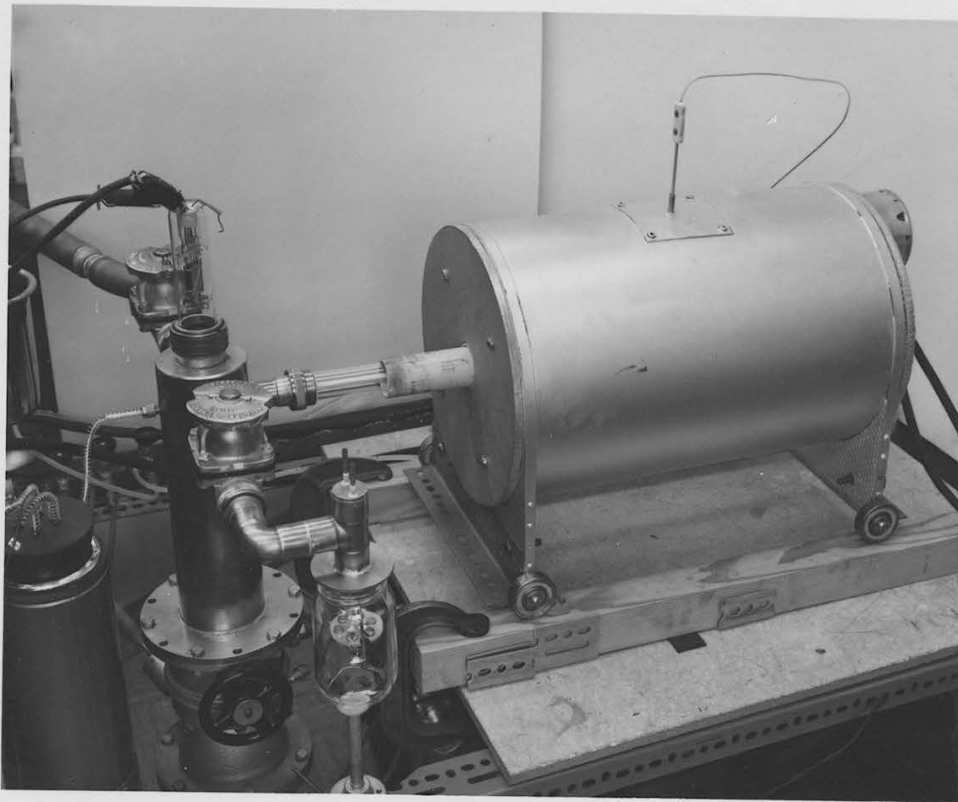


FIGURE IV - 3.3

TEMPERATURE PROFILE OF 'ROLL-ON FURNACE
FOR CENTER TEMPERATURE OF 959°C

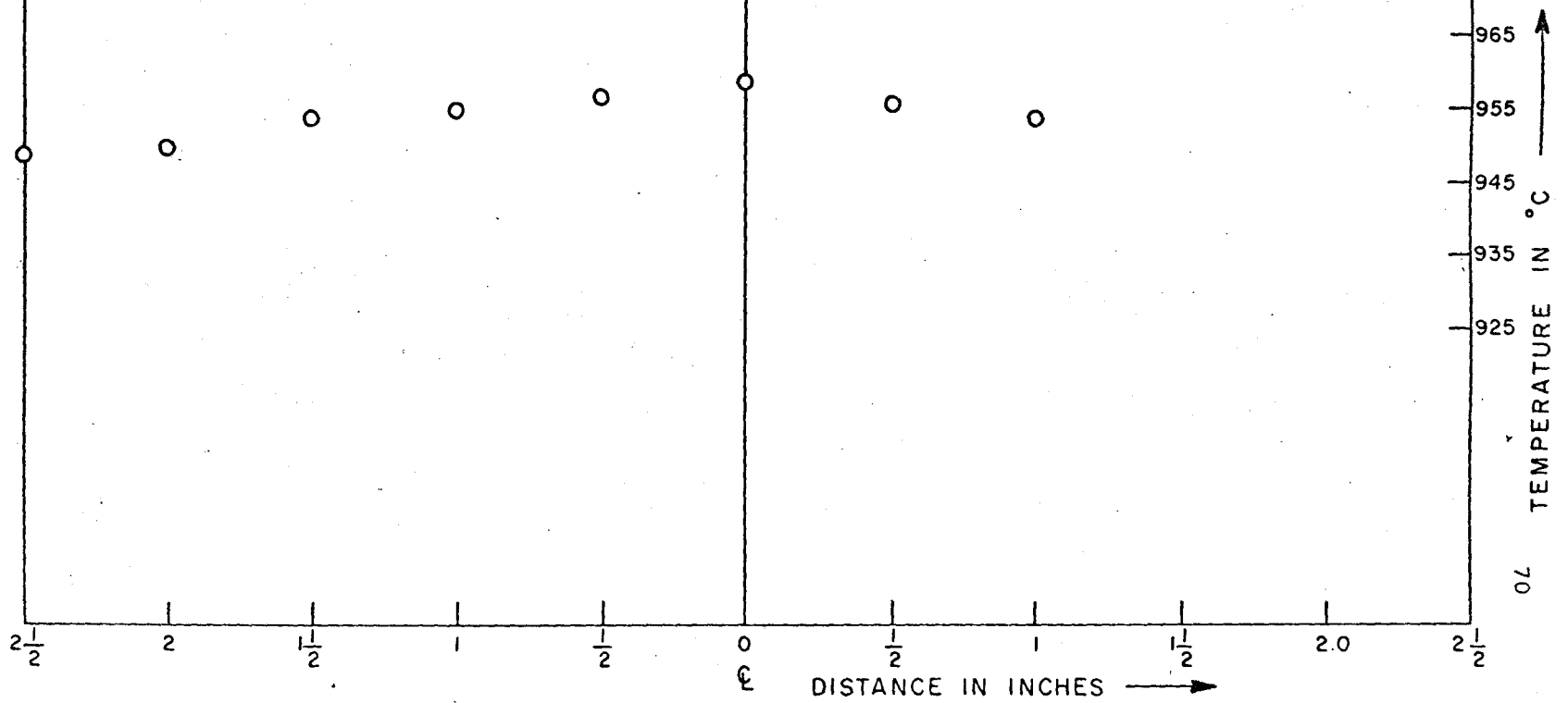


Fig. IV-3.4

Fig. IV-3.5

Details of High Vacuum Annealing Furnace

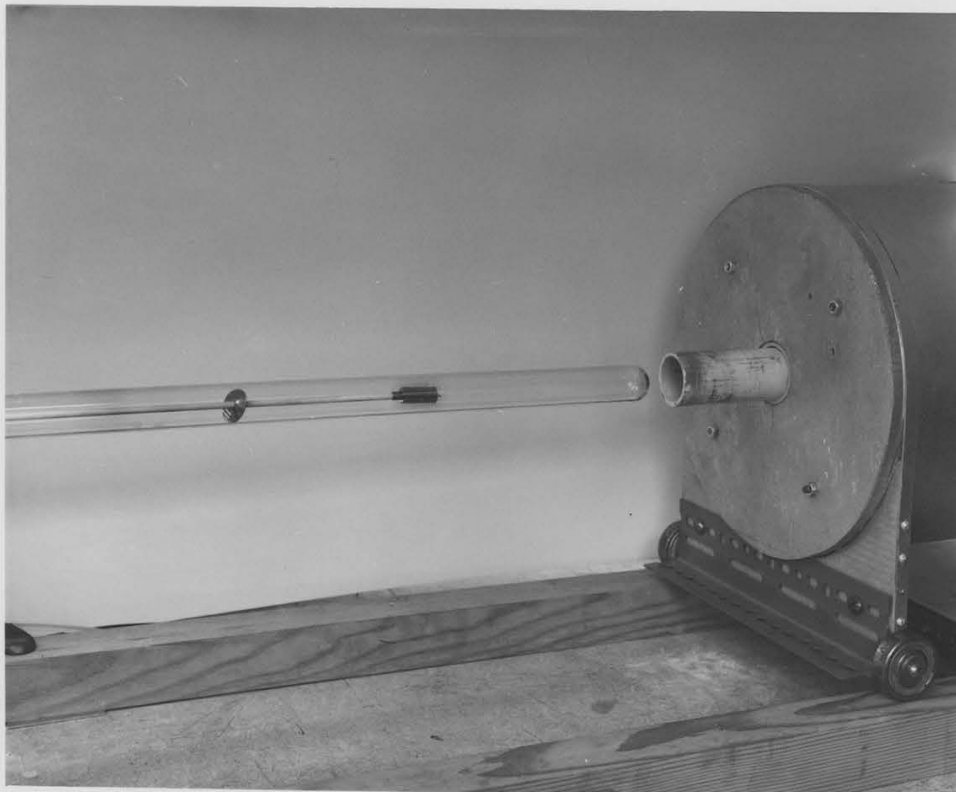
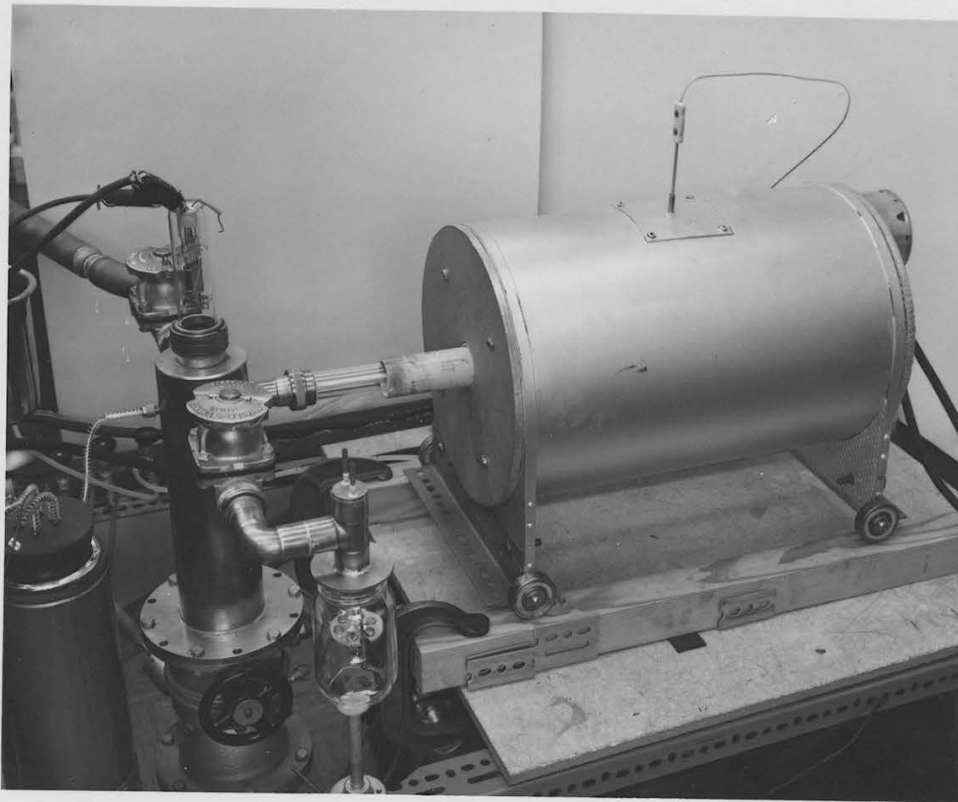


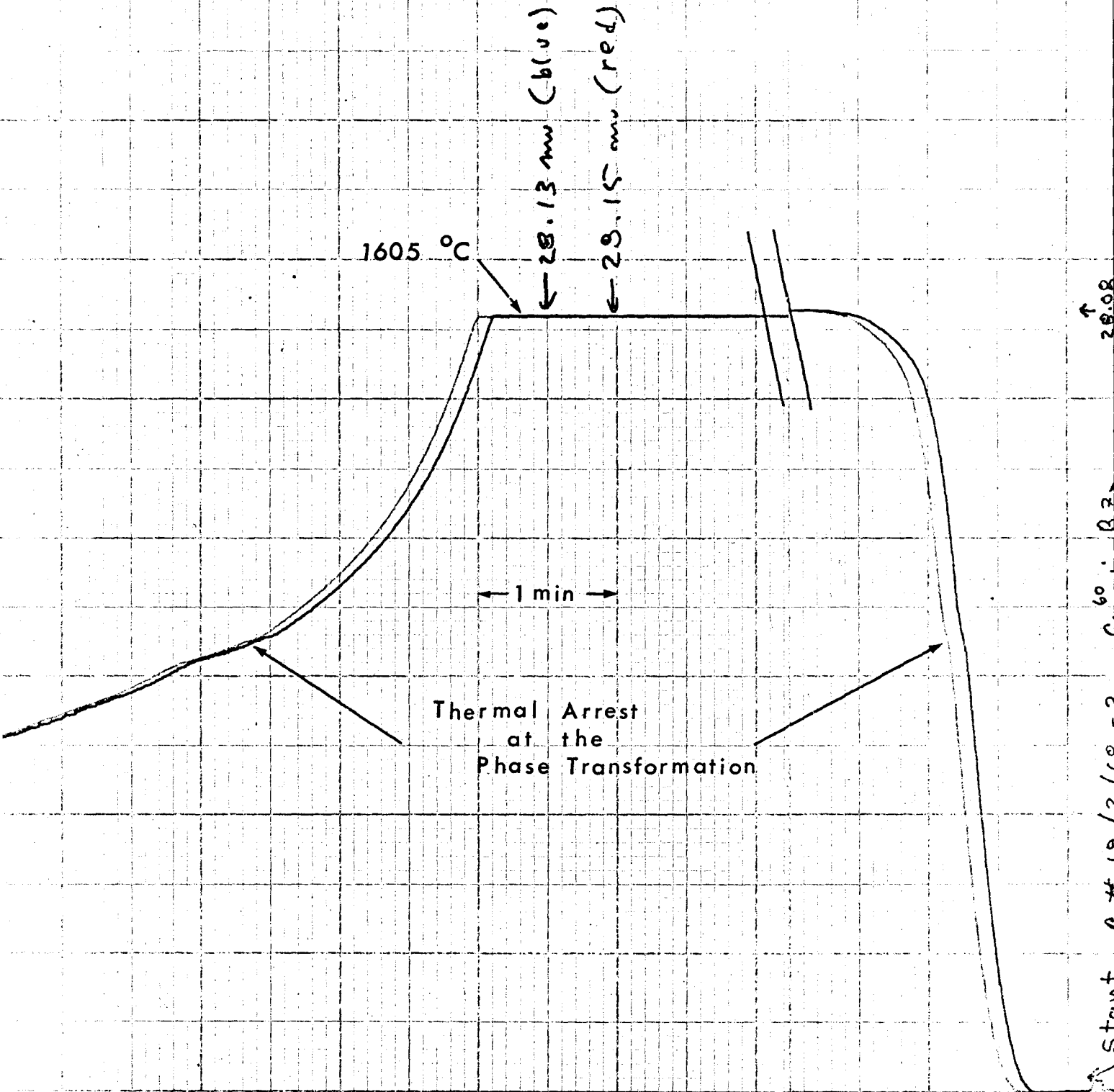
Fig. IV-3.6

Overall View of High Vacuum Annealing Furnace



Figure IV-3.7

Heating and Cooling Curve
in the High Temperature
Annealing Furnace



Following the diffusion anneal the specimens were mounted on a brass holder, using a high strength epoxy cement. The holder was identified by both the specimen and the run numbers* and then screwed to an adjustable ball and socket unit shown in figure IV-4.1.

This assembly was clamped in a four-jaw chuck on a precision lathe. The orientation of the specimen was carefully adjusted so that its surface was perpendicular to the lathe axis while its side was parallel. Although the former adjustment was sometimes made difficult by surface rumpling produced during the $\beta \rightarrow \alpha$ martensitic phase transformation, it could always be made accurate to ± 0.002 ", and frequently to ± 0.0005 ". The adjustment of the shoulder was less critical, but was usually within ± 0.002 ".

The specimen diameter was then reduced by about 0.100 inches to remove any contributions from diffusion along the specimen sides and hence into the bulk. The final diameter was carefully measured and recorded.

A transparent lucite chip collector was mounted on the lathe so that the specimen and cutting tool for removing sections were completely enclosed. This ensured that 100% of the chips were collected into pre-weighed, numbered bottles, screwed into the bottom of the plastic unit. The set-up is shown in figure IV-4.2. In most runs, a total of

* For example, if specimen #32 was used in the first run on the tenth day of the sixth month of 1967, the holder was stamped with R 10/6/67-1, Spec. 32.

40 slices was taken, the following being a typical set of nominal thicknesses: from 1-5, 0.001"; 6-15, 0.002"; and 16-40, 0.003".

The bottles were then re-weighed, to obtain the net chip weight, W_j , per slice. The slice thickness t_j was calculated from the chip weight W_j , the specimen diameter d and the zirconium density ρ , using

$$t_j = 4W_j / \rho d^2 \pi \quad \text{IV-4.1}$$

W_j was measured to ± 20 μ gms, and d to $\pm 1.27 \times 10^{-3}$ cm. The mid-point x_j of a slice, as measured from the surface, was then calculated from

$$x_j = t_j/2 + \sum_{i=1}^{j-1} t_i \quad \text{IV-4.2}$$

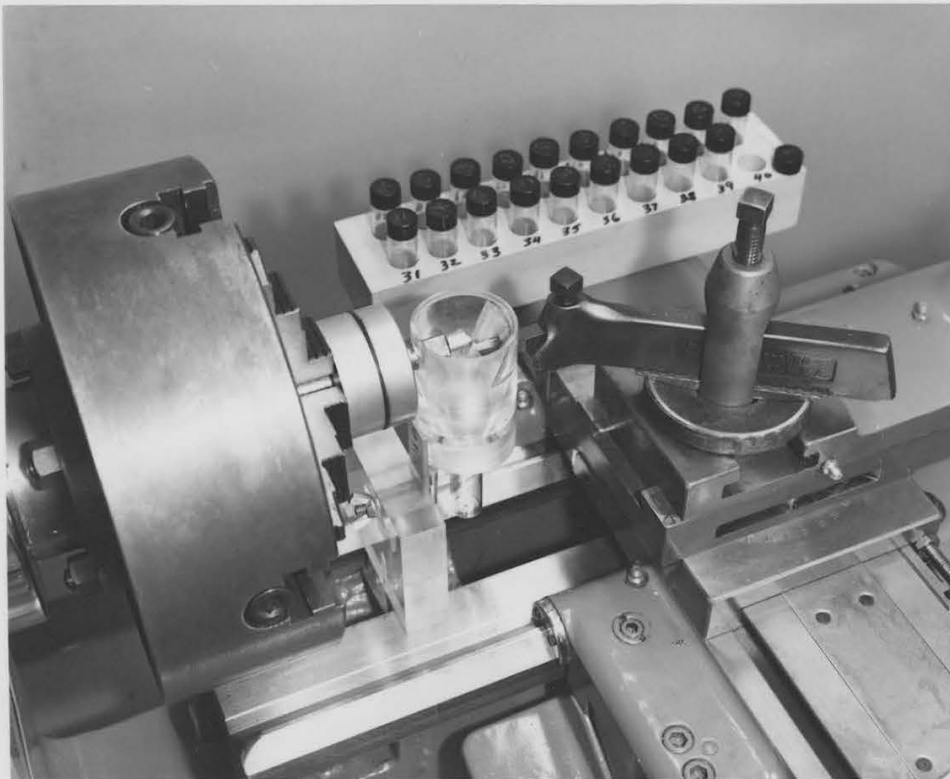
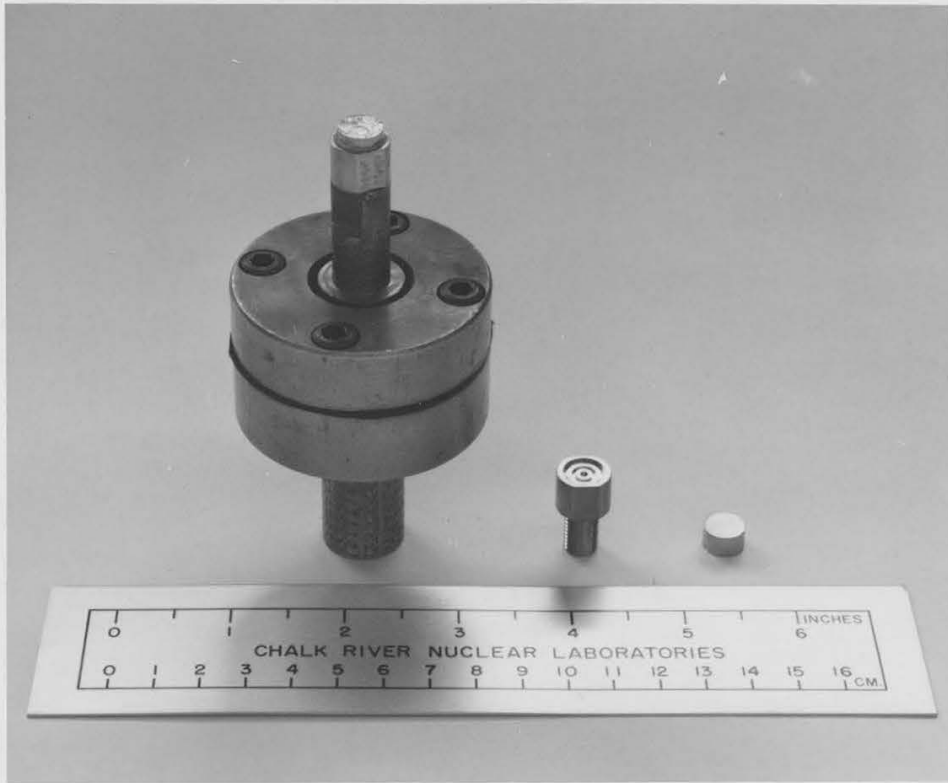
and hence x_j^2 and $x_j^{6/5}$. These calculations were done on a PDP8/S computer.

Fig. IV-4.1

Specimen on Adjustable Holder

Fig. IV-4.2

Lathe Sectioning Set-up



The concentration profiles were determined from measurements of the specific gamma ray activities of the slices. To provide a well defined and constant geometry for the γ -counting, the specimen chips were dissolved by adding 2 mls. of the chemical polishing solution to each bottle.

The activity measurements were made using facilities established in the Research Chemistry Branch at CRNL. A bottle of dissolved chips was centrally located by means of a lucite plate, on the surface of a 3" x 3" thallium activated, sodium iodide scintillation crystal. This was optically coupled to a photomultiplier tube and the assembly housed in a large lead shielding box, measuring 32" x 32" x 32" inside and having 4" thick walls.

The light pulses, produced by interaction between the γ -photons and the NaI crystal, were converted to charge pulses and amplified in the photomultiplier tube. These in turn were converted to voltage pulses, amplified and fed to the input of the pulse-height analyser. Here they were registered in 1 of a 100 channels, according to the size of the voltage pulse. The latter was directly proportional to the energy of the γ -photon.

The data thus collected could be read-out either on punched tape or on a teletypewriter. Figure IV-5.2 shows the γ spectrum of ^{60}Co plotted on a linear scale of counts/channel vs. channel number. The two photo-peaks occur at

1.17 and 1.33 MeV respectively and are separated from the Compton Scattering plateau by a well-defined valley. By setting the bias and gain controls of the analyser so that most of the Compton plateau was cut off from the registered counts, the dead-time losses in the system were reduced and only the first 35 to 40 channels were required to be read-out.

In recording the gross number of counts in a given section, only those falling within the channels indicated in figure IV-5.2 were used, thereby reducing the background counts to those coinciding with this restricted energy range*.

The sequence of counting adopted, designed to reduce short-term systematic errors due to drift in the system, was as follows:

Bkgd. - Std - S₁ - S₃ - S₅ - S₇ - Bkgd. - Std - S₉ ...
 " " - S₂ - S₄ - S₆ - S₈ - " "

The gross section and standard counts were generally greater than 10,000, to keep random statistical errors to about ±1%. Background counts were taken over a time period comparable to that of an associated section count. Dead time losses were automatically registered as a percentage of the gross counts.

* Unfortunately, a background 1.29 MeV peak from ⁴¹A was sometimes present when the wind conditions created a downdraft from the reactor stacks. On such days, counting was discontinued.

The gross section counts were corrected for dead-time losses and background, reduced to counts/min/mgm and normalised by dividing by the net corrected standard count appropriate to the mid-time of the section count. This latter procedure corrected all counts for radioactive decay during the time of data collection. It served also to reduce errors due to drift or instability in the counting system.

Where appropriate, the data were processed during the counting period and plotted as \ln (specific activity) vs x^2 . Points obviously in error were rechecked immediately.

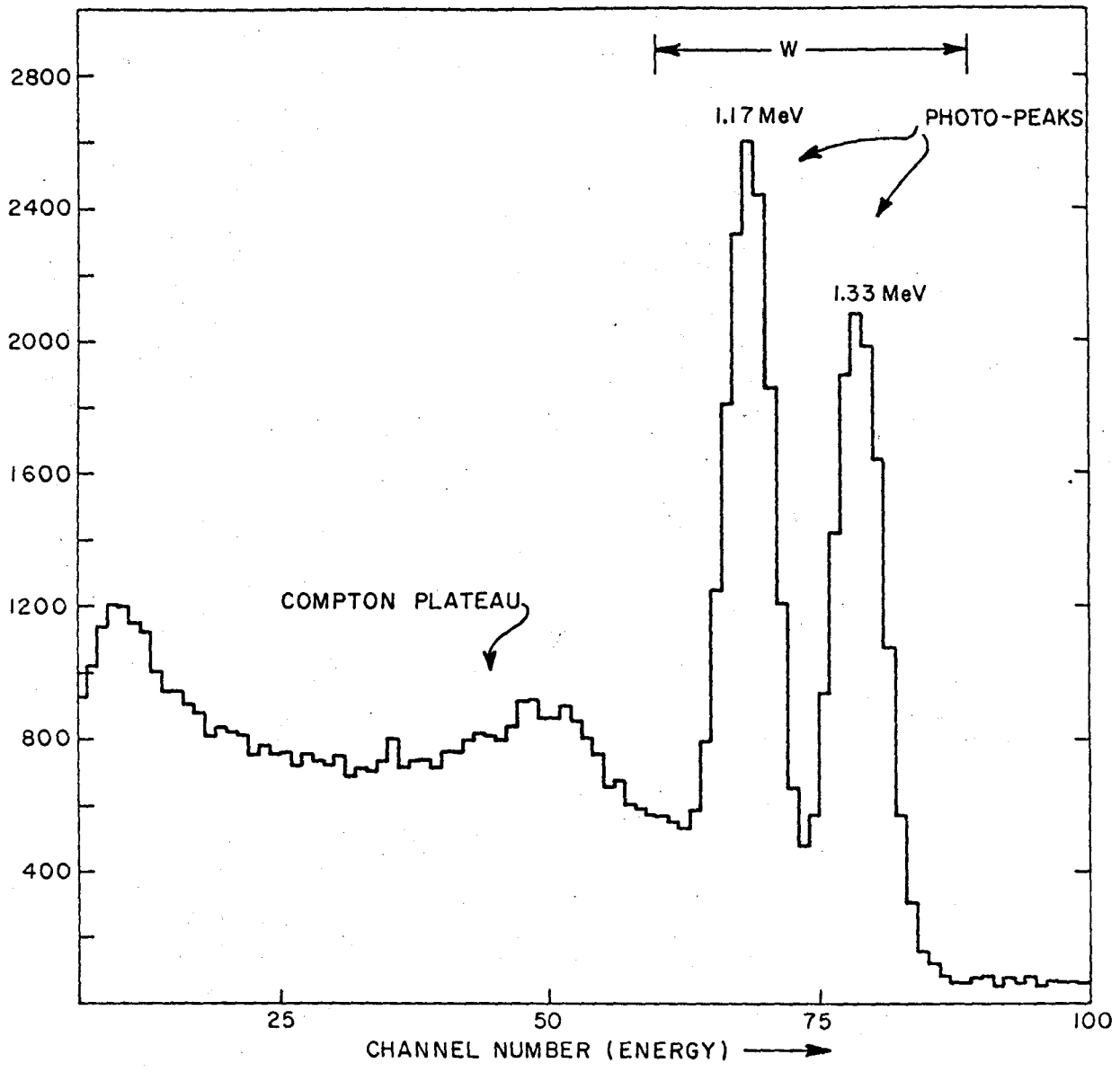


FIGURE IV-5.2
GAMMA RAY SPECTRUM OF ^{60}Co .

W INDICATES THE CHANNELS OVER WHICH
COUNTS WERE RECORDED

The diffusion of ^{60}Co in the β phase of pure zirconium was measured at temperatures ranging from 875 to 1700°C. The initial runs at 875 and 893°C for annealing times of 25 hr 40 min and 24 hr respectively, indicated that the diffusion rates were very much higher than anticipated from the work reported on solute diffusion in β Ti⁽⁵⁴⁾. The concentration profiles are shown in figure V-6.1 as $\log C$ vs x^2 .

The annealing times of subsequent runs were reduced to less than 3 hours and the results plotted in the form $\log C$ vs x^2 on the assumption that they could properly be represented by equation II-1.1. It was evident, however, that marked and consistent departures from this relation occurred for points near the surface and, in some cases, in the regions of deepest penetration as well. The origin and significance of these departures are believed to be understood and will be discussed more fully in chapter V.

The remaining points, for which equation II-1.1 did appear to apply, were treated by a least squares analysis, assuming that both the C and x^2 values were liable to error. Figures IV-6.2 to IV-6.16 show the experimental results plotted as $\log C$ vs x^2 , the line of best fit through them, the slope of the curve and the accuracy of the slopes. The statistical treatment of the data and the method of estimating maximum errors in the measurements are discussed in appendix III. The points indicated by the closed circles in the figures are those omitted from the least squares analysis.

It will be noted that in general the extent of the departures from the linear relation between $\log C$ and x^2 was most pronounced in the lower temperatures runs.

Below 1000°C the specimens were annealed in pairs in the roll-on furnace. In several cases samples were deliberately selected with different metallurgical conditions in order to check the sensitivity of the results to this factor. The specific histories of the specimens are indicated in the figures and the significance of any differences noted in their behaviour will be discussed in chapter V.

The diffusion coefficients, corrected for heat-up and cooling times are plotted as $\log D$ vs $1/T$ in figure IV-6.17.

Fig. IV-6.6

R# 4/8/67-1

Spec.# 7

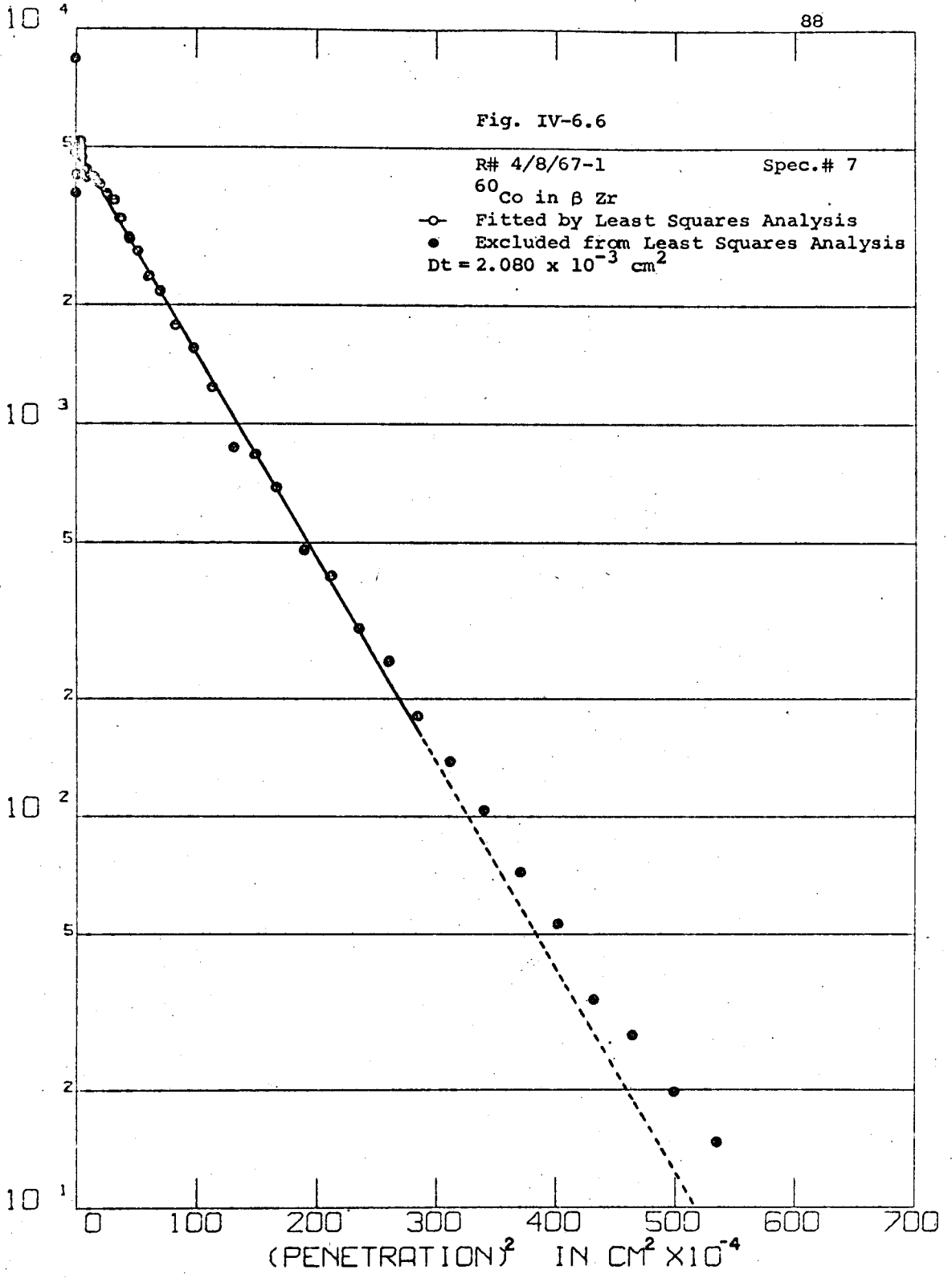
⁶⁰Co in β Zr

○ Fitted by Least Squares Analysis

● Excluded from Least Squares Analysis

Dt = 2.080 x 10⁻³ cm²

(CONCENTRATION) IN ARBITRARY UNITS



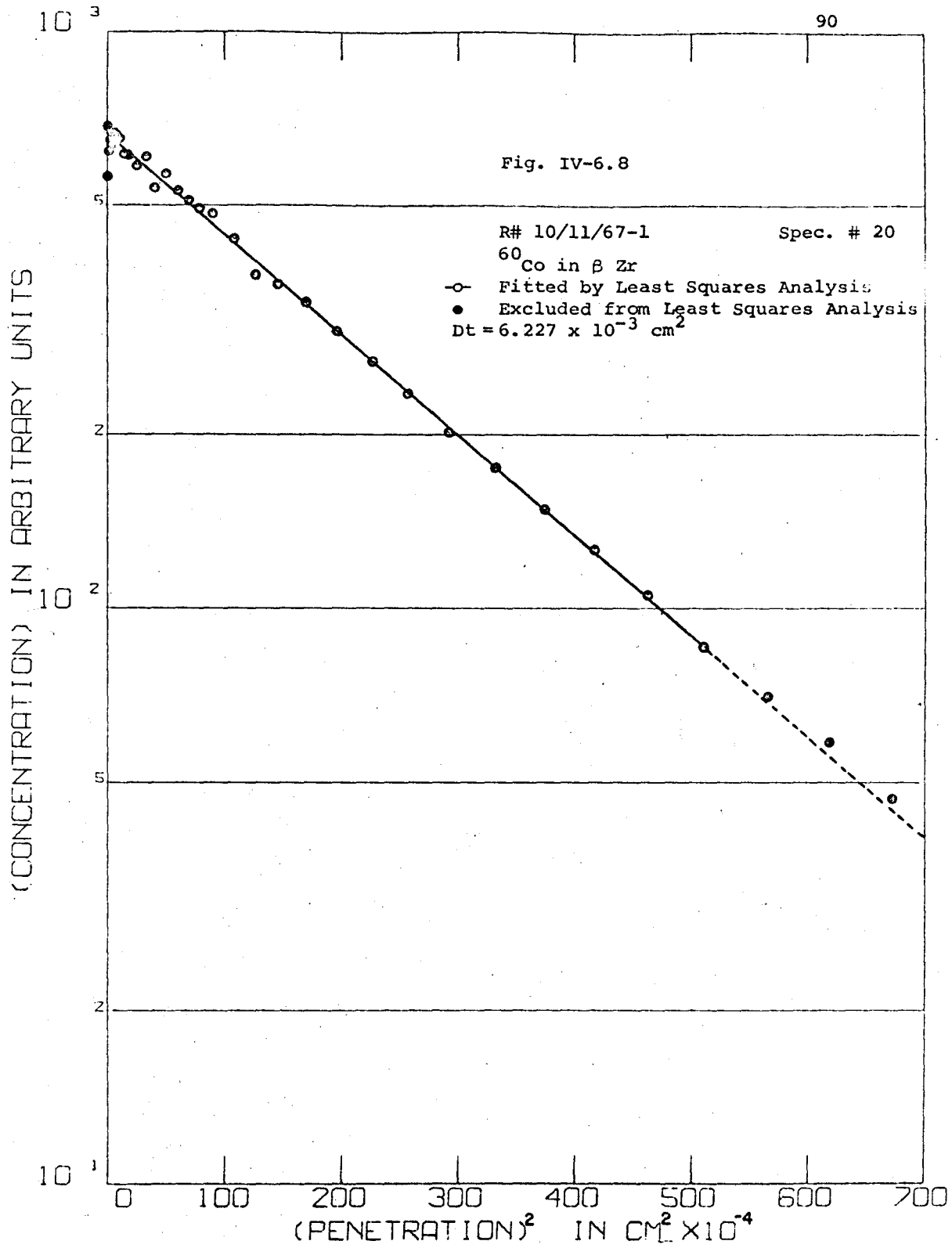
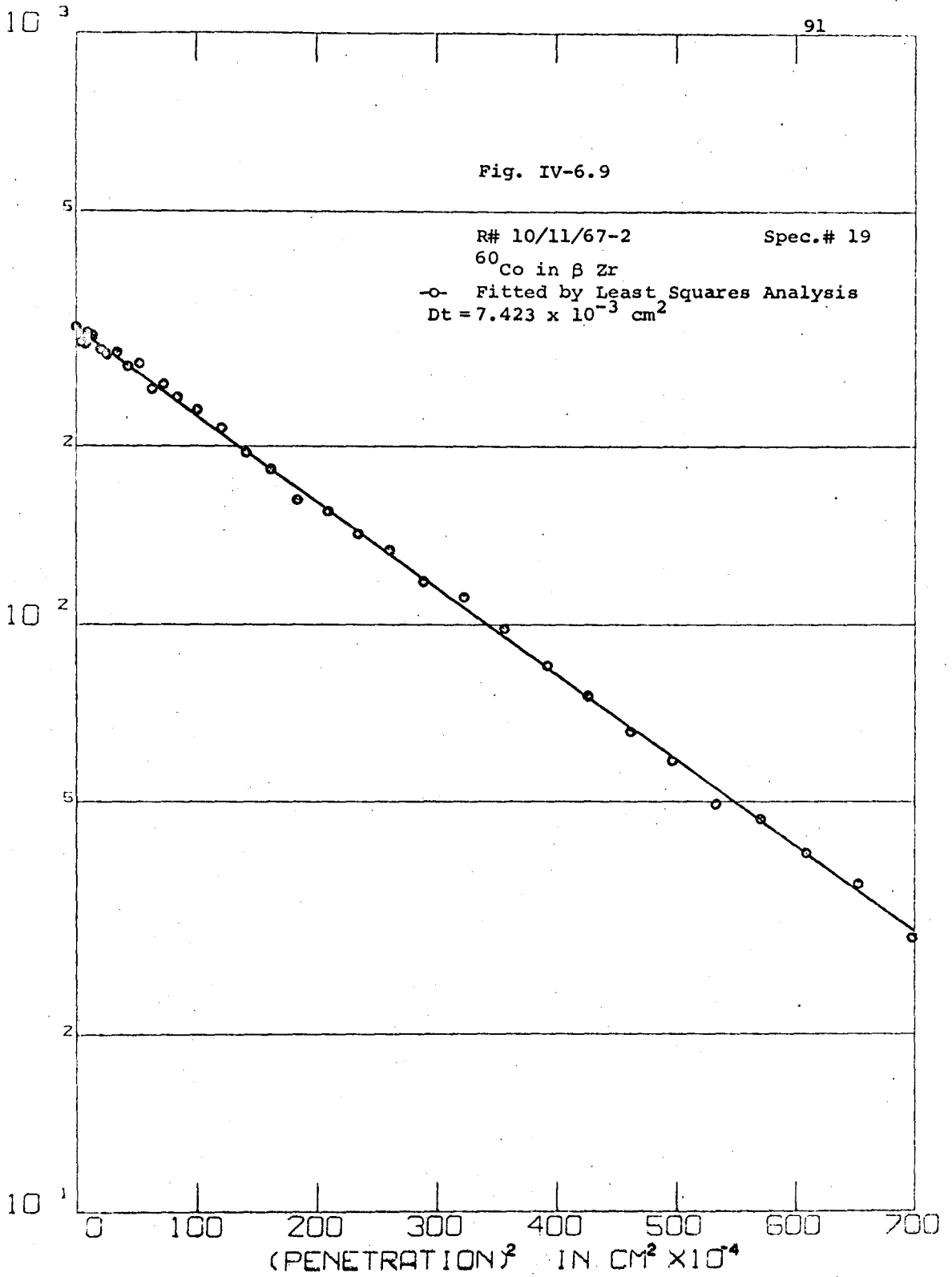


Fig. IV-6.9

(CONCENTRATION) IN ARBITRARY UNITS



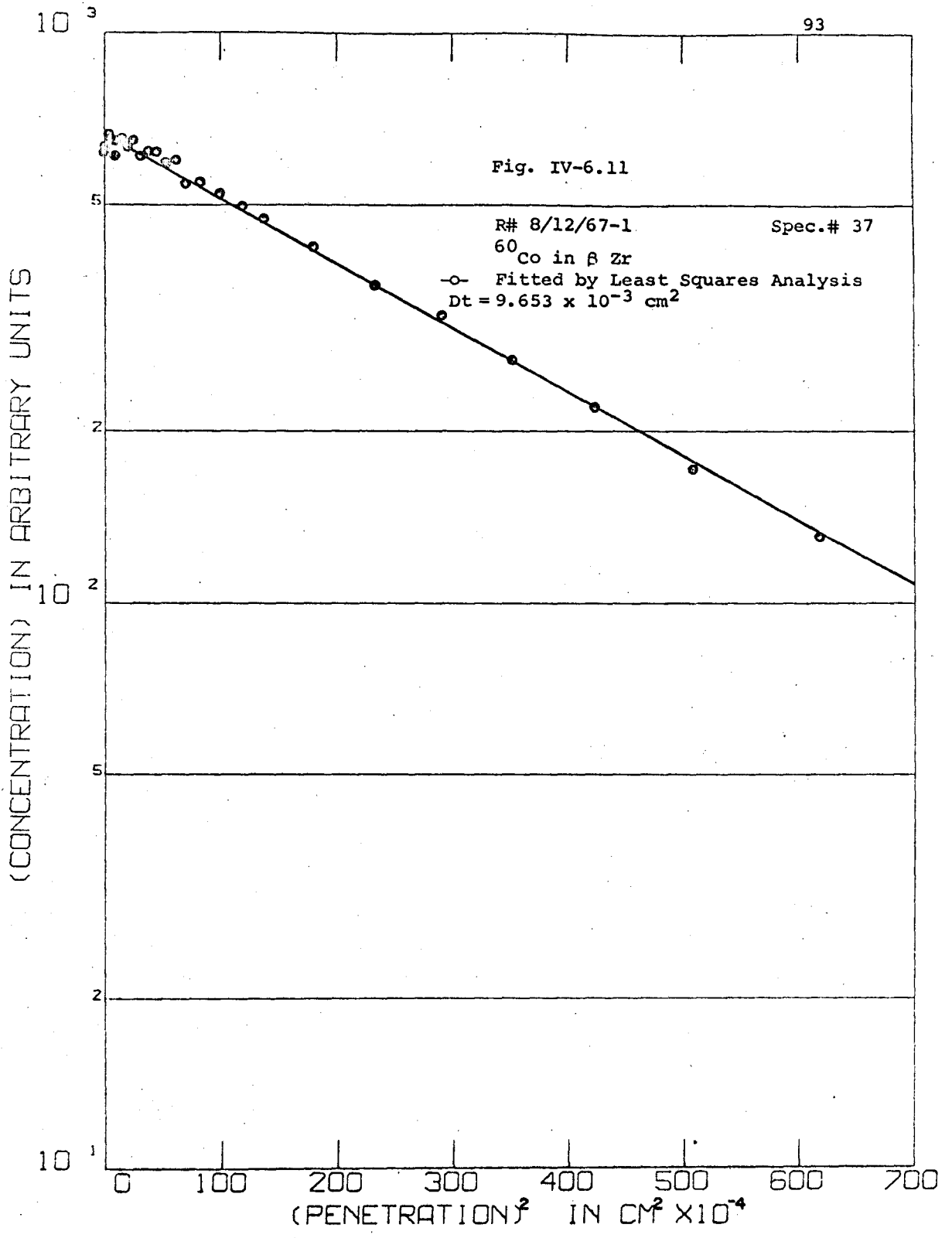
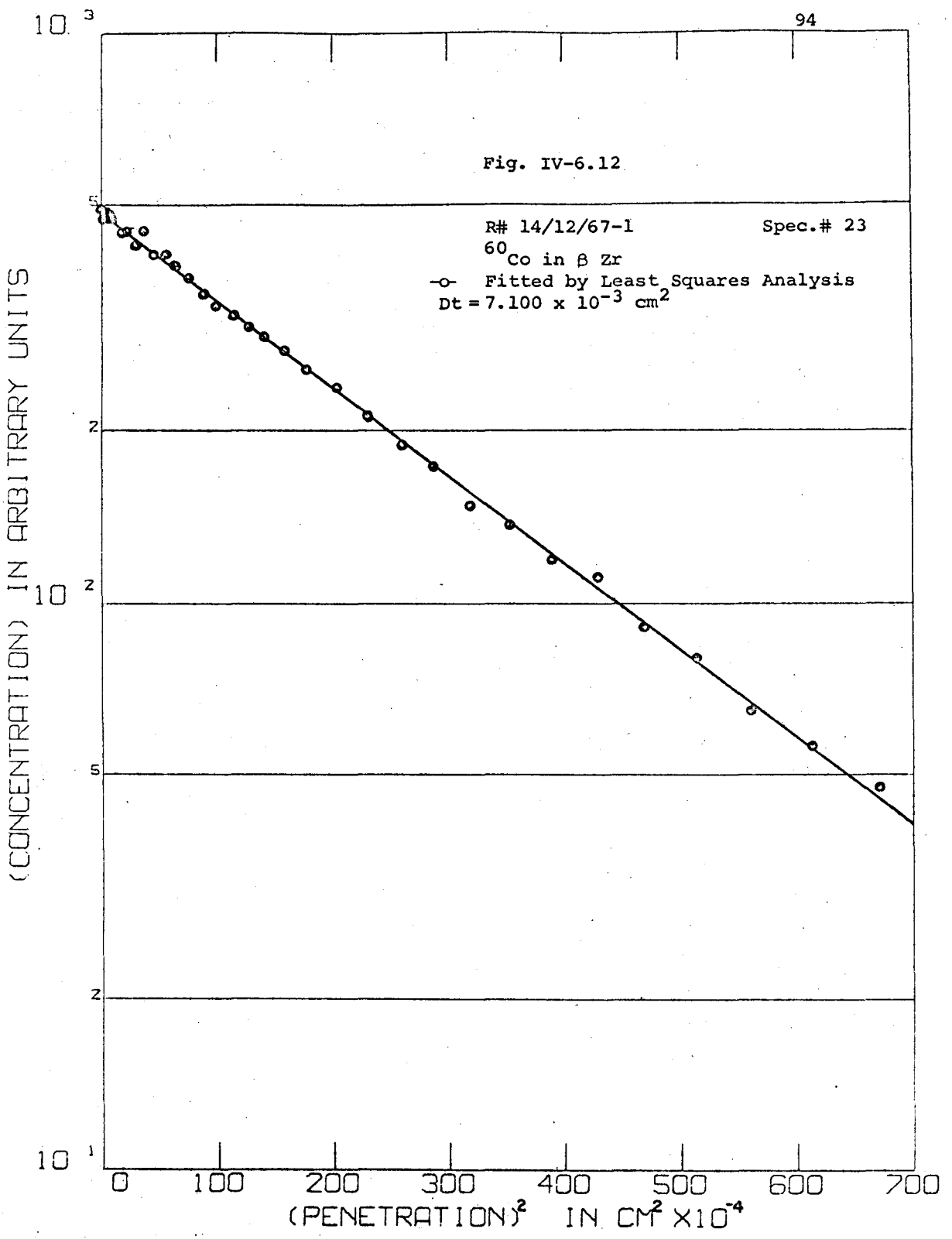
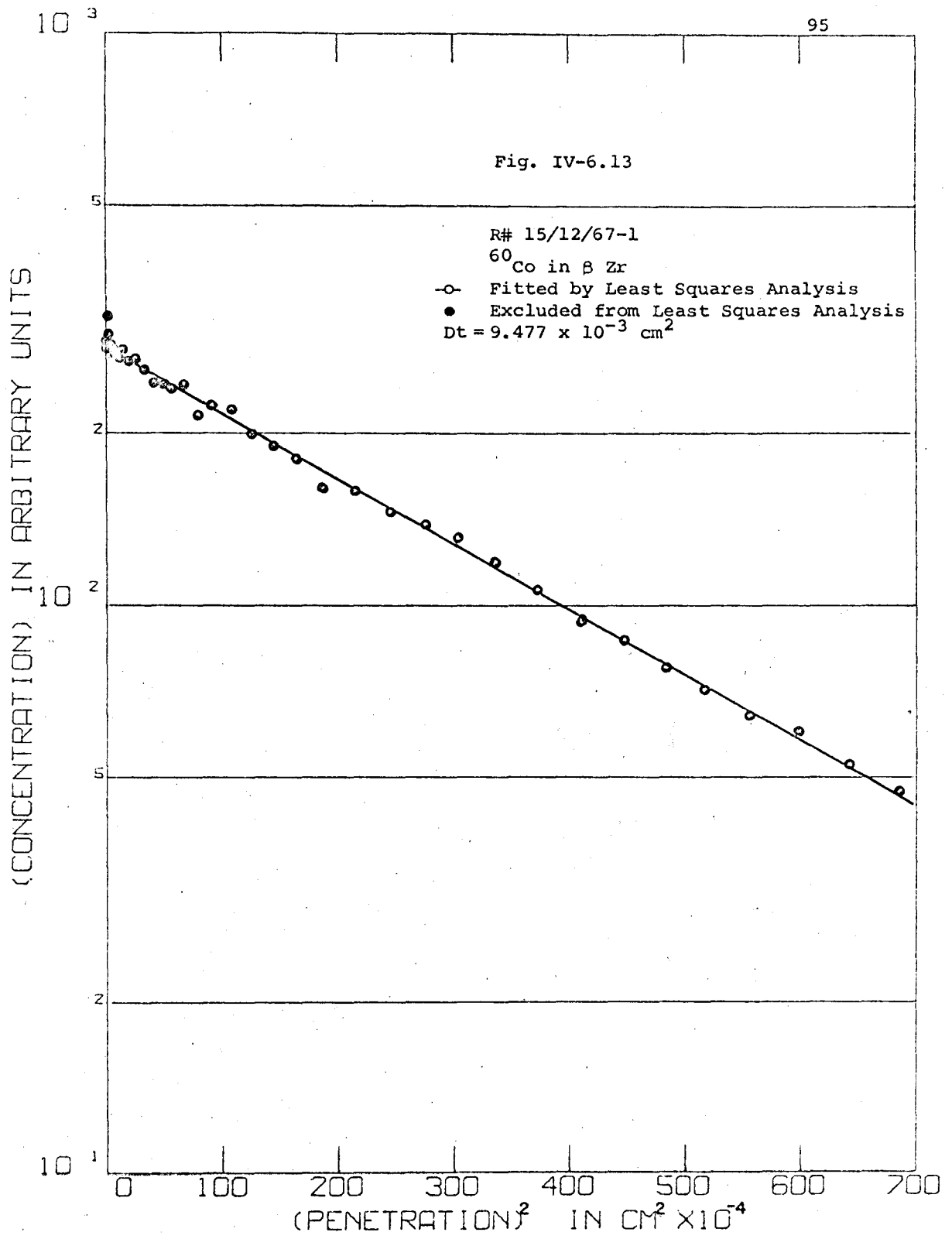
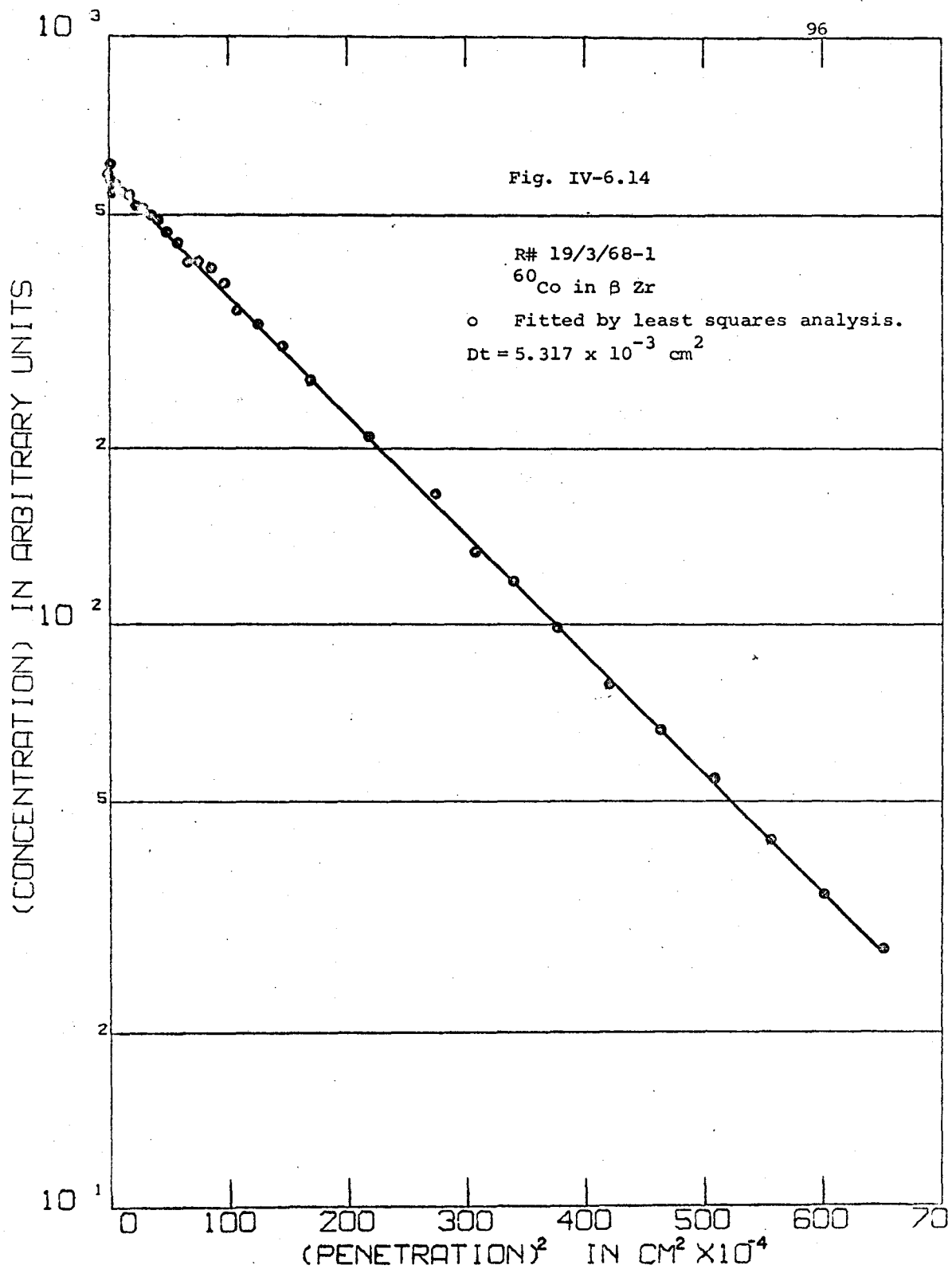


Fig. IV-6.12







10³

97

Fig. IV-6.15

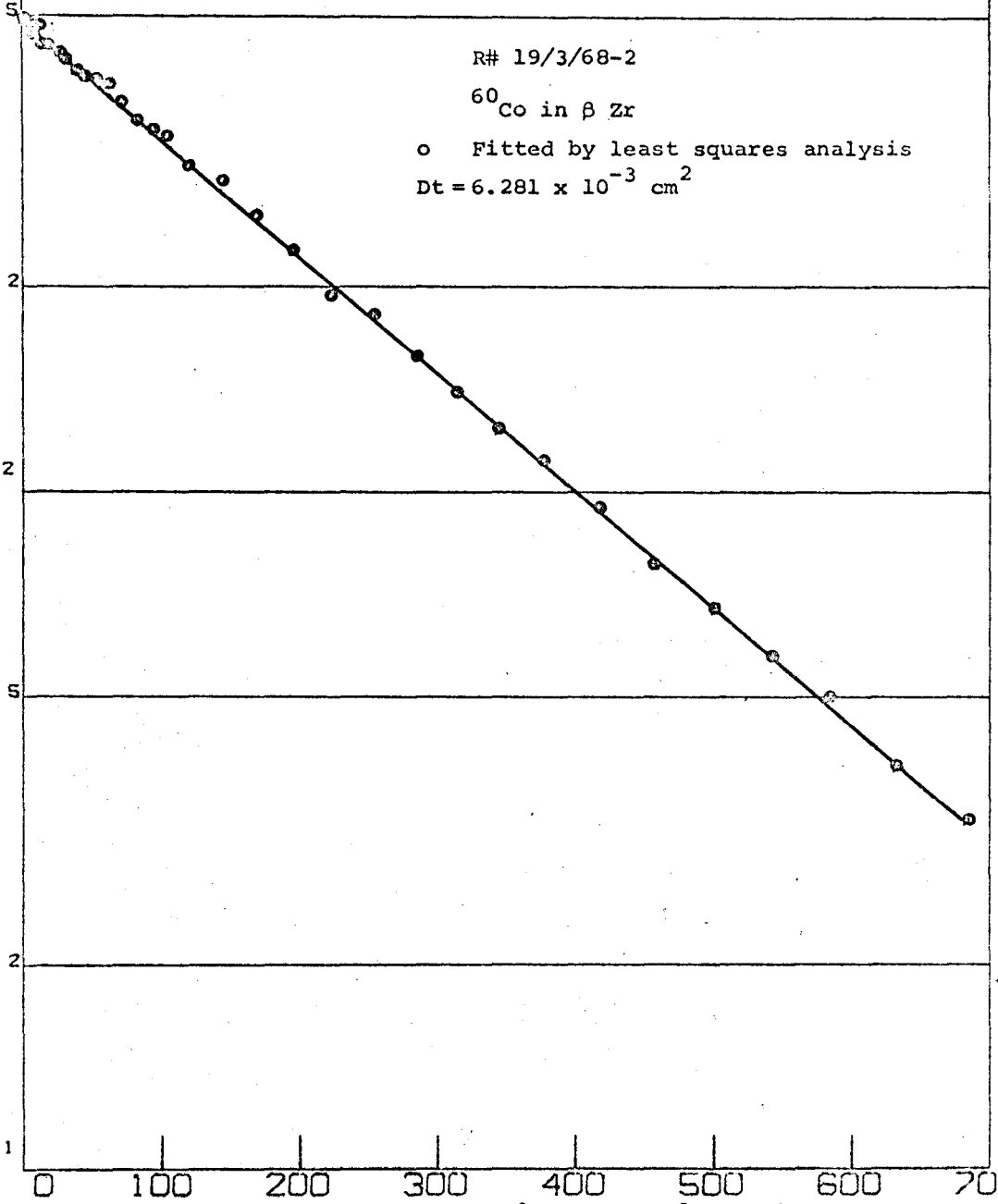
(CONCENTRATION) IN ARBITRARY UNITS

R# 19/3/68-2

⁶⁰Co in β Zr

o Fitted by least squares analysis

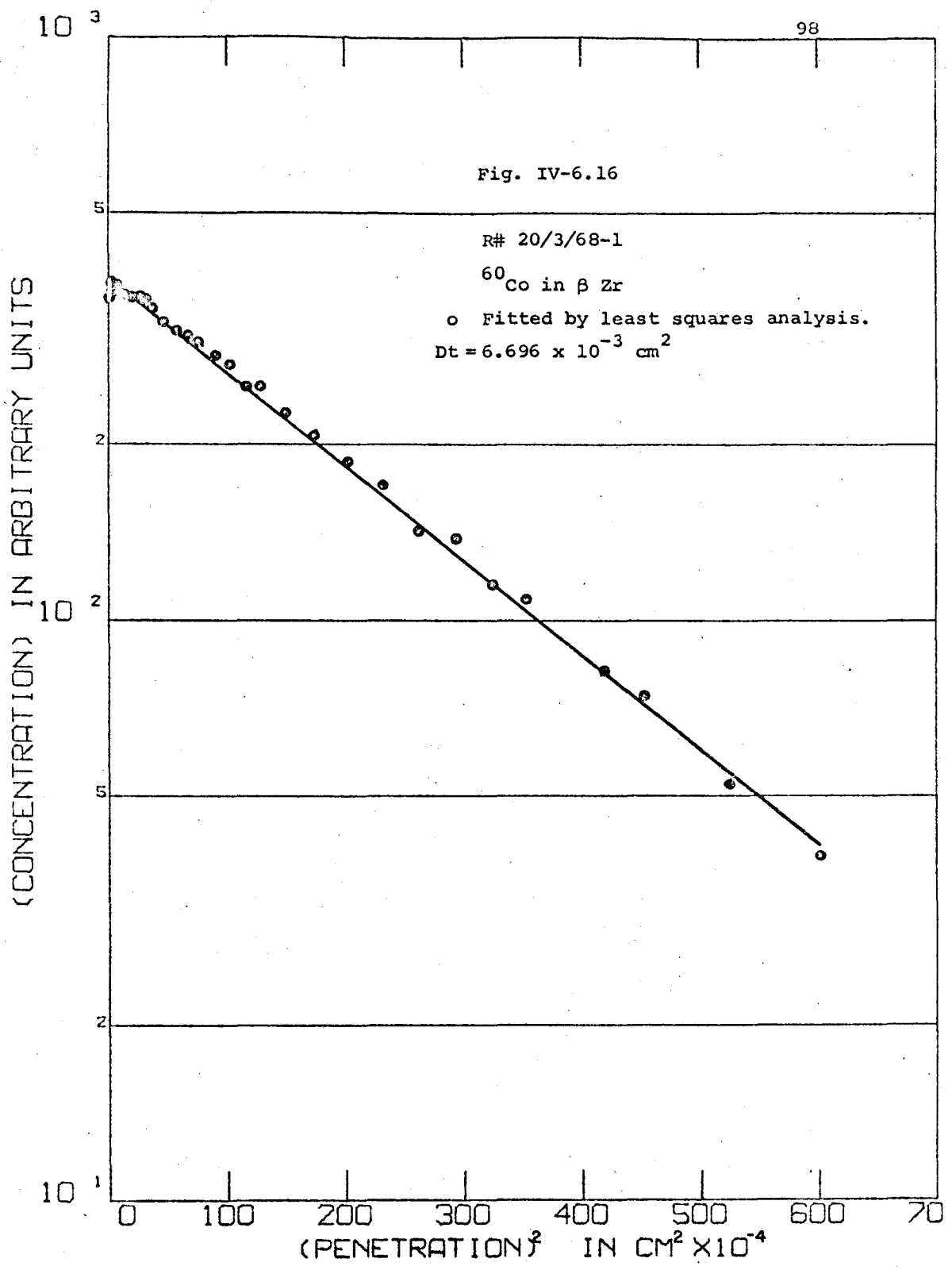
Dt = 6.281 x 10⁻³ cm²

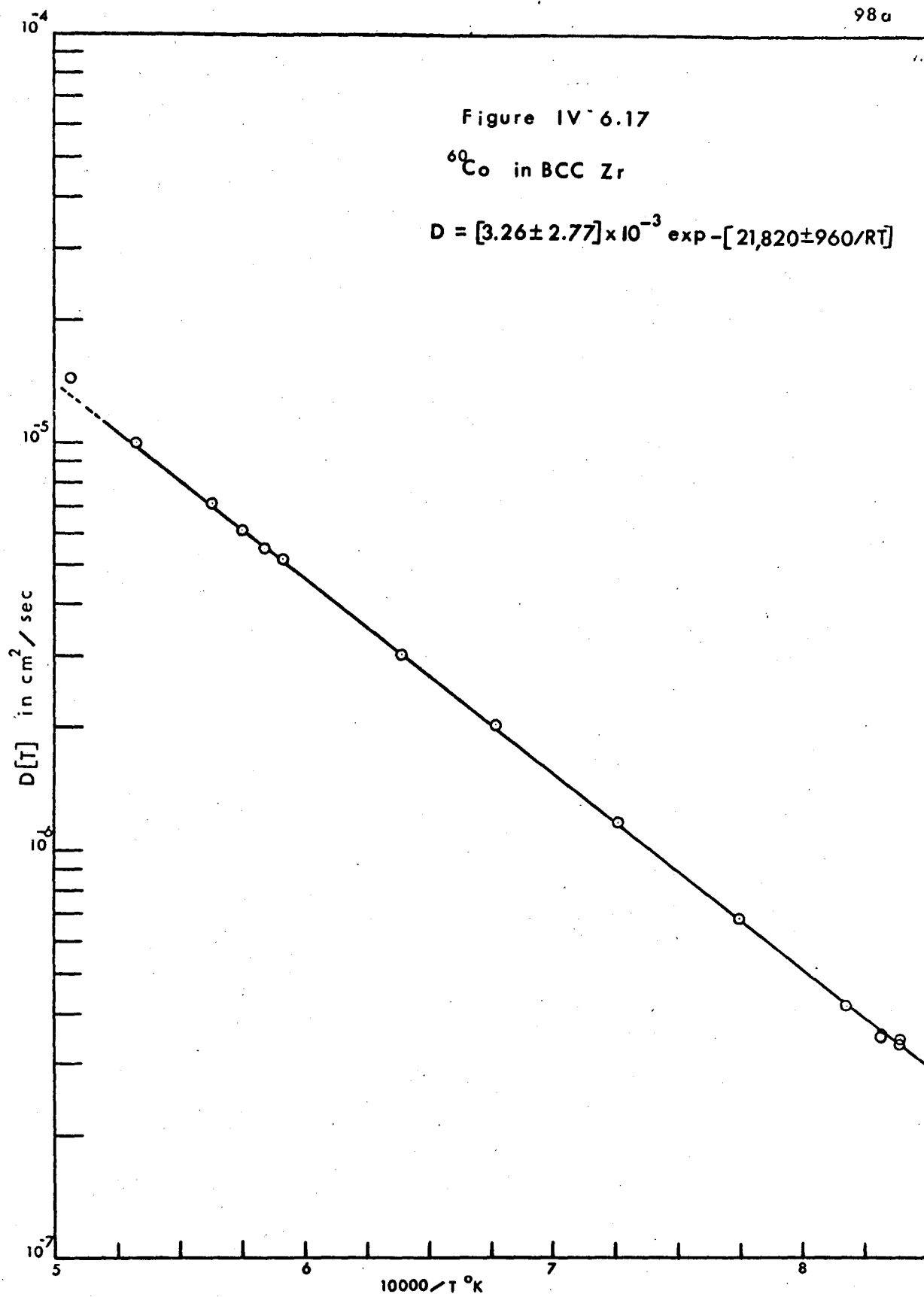


10¹

(PENETRATION)² IN CM² X 10⁻⁴

Fig. IV-6.16





IV-7 THE DIFFUSION OF ^{95}Zr IN DILUTE Zr-Co ALLOYS

A thin layer of the radioactive tracer isotope ^{95}Zr was evaporated onto a group of specimens prepared from the dilute Zr-Co alloy rods. The specimens were then assembled in a zirconium annealing capsule as indicated in figure IV-7.1. The capsule, attached to the thermocouple insulator tube of the roll-on furnace, was positioned so as to minimize temperature differences along its length during annealing*. The specimens were annealed together at 933°C for 2 days in a vacuum of 2×10^{-6} torr, removed and analysed as outlined in IV-6.

The results are shown in figs. IV-7.2, 7.8. In table V-7.1, ratios are given of the diffusion coefficients of ^{95}Zr in the alloys to those in the adjacent pure zirconium specimen.

The individual self diffusion results agreed with one another within experimental error, and within 8% with those reported by Lundy and Federer⁽⁴⁸⁾.

* Previous calibration of the furnace indicated a maximum difference of ± 3 °C for a central temperature of 960°C.

TABLE IV-7.1

RATIO OF SOLVENT DIFFUSION COEFFICIENT IN THE ALLOYS
TO SOLVENT DIFFUSION COEFFICIENT IN THE PURE METAL

<u>Nominal Composition at.%</u>	<u>Actual Composition at.%</u>	<u>Measured Dt</u>	<u>Ratio</u>
0.00 (A)		1.7238 x 10 ⁻⁴	
0.00 (J)		1.6860 x "	
0.4	0.395	1.6346 x "	0.948
0.80	0.74 ₇	2.2553 x "	1.3228
1.20	1.22	2.8440 x "	1.668
1.60	1.61	3.6136 x "	2.1433
2.00	1.99 ₅	3.7495 x "	2.2239

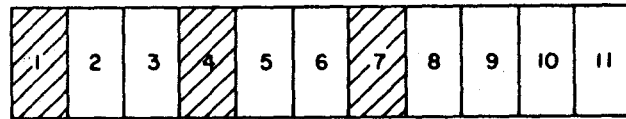


FIGURE V-7.1(a) POSITIONS OF DIFFUSION SPECIMENS CUT FROM Zr-Co ALLOY RODS



USED IN DIFFUSION MEASUREMENTS



SENT FOR ANALYSIS OF Co AND O CONTENT

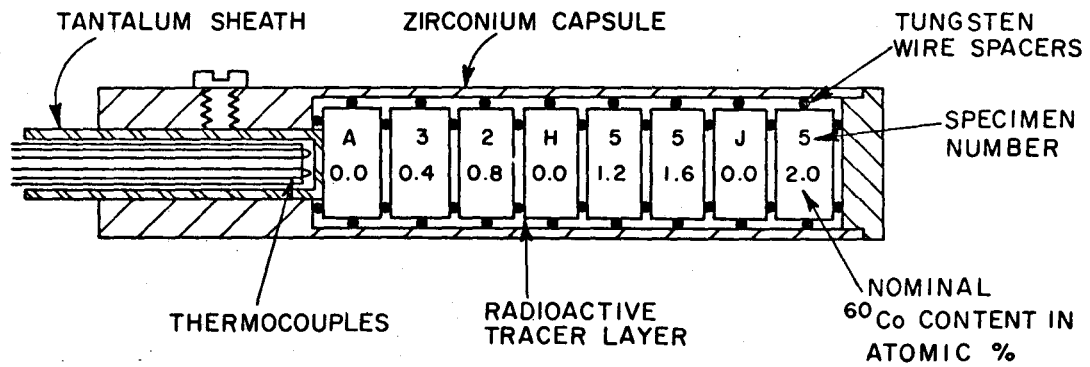
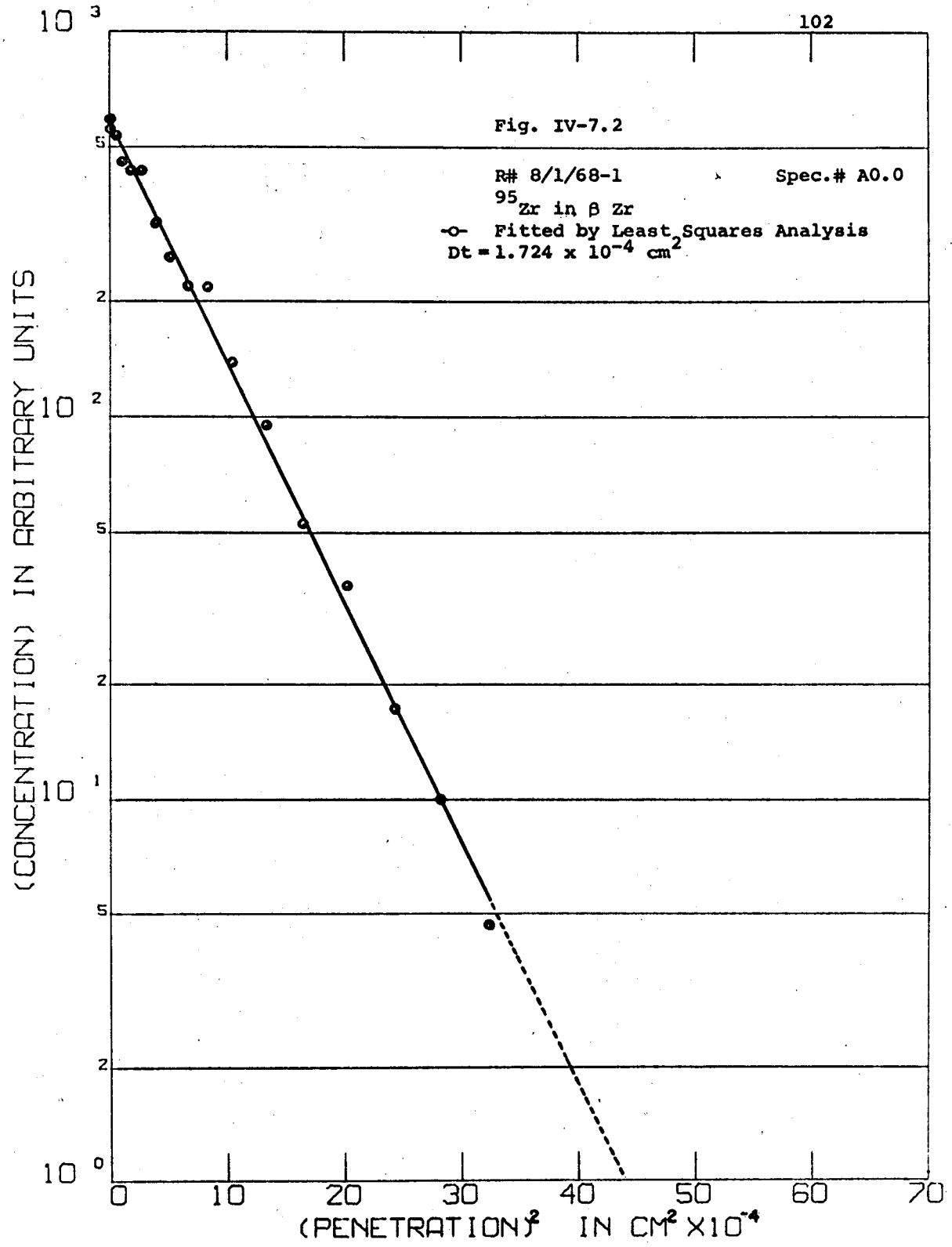
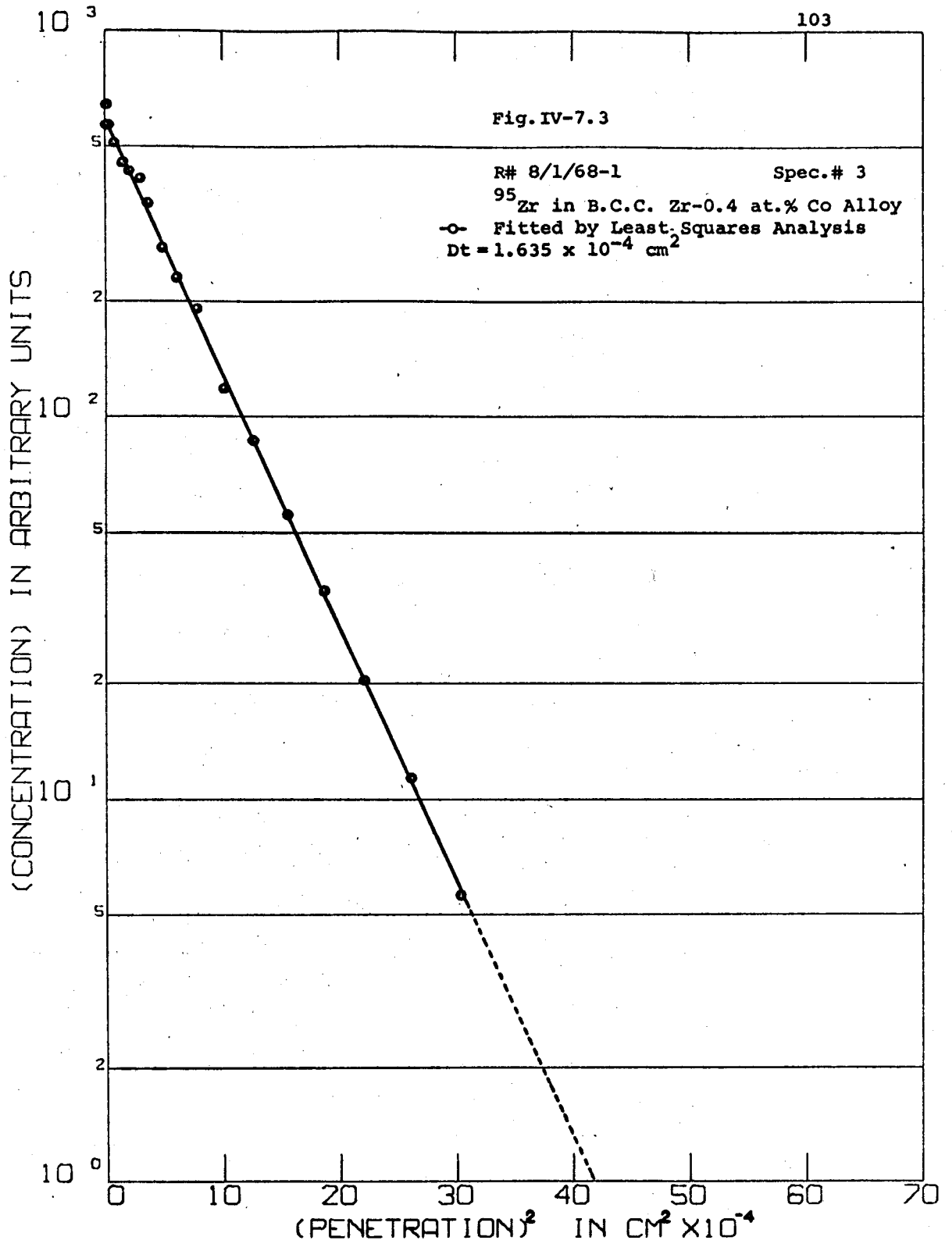
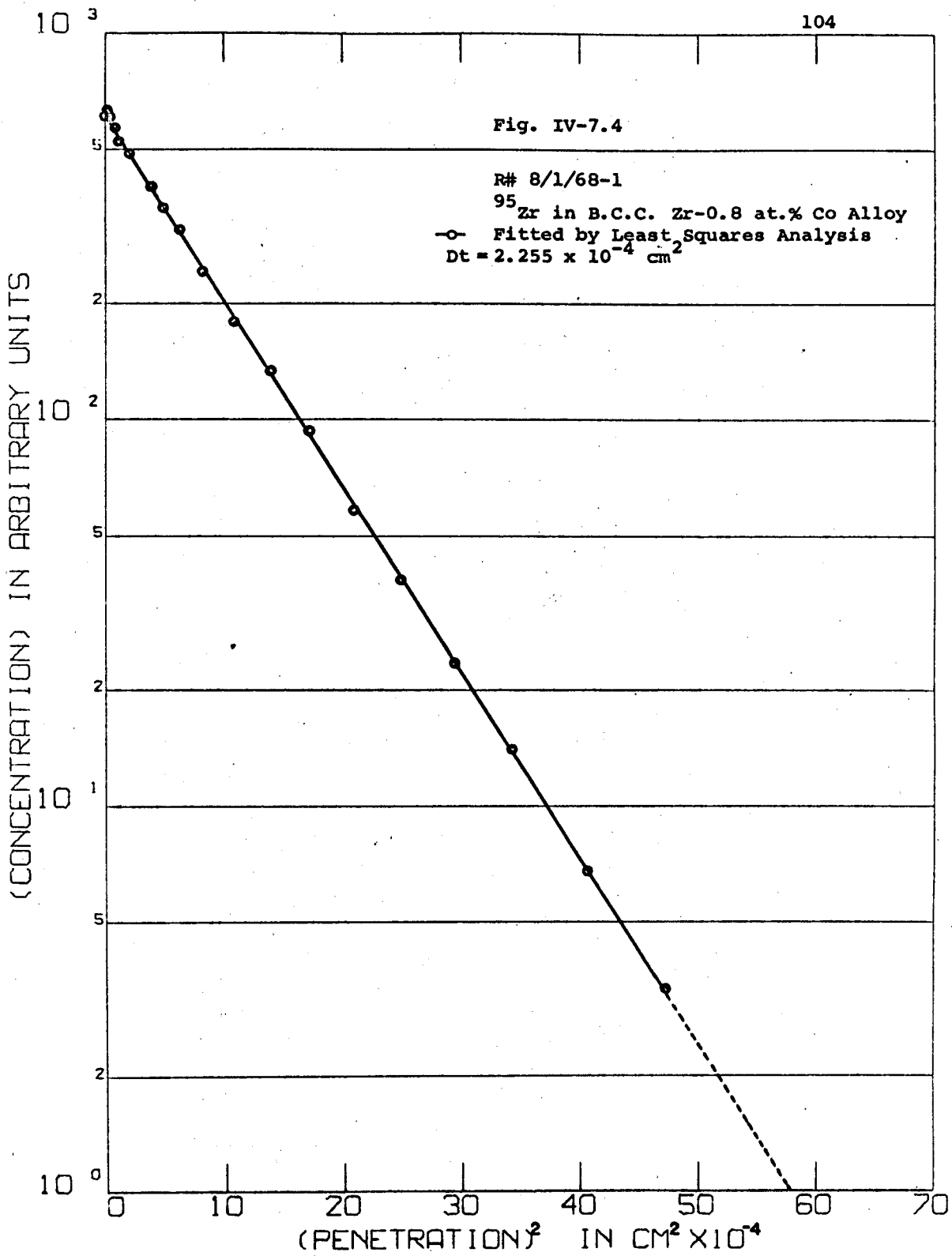


FIGURE V-7.1(b) ANNEALING CAPSULE FOR DIFFUSION OF ^{95}Zr IN DILUTE Zr-Co ALLOYS IN R# 8/1/68-1







10³

105

(CONCENTRATION) IN ARBITRARY UNITS

Fig. IV-7.5

R# 8/1/68-1

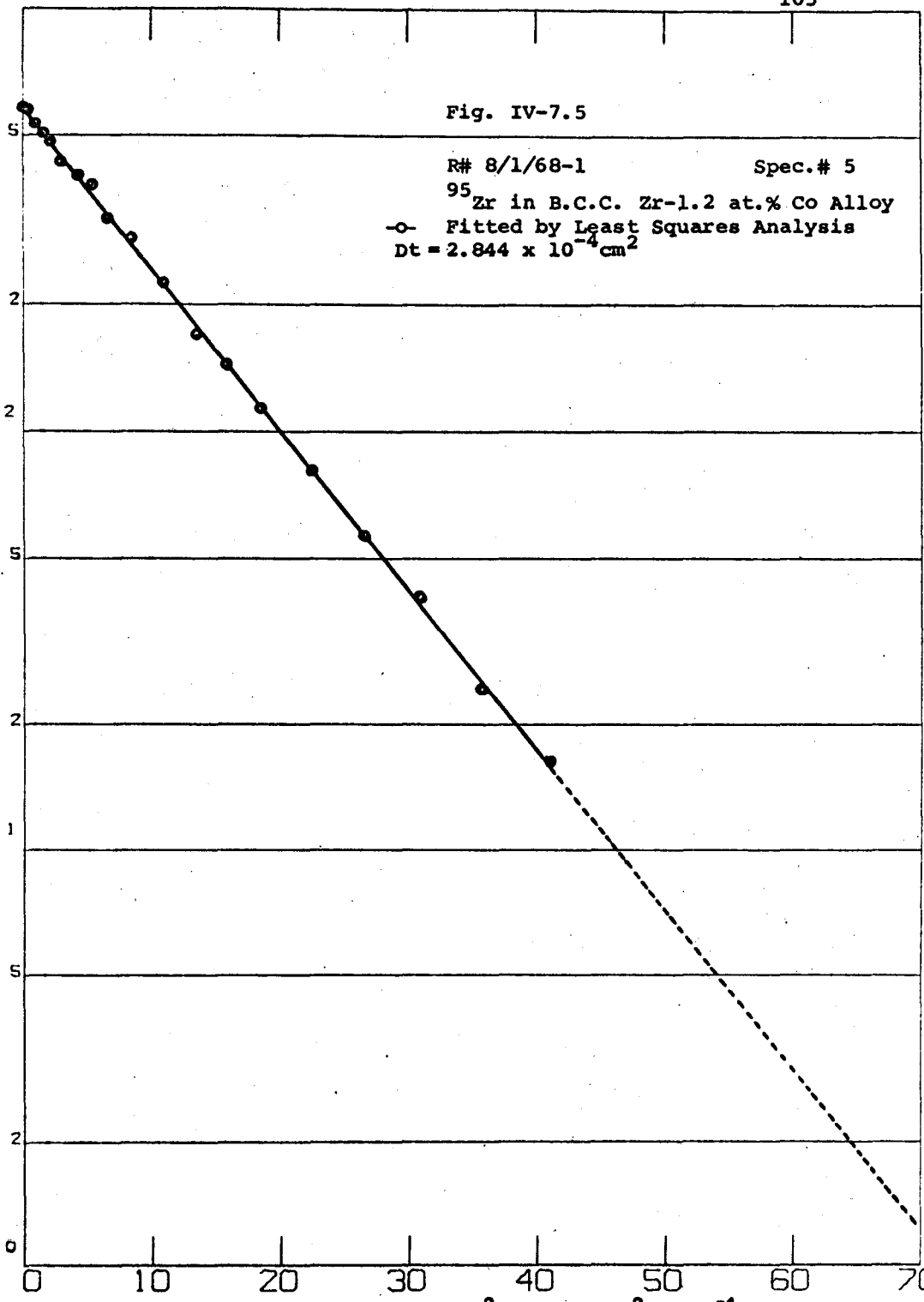
Spec.# 5

⁹⁵Zr in B.C.C. Zr-1.2 at.% Co Alloy

○ Fitted by Least Squares Analysis

Dt = 2.844 x 10⁻⁴ cm²

10²



10⁰

(PENETRATION)² IN CM² X 10⁻⁴

10³

Fig. IV-7.6

R# 8/1/68-1

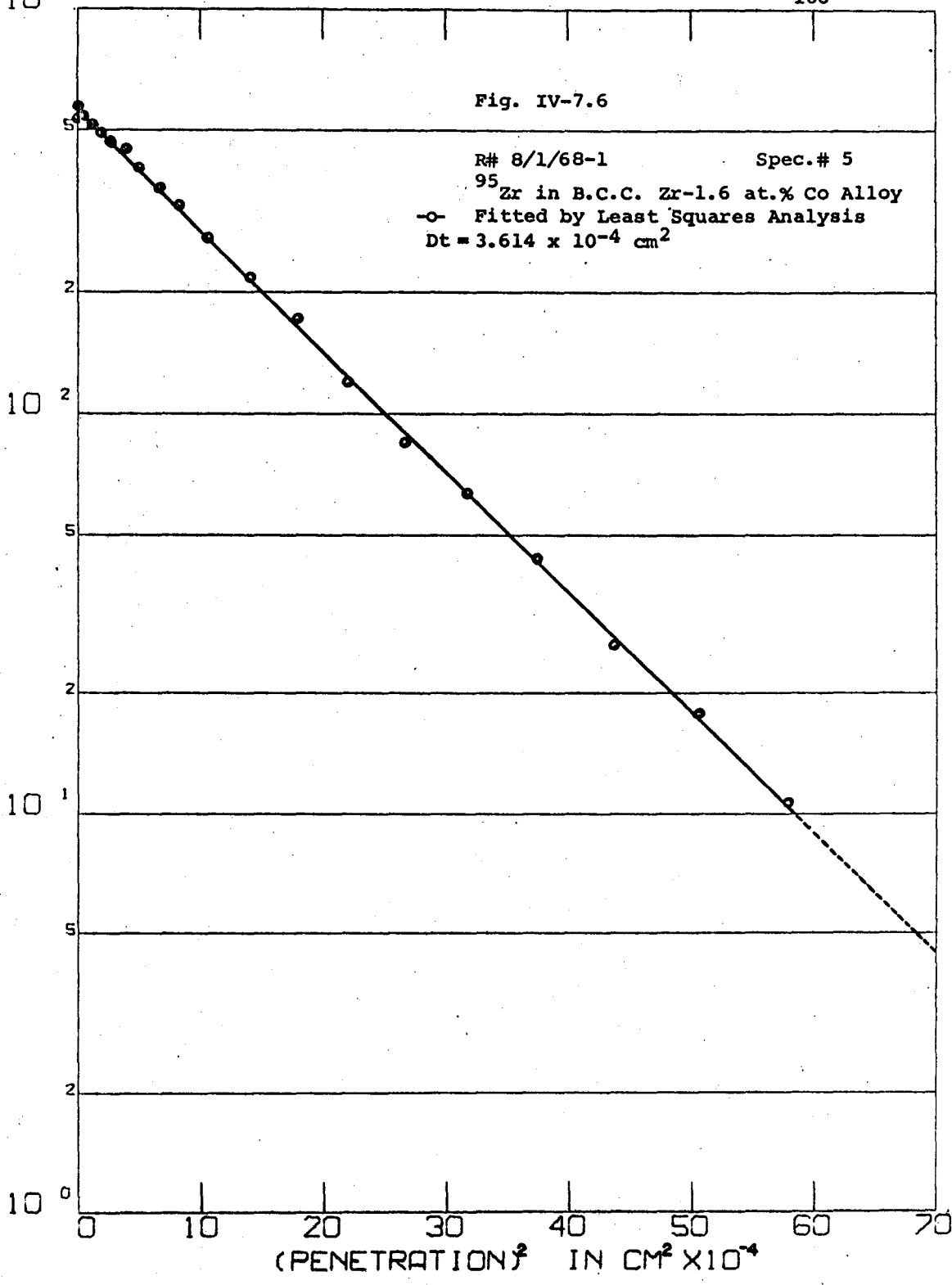
Spec.# 5

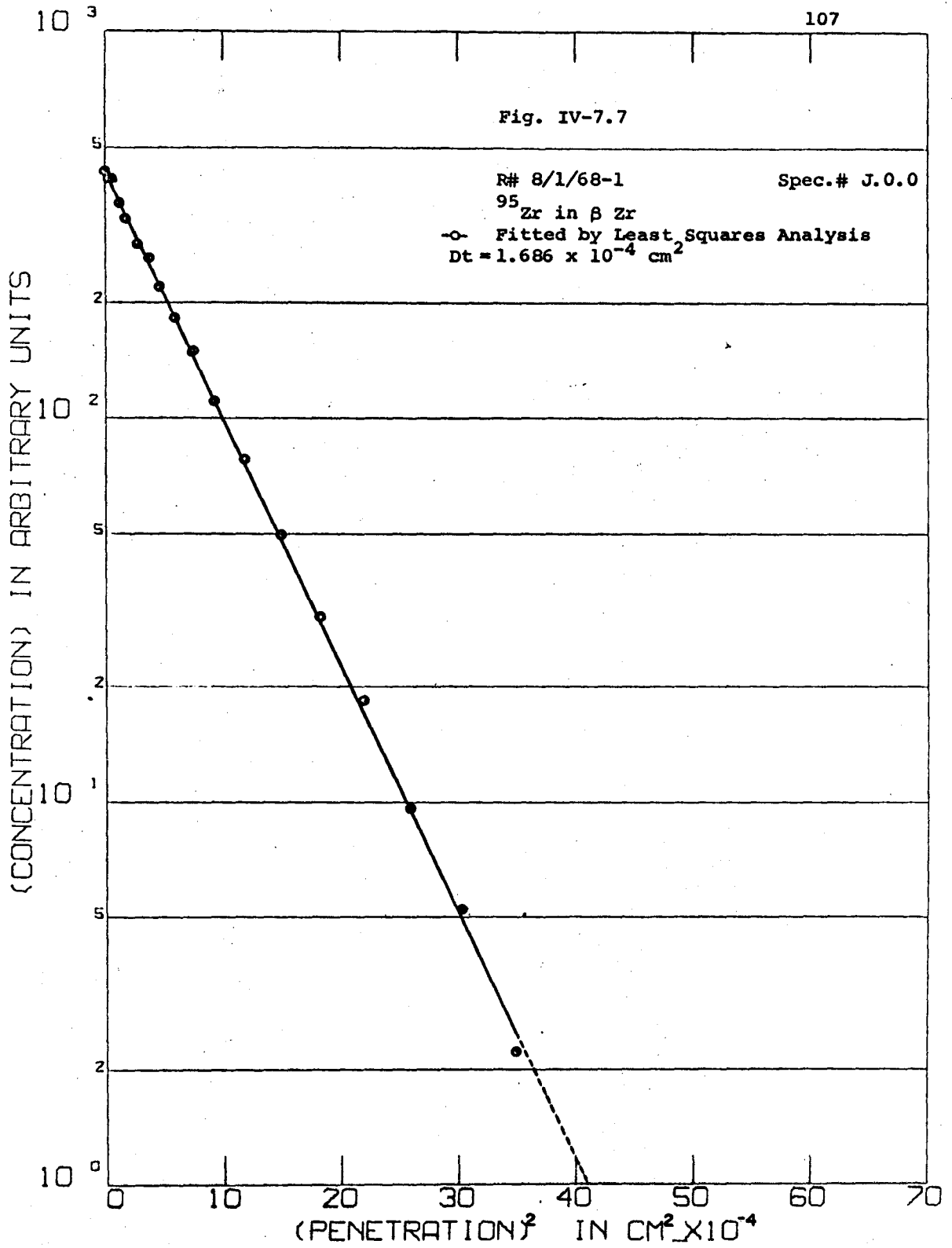
⁹⁵Zr in B.C.C. Zr-1.6 at.% Co Alloy

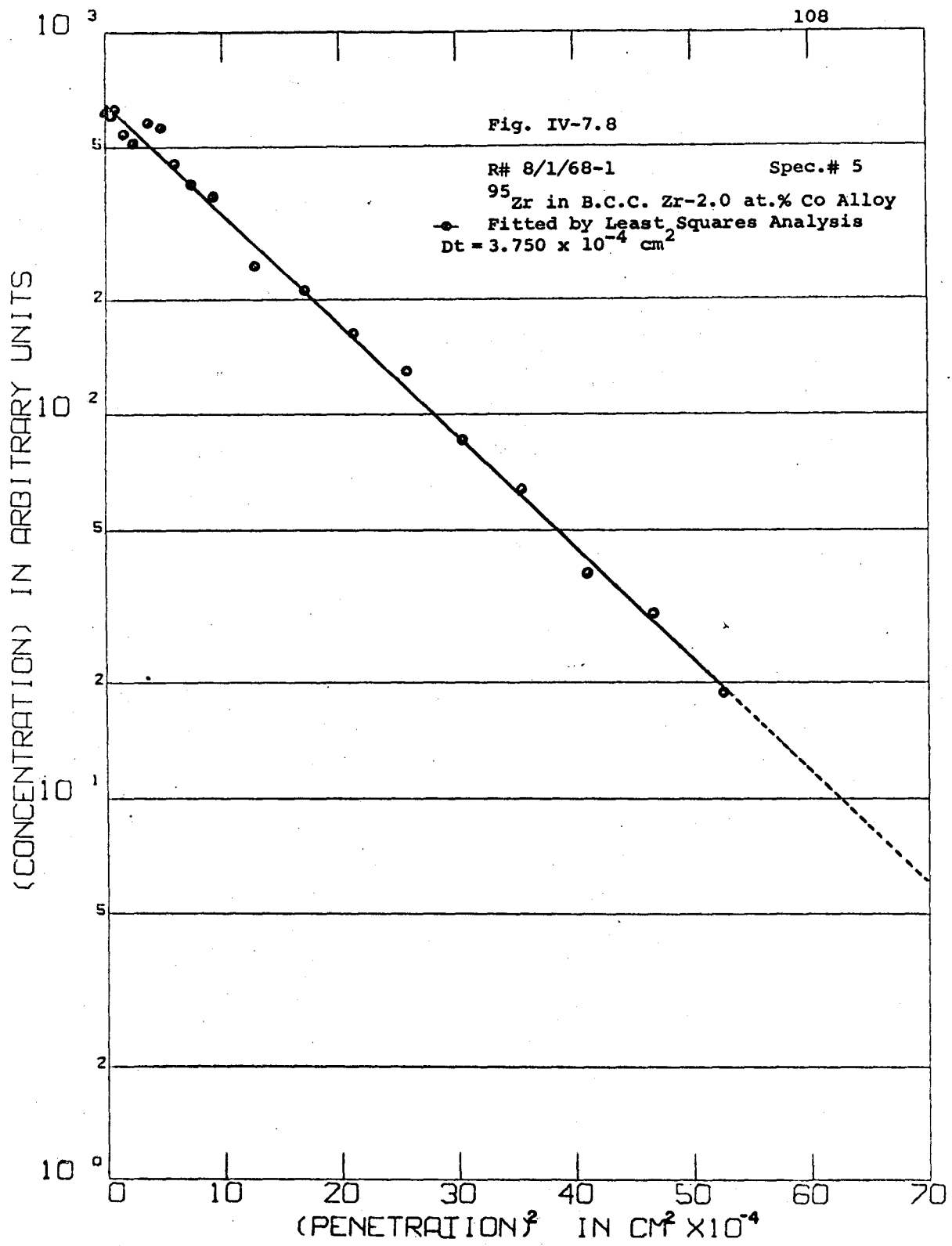
○ Fitted by Least Squares Analysis

Dt = 3.614 x 10⁻⁴ cm²

(CONCENTRATION) IN ARBITRARY UNITS







IV-8 THE DIFFUSION OF ^{60}Co IN DILUTE Zr-Co ALLOYS

A set of runs were made, as in V-7, but using ^{60}Co in place of ^{95}Zr . The results are shown in figures V-8.1 - 8.4.

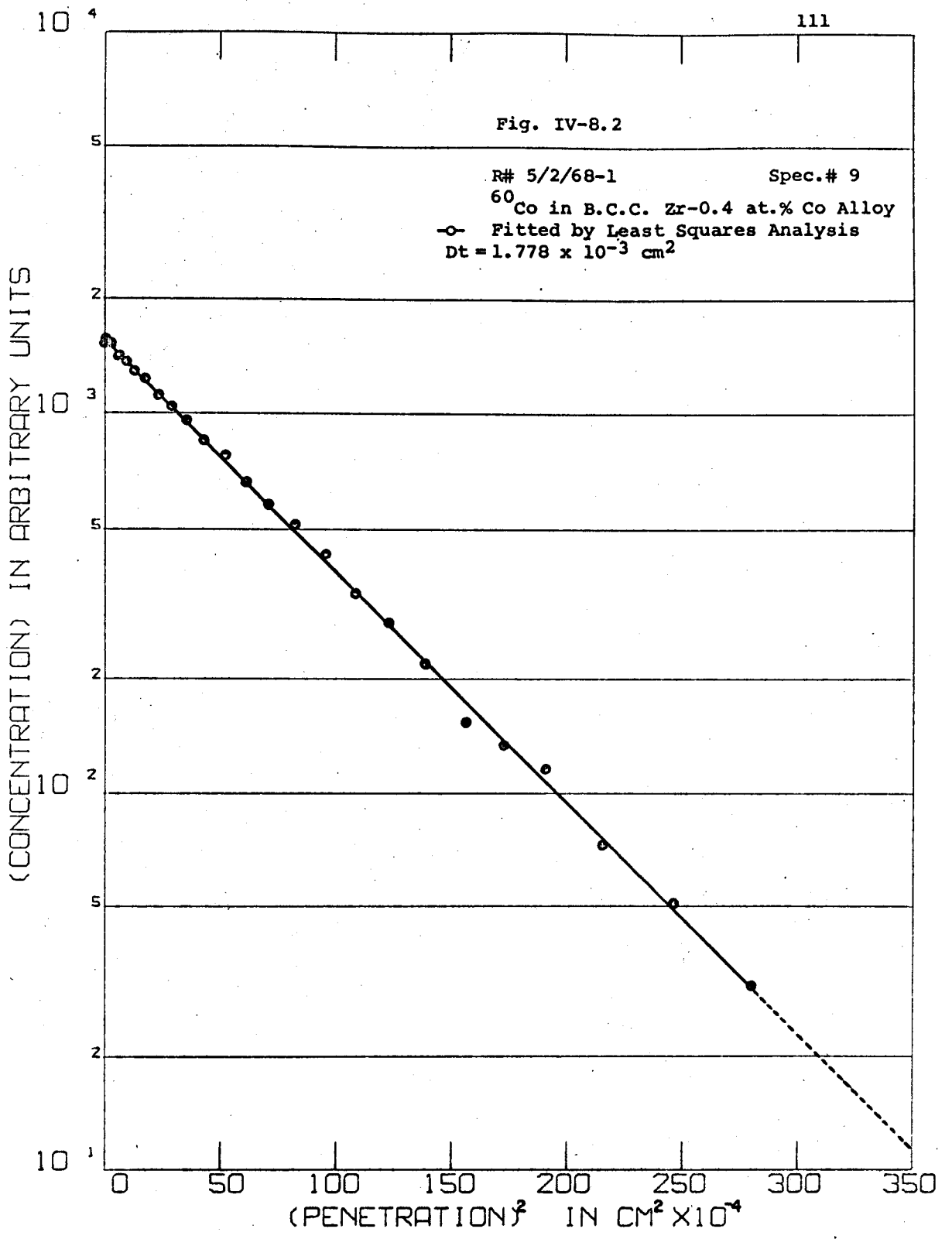
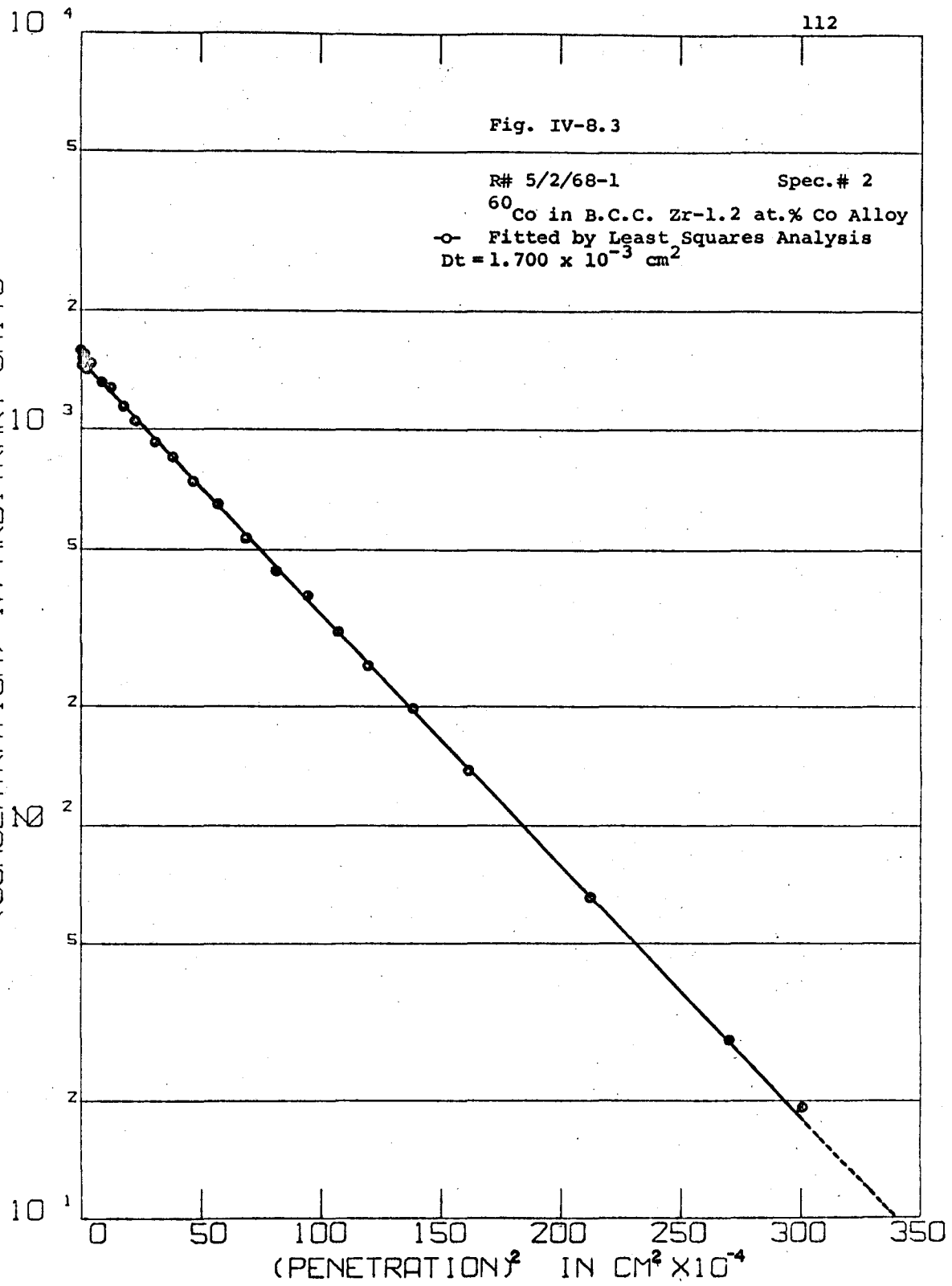
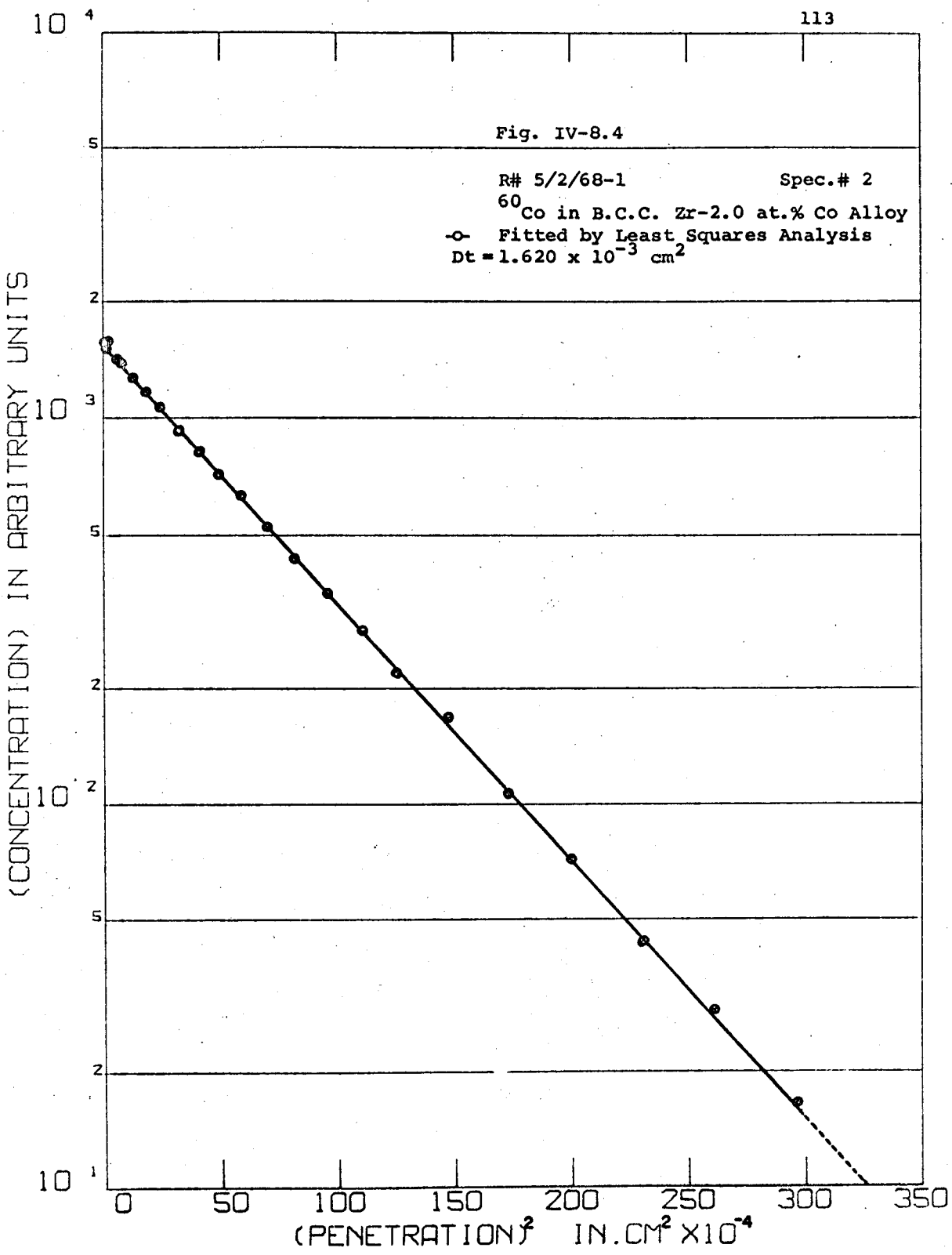


Fig. IV-8.3

R# 5/2/68-1 Spec.# 2
⁶⁰Co in B.C.C. Zr-1.2 at.% Co Alloy
-o- Fitted by Least Squares Analysis
Dt = 1.700 x 10⁻³ cm²

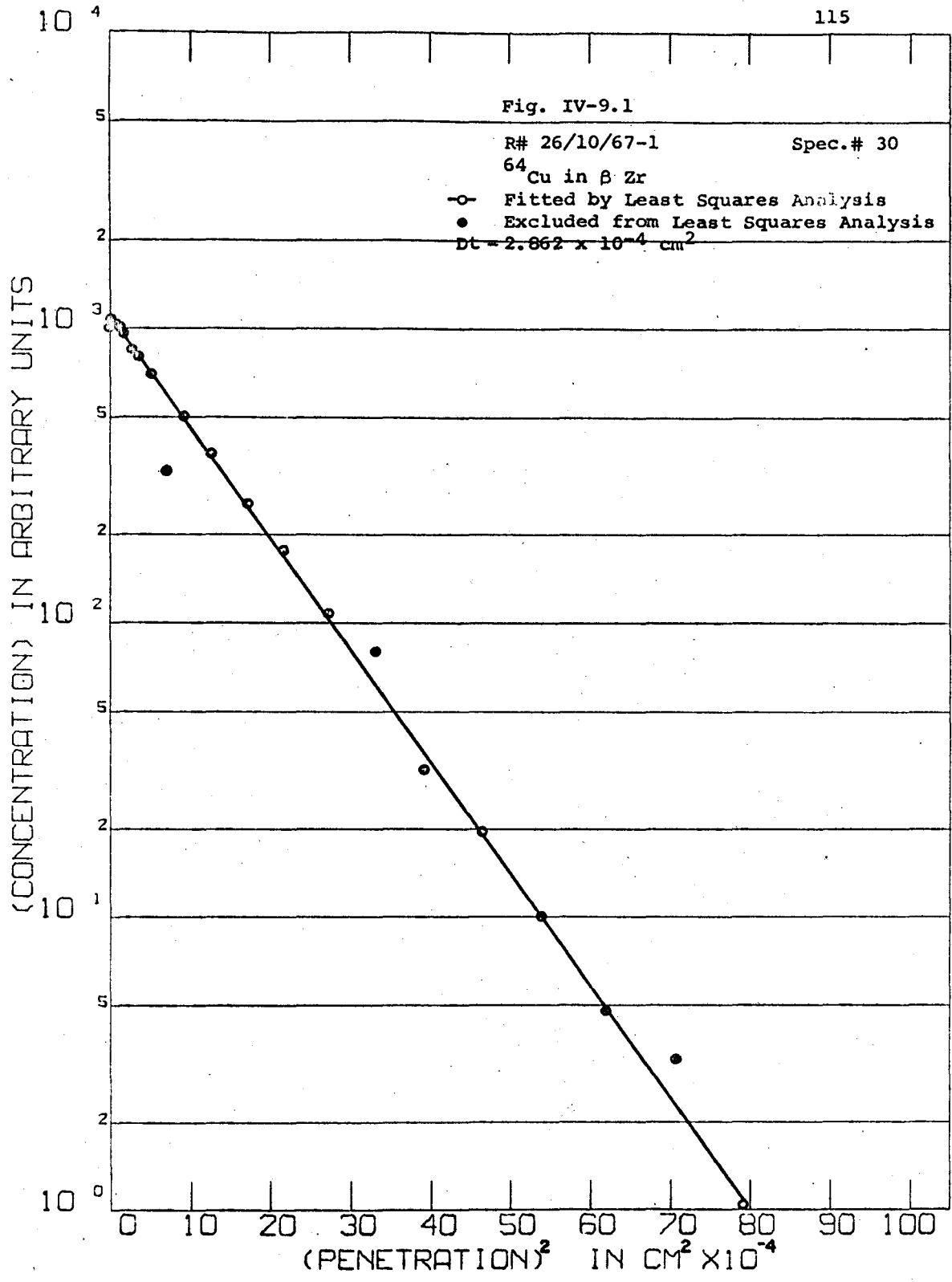
(CONCENTRATION) IN ARBITRARY UNITS





A single measurement of the diffusion of ^{64}Cu in β Zr was made at 900°C for an annealing time of $2\frac{1}{2}$ hours. The specimen, cut from the swaged rod, had been pre-annealed at 840°C for 5 days to give an α grain size of about 2 mm.

The concentration profile was entirely characteristic of normal volume diffusion. The diffusion coefficient of $3.12 \times 10^{-8} \text{ cm}^2/\text{sec}$ was about 60 times greater than that for self diffusion but about $1/10^{\text{th}}$ that for ^{60}Co diffusion at the same temperature. The concentration profile is shown in figure IV-9.1.



IV-10 THE TIME AND TEMPERATURE DEPENDENCE
OF THE QUALITY OF LAUE X-RAY DIFFRACTION SPOTS
FROM MARTENSITICALLY TRANSFORMED β Zr

It was suggested in II-4 that the most straightforward model proposed to account for the unusual diffusion behaviour of β Zr, β Ti and possibly γ U assumed that dislocations are generated during the martensitic $\alpha \rightarrow \beta$ phase transformation, that these remain stable to relatively high temperatures and that they provide paths for rapid diffusion. The chief difficulty of the model lies in the high density and stability of the dislocation network required to account for the pre-exponential factors derived from the Arrhenius curves.

It was felt, therefore, that a qualitative examination of the structural perfection of the material, as a function of annealing time and temperature after the $\alpha \rightarrow \beta$ transformation would be of considerable value in assessing the model.

This section of chapter IV describes the design, operation and results obtained from a high temperature, high vacuum Back Reflection Laue X-ray Diffraction Camera. It was built with the aim of observing any changes in the diffraction spots that could be associated with the behaviour of dislocations in the β phase.

Conversely, if sharp spots, characteristic of good quality crystals, were developed in the β phase in times short, or at most comparable to those required for diffusion measurements, the dislocation hypothesis could be discounted.

The main body of the camera consisted of a stainless steel pot, an 8 liter per second Varian Vac-Ion pump, a high vacuum Hoke valve and a 1" diameter, 0.011" thick Be window for the transmission of the X-ray beam.

The specimens themselves were initially in the form of 1/4" wide strips, cut from a 0.015" thick cold rolled sheet and bent to the shape shown in figure V-10.1. W + 5% Re - W + 26% Re thermocouple wires, 0.005" in diameter were spot welded to the back central portion as shown. Strong, well behaved junctions were made by then spot welding a small disc of Zr foil over the thermocouple wires so as to enclose them in an envelope.

The specimen filaments were bolted to two water cooled power leads vacuum sealed and electrically isolated in a stainless steel base plate. The thermocouple wires were fed through a ceramic insulator in the base plate and sealed with a high vacuum epoxy resin.

The unit was assembled into the main Camera body as shown in figure IV-10.2.

The system was attached via the Hoke high vacuum valve, to the vacuum system of the roll-on furnace, pumped down to 10^{-6} torr and the specimen degassed. Once the degassing, due mainly to hydrogen, was complete at about 800°C, the Vac-Ion pump was switched on, the specimen current turned off and the Hoke valve sealed.

The unit was then pumped to about 5×10^{-8} torr, the Vac-Ion pump switched off and the complete assembly, including the power supply, vacuum control unit and temperature recorder transferred to the X-ray laboratory, where they were re-assembled on a Philips X-ray Unit.

Figure IV-10.2 shows an overall view of the camera, the X-ray unit, the Polaroid film holder and the associated gear.

Preliminary runs established that the Vac-Ion pump could maintain a vacuum of 5×10^{-8} torr to 1×10^{-6} torr when the specimen temperature was raised to 1400°C . The water-cooling on the camera body kept it and the Be window cool. A convenient internal check on the behaviour of the thermocouple was provided by a sharp thermal arrest at the transformation temperature during cooling from the β to the α phase.

The specimen could be heated quickly to a desired temperature and maintained there by manually adjusting the power input to the current leads via a Variac autotransformer coupled to a high current step-down transformer. Examples of both the controlled heating and the large thermal arrest on cooling are shown on the recorder chart in figure IV-10.9.

The X-rays were supplied from a copper target tube operated at 35 kV and 20 m.a. A collimated beam passed through a central hole in the Polaroid film holder to the Be window and thence to the specimen. The very fine grain size of the Be window gave rise to spotty rings as shown in figure IV-10.4, for which no specimen was in the camera.

Figure IV-10.5 shows diffraction spots produced from an α annealed fine grained zirconium filament, held in the camera at room temperature. The horizontal shadows are due to two stainless steel braces behind the Be required to support the window under vacuum.

While the spots were small and fell in a ring similar to those from the Be, it was hoped that they would persist

up to the $\alpha \rightarrow \beta$ transformation to provide a reference for a comparative assessment of the β phase diffraction spots.

Two unforeseen difficulties were encountered when the specimen was heated. These can be seen in the sequence of films shown in figure IV-10.6. The first was purely geometrical; as the temperature increased, the lattice parameter increased with a consequent increase in the diameter of the ring formed by the spots.

This eventually merged with that of the Be window, making further observations extremely difficult. The second effect was associated with the decrease in spot intensity due to the increased vibrational amplitude of the atoms as the temperature was increased. This resulted in most of the spots disappearing completely below the transformation temperature.

Figure IV-10.7 shows the diffraction pattern of a large grained specimen taken at room temperature in the camera. The relatively high intensity of the spots suggested that either single crystalline or large grained polycrystalline α Zr specimens would overcome the second of the two difficulties. Attempts to grow large grains in the filaments themselves were not successful; the grains appeared to stabilize at a size of the order of the thickness of the filament and did not grow further even after 5 days annealing at 840°C.

As an alternative a disc 0.040 inches thick was carefully cut from a 3/8 inch diameter large grained diffusion specimen and thinned down to 0.020" by chemical polishing. It was then carefully spot welded around its rim to a normal filament that had a 3/16" diameter hole cut in

its central portion. Thermocouple wires were attached in the usual way directly to the back of the large grained disc. The specimen is shown in figure IV-10.1.

At the same time, the camera mount was modified to provide effective translational and rotational movements of the specimen with respect to the incoming X-ray beam. This was aimed at increasing the probability of a major diffraction spot falling within the restricted field of view of the camera.

These two modifications worked well and provided data of considerable interest.

Figure IV-10.8 shows the temperature record during the run. The complete annealing history of the specimen in the β phase was as follows:

10	minutes	at	945°C
68	"	"	1060°C
22	"	"	945°C
85	"	"	1080°C
25	"	"	940°C
20	"	"	1342°C
40	"	"	940°C

Films shown in figure IV-10.9 were taken at the points indicated by arrows on the chart.

The slightly smeared patterns in the low temperature films (figure IV-10.7) were probably due to the distortion introduced into the crystal during the spot welding to the filament. The rapid decrease in spot intensity between room temperature and 664°C is seen in the figures IV-10.10(a) and 10.10(b).

The initial films taken after the $\alpha \rightarrow \beta$ transformation did not show any spots at all (figure IV-10.10(c)).

The specimen temperature was increased from 945 to 1080°C and a single, faint spot appeared at about "7 o'clock" on the film (figure IV-10.10(d)). This was observed over a period of 1 hour, but it gradually faded and disappeared completely. The temperature was then decreased to 945°C again, and the field of view carefully scanned by shifting and rotating the specimen relative to the X-ray beam. This finally revealed another diffraction spot, now at "11 o'clock" on the film (figure IV-10.10(e)). On raising the specimen temperature to 1080, the spot disappeared, but reappeared on returning the temperature to 945°C. Finally, the temperature was raised to 1342°C and held there for 20 minutes, then lowered to 940°C. What was formerly a single faint spot was now transformed to a cluster of about 8 small but relatively bright spots, as shown in figure IV-10.10(f).

Fig. IV-10.1

Large Grained X-ray Specimen

Fig. IV-10.2

High Vacuum, High Temperature Laue Camera
on X-ray Unit

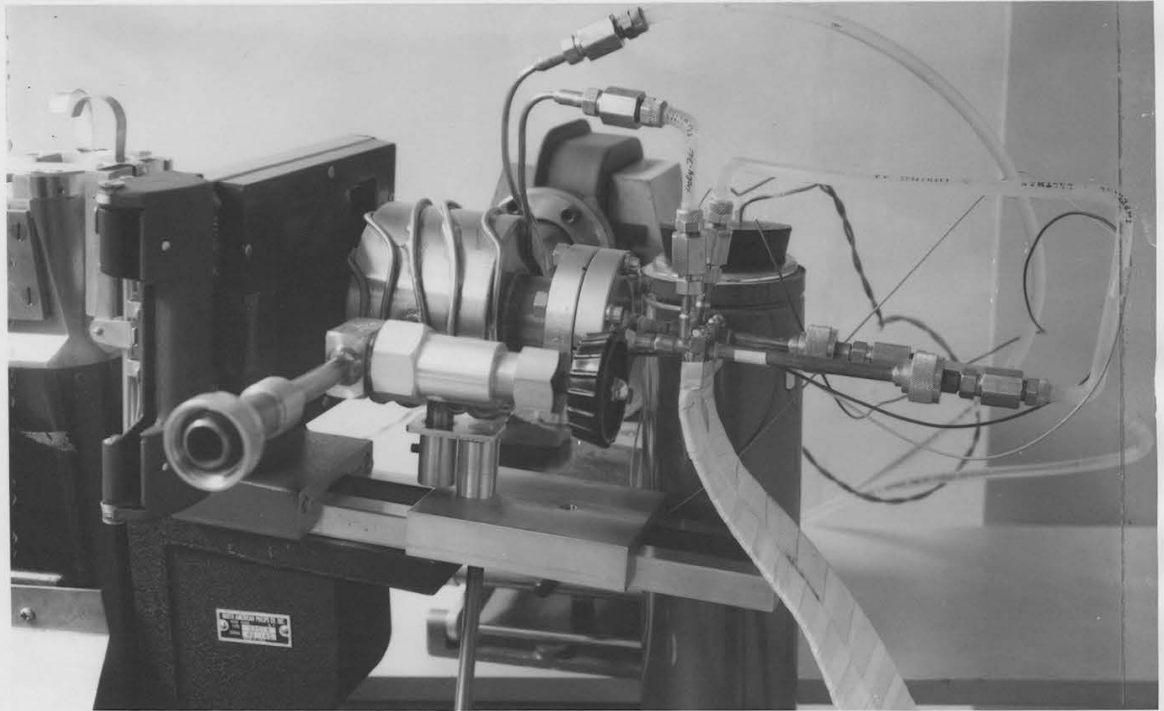
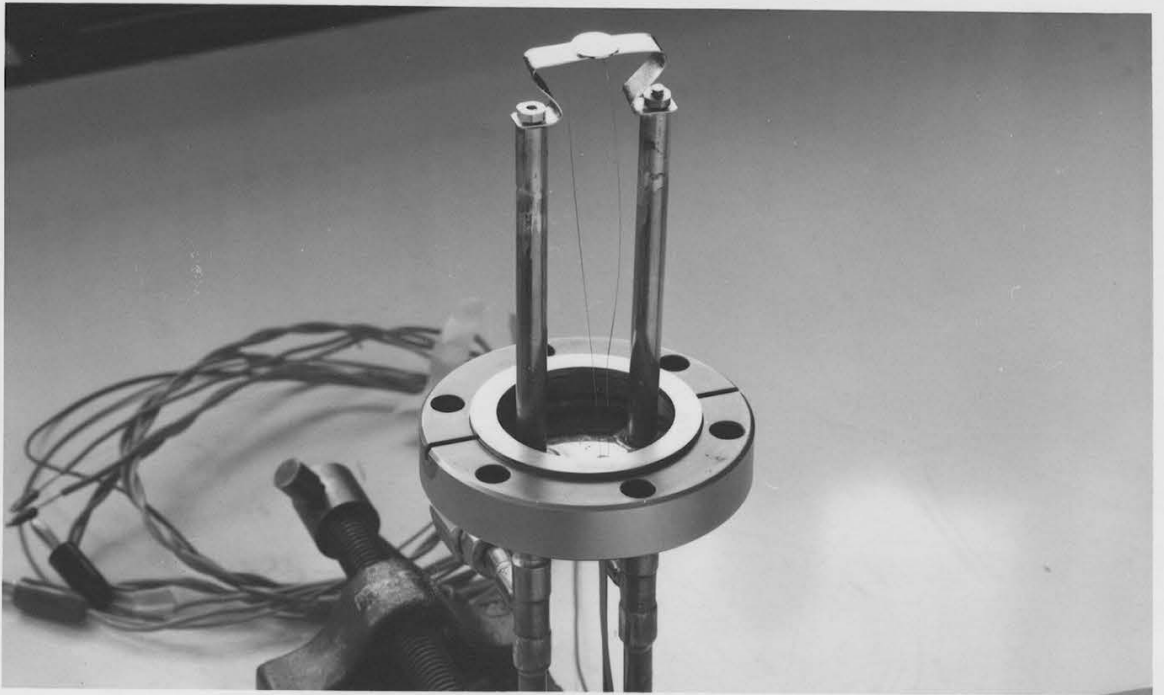


Fig. IV-10.4

Spotty rings from Beryllium
window

Fig. IV-10.5

Diffraction spots from fine
grained α Zr at room temperature

Fig. IV-10.6(a)

As in 10.5 at 357°C

Fig. IV-10.6(b)

As in 10.5 at 750°C

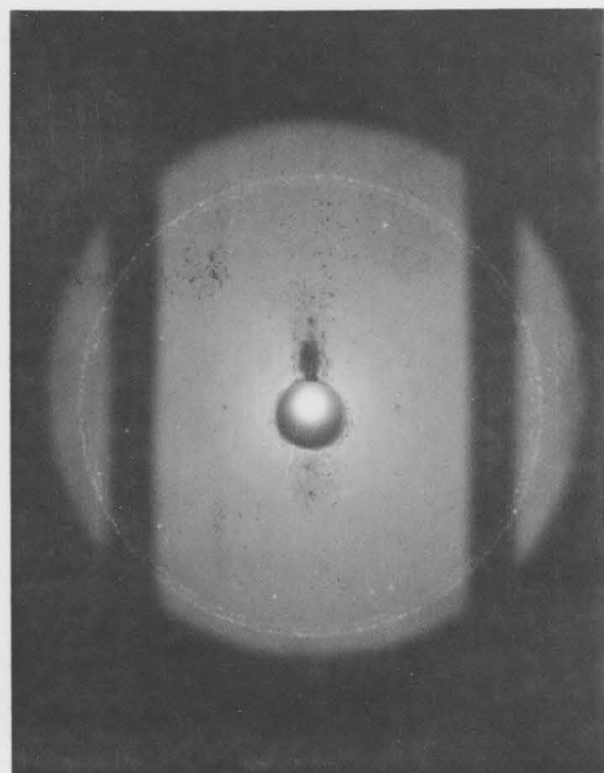
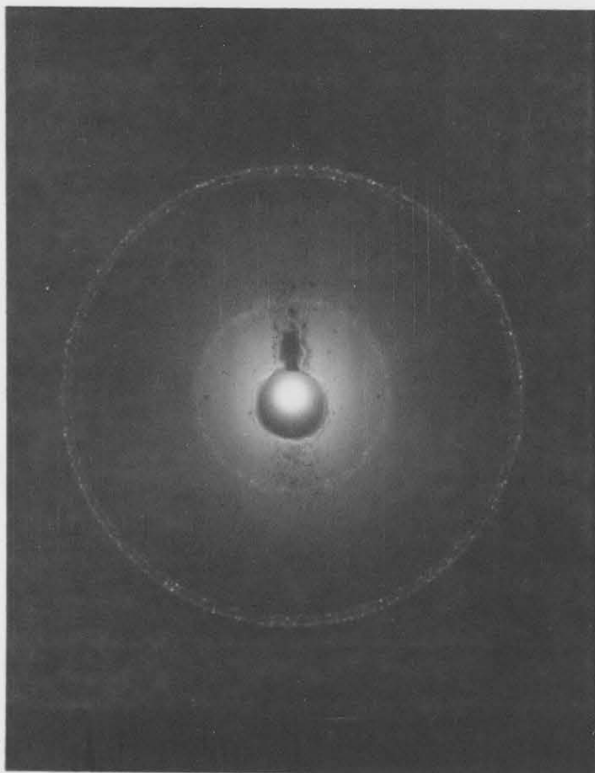
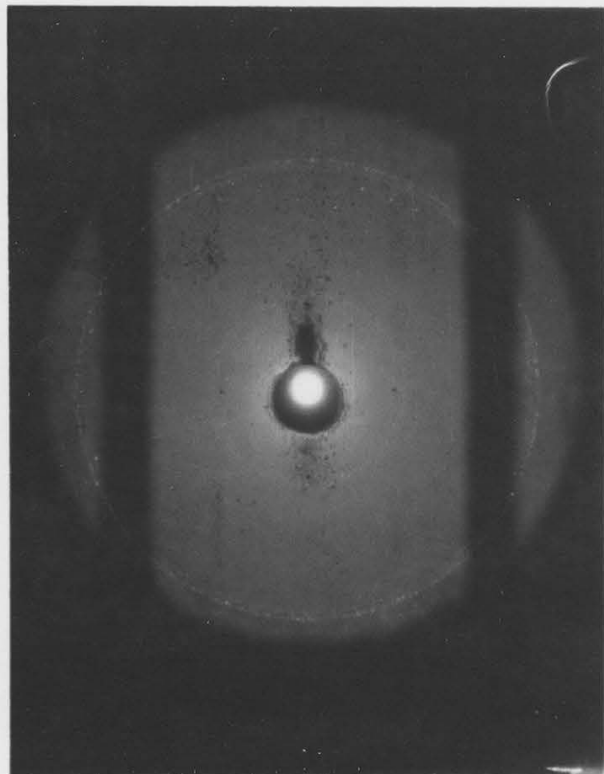
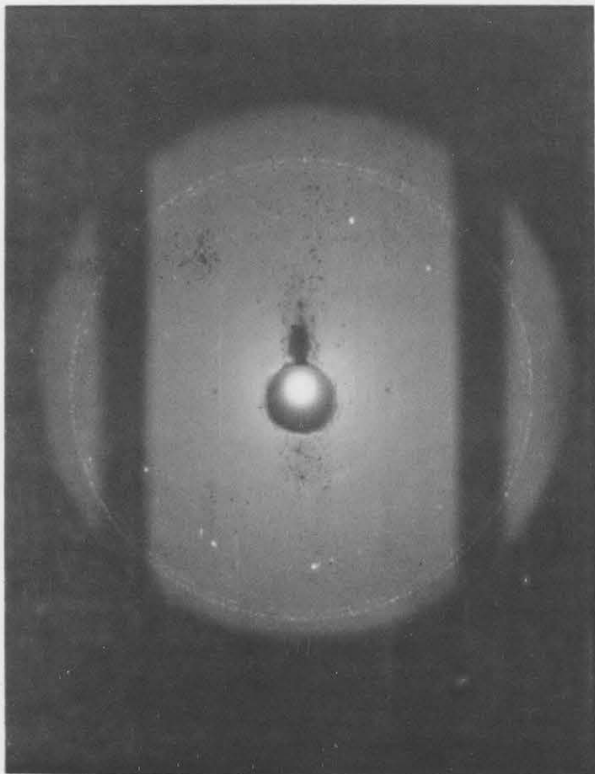


Fig. IV-10.7

Diffraction spots from the
large-grained α -Zr specimen
at room temperature

Fig. IV-10.10(a)

As in IV-10.7 showing decrease
in spot intensity with in-
creasing temperature.
T = 357°C

Fig. IV-10.10(b)

As in IV-10.10(a)

T = 664°C

Fig. IV-10.10(d)

Transient spot at "7 o'clock"
in specimen after $\alpha \rightarrow \beta$ trans-
formation.

(note change in sequence of
photographs: Fig. IV-10.10(c)
precedes 10.10(d) in the text)

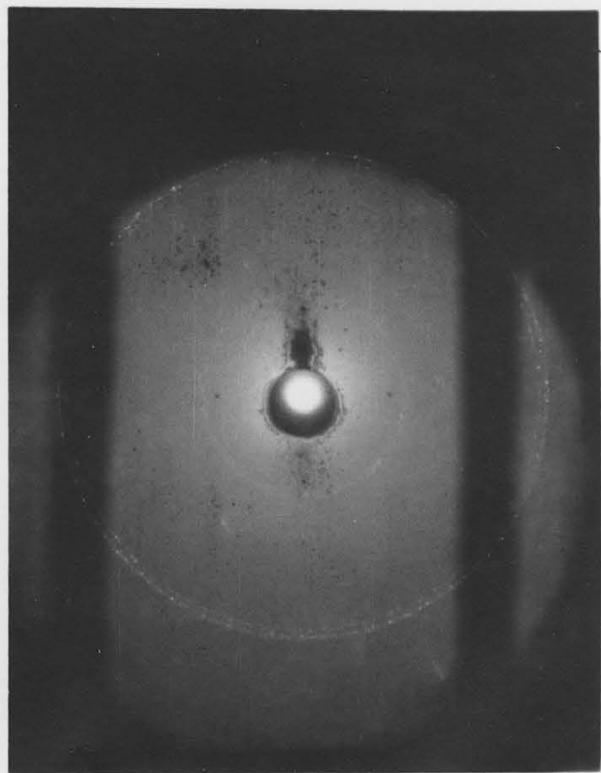
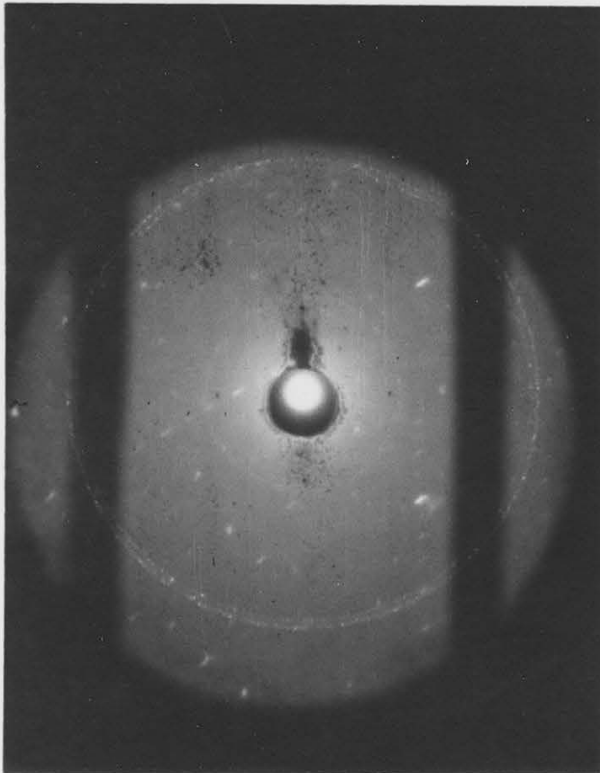
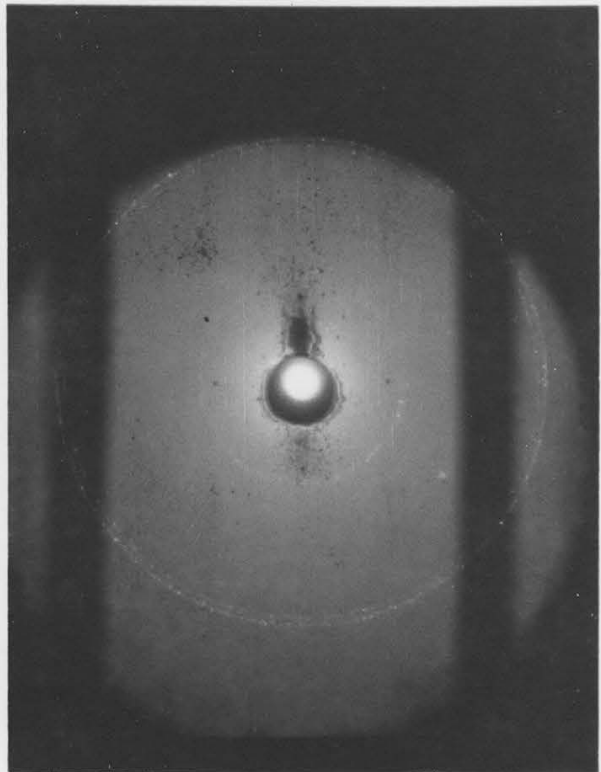
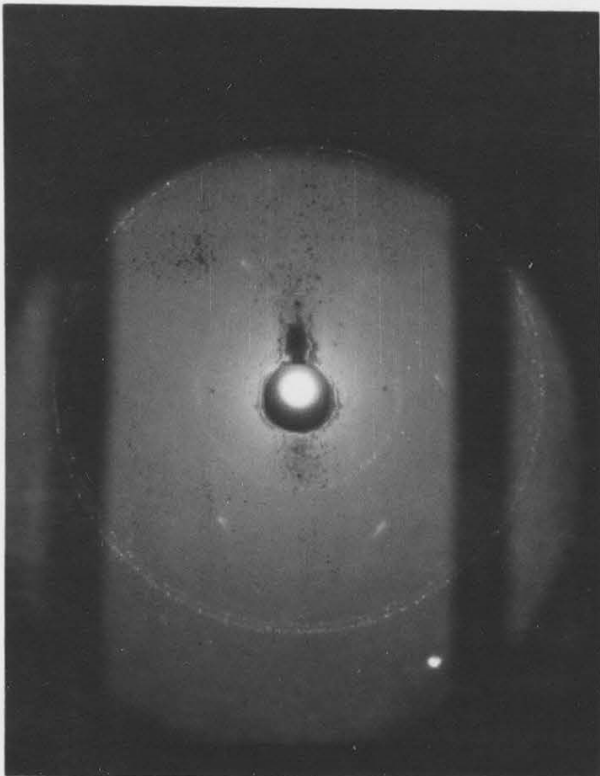


Fig. IV-10.10(c)

Lack of diffraction spot from β -Zr for 10 minutes after the $\alpha \rightarrow \beta$ transformation.

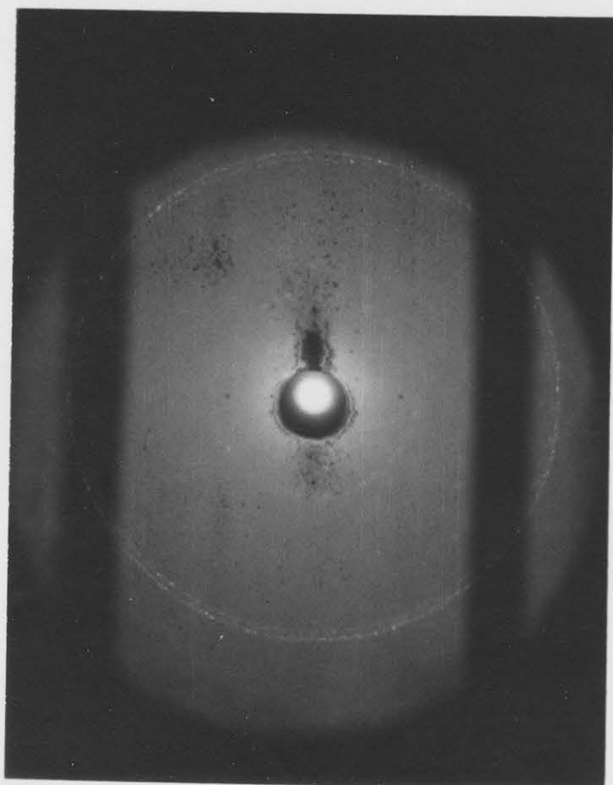
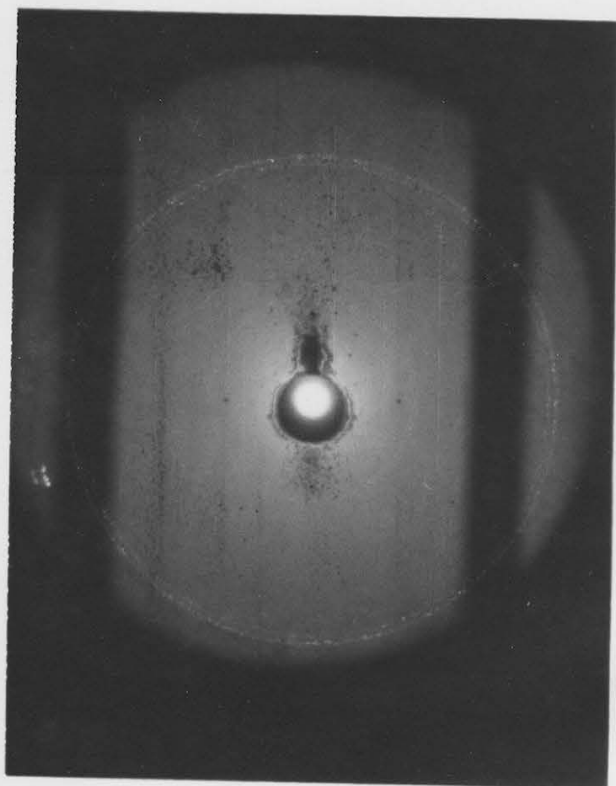
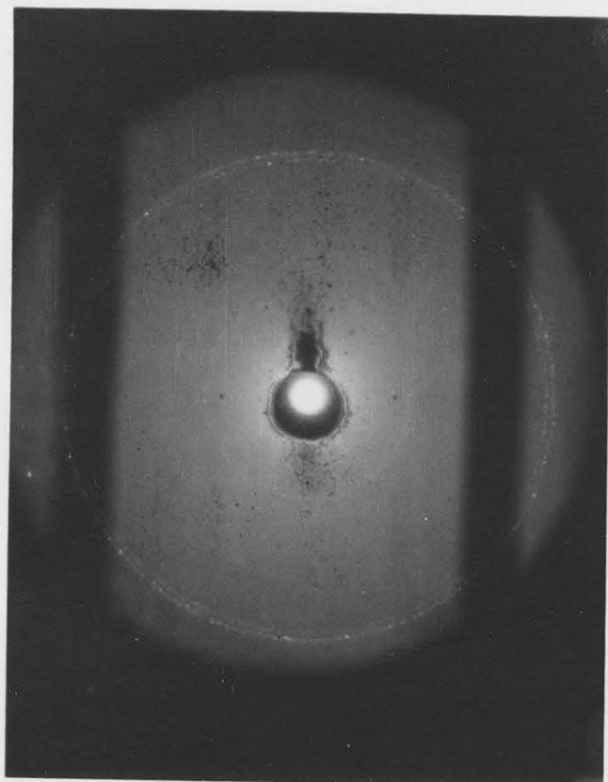
Temp. = 945°C

Fig. IV-10.10(e)

Faint diffraction spot at 11 o'clock (see text)

Fig. IV-10.10(f)

Multiple diffraction spots after annealing 20 minutes at 1342°C.



The low neutron capture cross section of zirconium makes it particularly useful as a structural component of nuclear reactors. For the purposes of alloy development in this field, there is a need for measurements of both self and solute diffusion in the low temperature close packed hexagonal α phase. A compilation of the available data has been given by the author in a review article⁽⁷⁷⁾. In general, such measurements are made difficult by a combination of very low diffusion rates and a lack of good quality single crystals. Typical values of the diffusion coefficients at about 820°C range from 10^{-13} to 10^{-11} cm²/sec.

In view of the very rapid diffusion of ^{60}Co in β Zr, however, a few exploratory measurements were made in the α phase as well. The primary aim was to assess the extent to which the rapid diffusion was dependent on the crystal structure alone.

The initial run was made at 820°C for 21 hours. One of the specimens came from the swaged rod and had been pre-annealed at 840°C for 5 days to give a mean grain size of 1.2 mm. The other was cut from the M.R.C. crystal and exhibited the large degree of persistent substructure indicated in figure IV-2.1(b).

The results, shown in figure IV-11.1 in the usual form of $\log c$ vs x^2 , were both unexpected and startling in that complete homogenization appears to have occurred throughout the specimens. The immediate implication, of course, was that the high rates of diffusion of ^{60}Co in β Zr

were matched by those in the α phase. In order to obtain quantitative measures of the diffusion coefficients as well as more informative concentration profiles, further runs were made at lower temperatures and for times of the order of 2 hours. Again, specimens of different metallurgical conditions were annealed in pairs.

The results, when plotted in the usual manner as $\log C$ vs x^2 , showed in all cases a continuous positive curvature characteristic of diffusion occurring predominantly along grain boundaries. When replotted as $\log C$ vs $x^{6/5}$, the major portion of the curves were linear and generally conformed to the theoretical shape predicted by Suzuoka⁽³⁴⁾, as indicated in figures IV-11.2 to 11.5.

In run # 30/8/67-2 one of the samples was cut from the swaged rod and given a short pre-anneal in the α phase to produce a fine grain size, the other was a large grained specimen obtained after prolonged pre-annealing. In both cases Laue X-ray examination showed sharply defined spots. While both plots of $\log C$ vs $x^{6/5}$ were linear, their slopes differed significantly, as shown in figure IV-11.6.

10³

129

Fig. IV-11.1(a)

R# 3/8/67-1

Spec.# 15

⁶⁰Co in α Zr

o Fitted by least squares analysis.

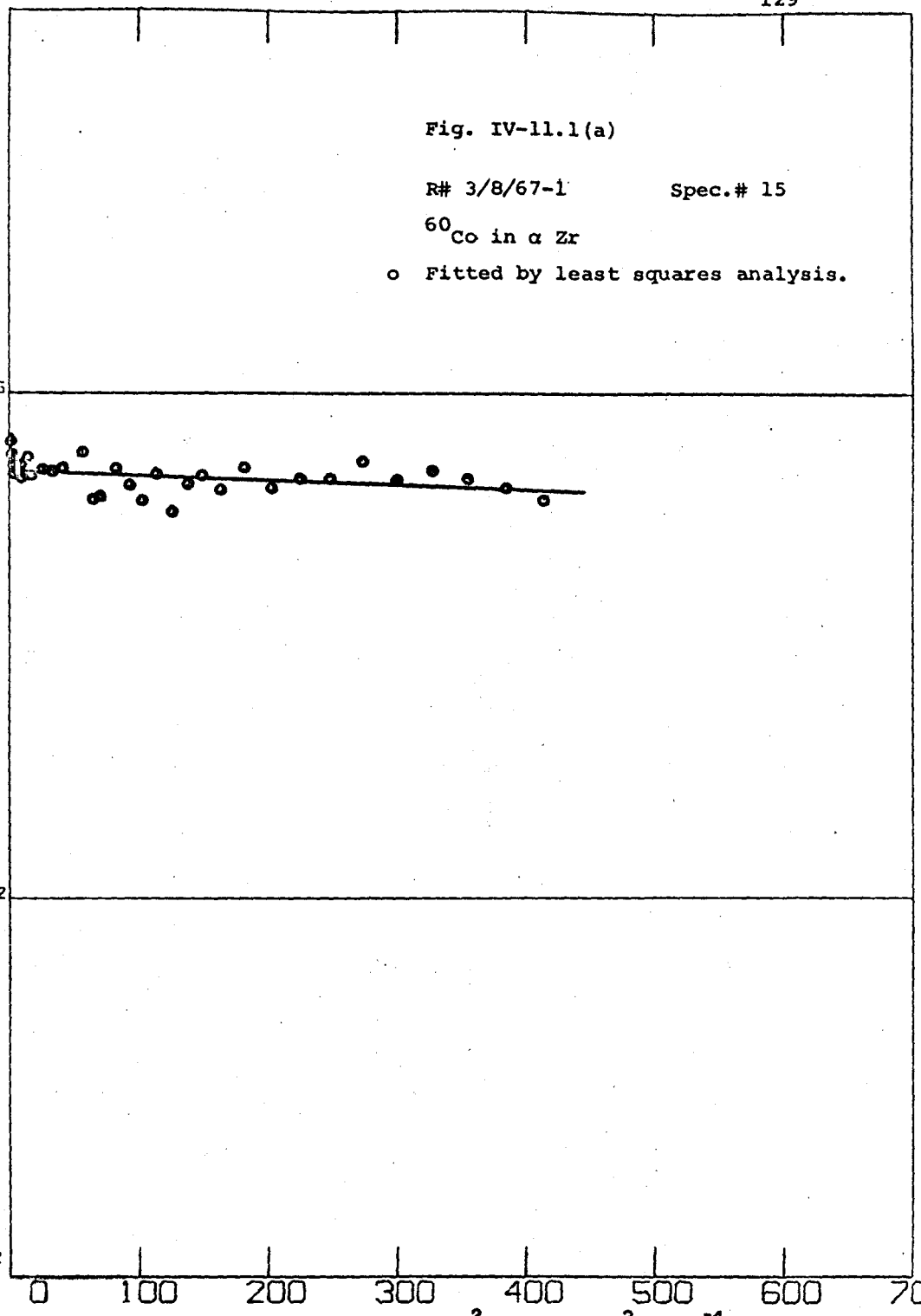
(CONCENTRATION) IN ARBITRARY UNITS

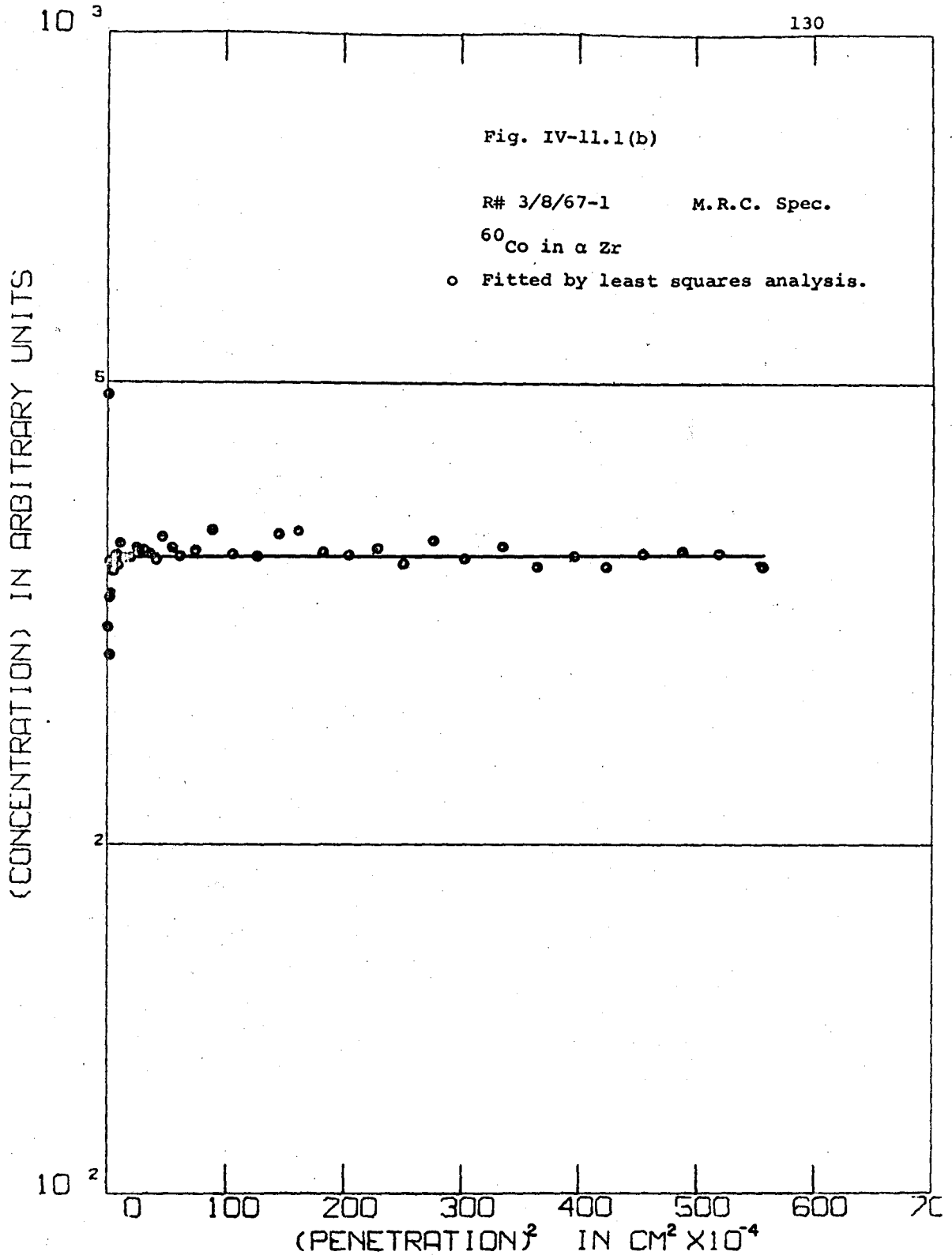
5

2

10²

(PENETRATION)² IN CM² X 10⁻⁴





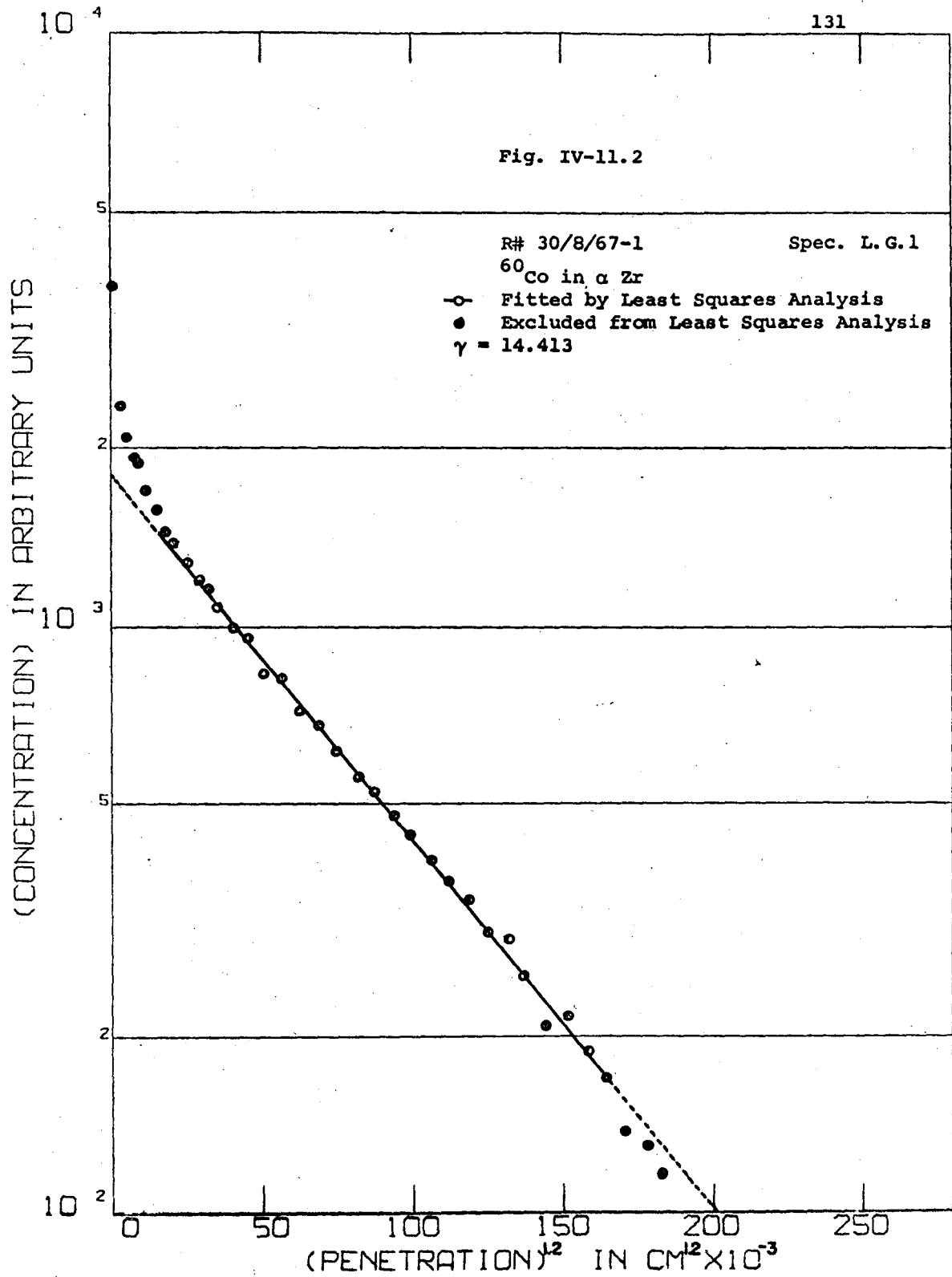
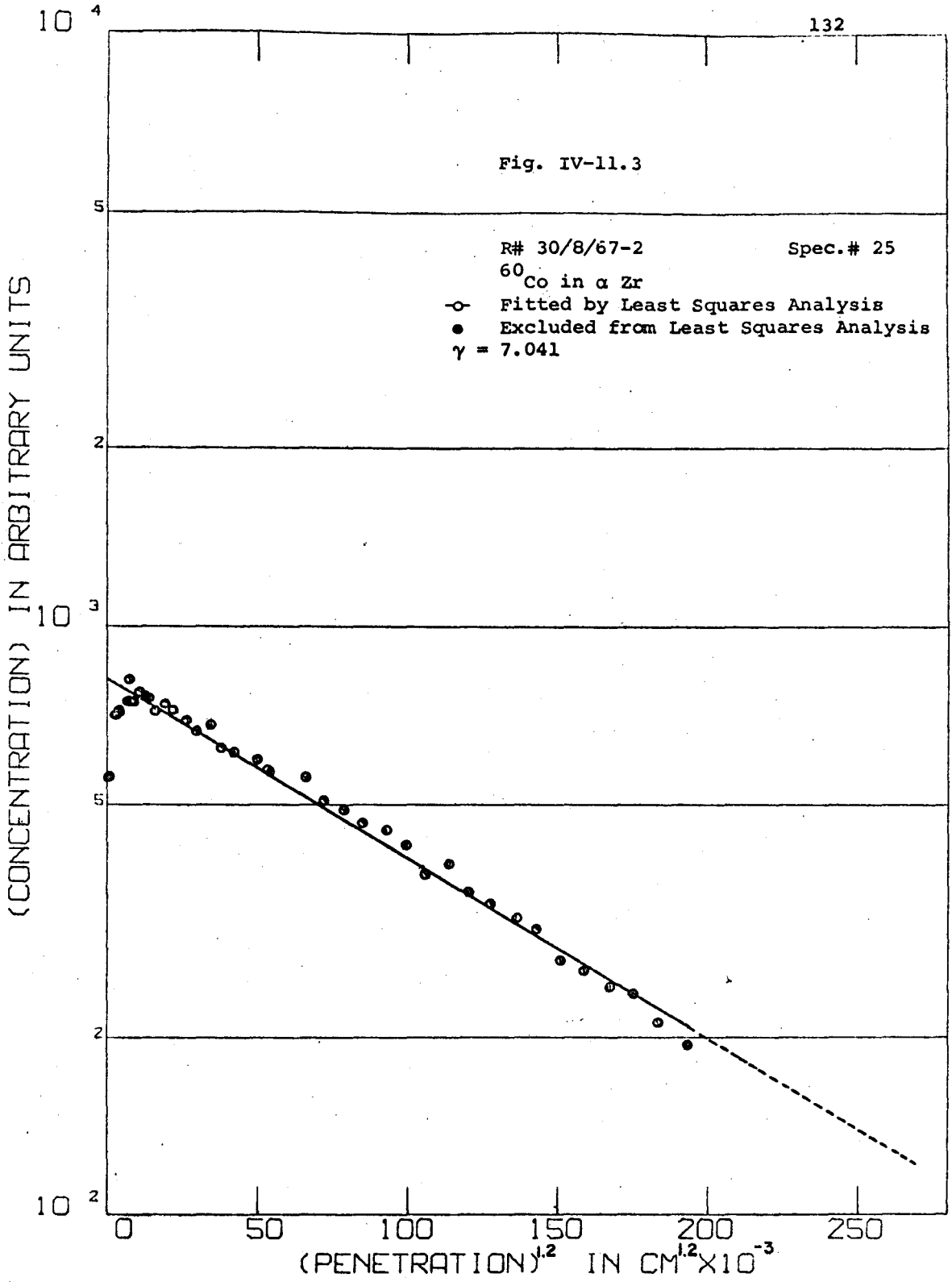
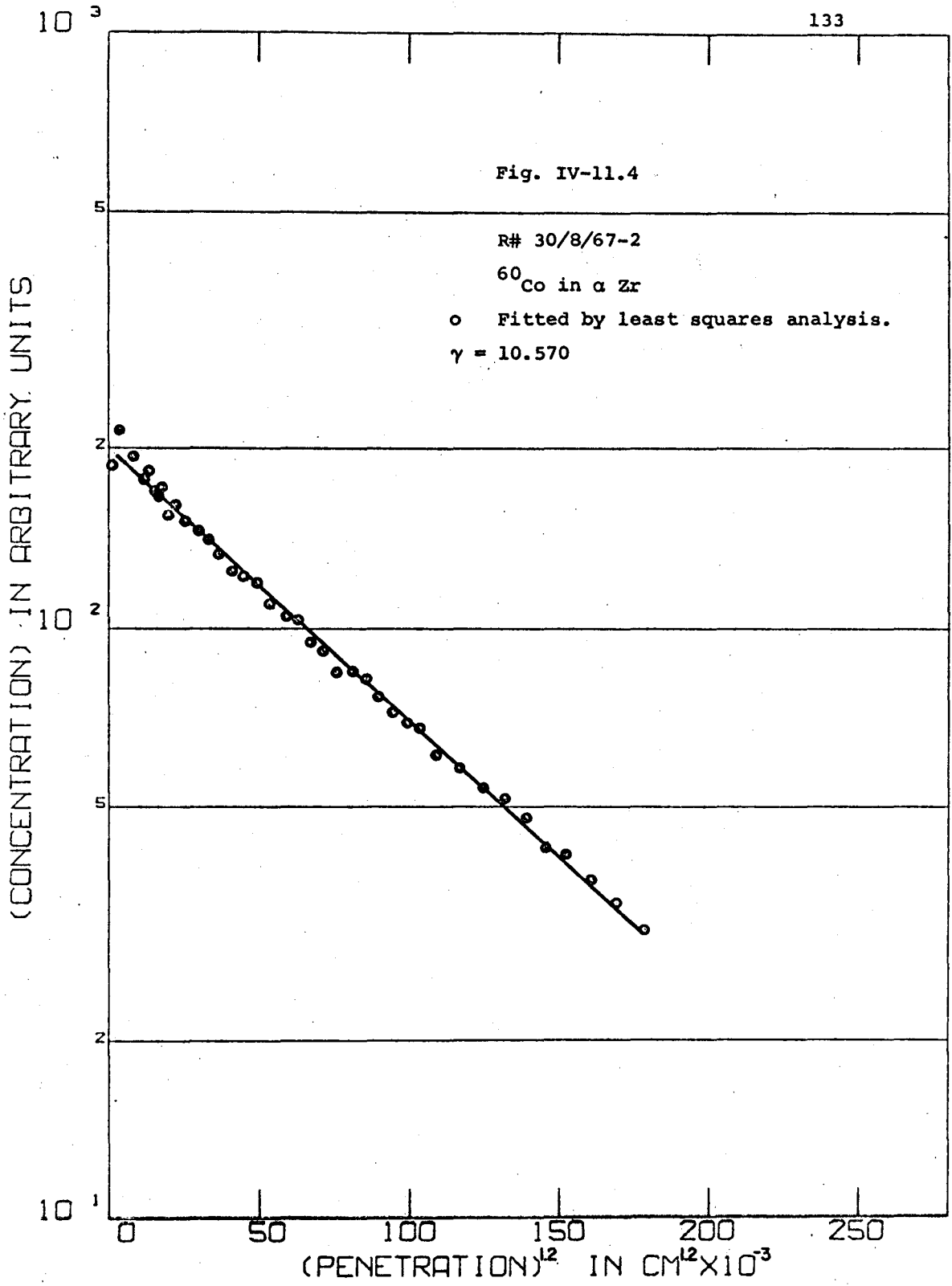


Fig. IV-11.3





10³

(CONCENTRATION) IN ARBITRARY UNITS

Fig. IV-11.5

R# 31/8/67-1

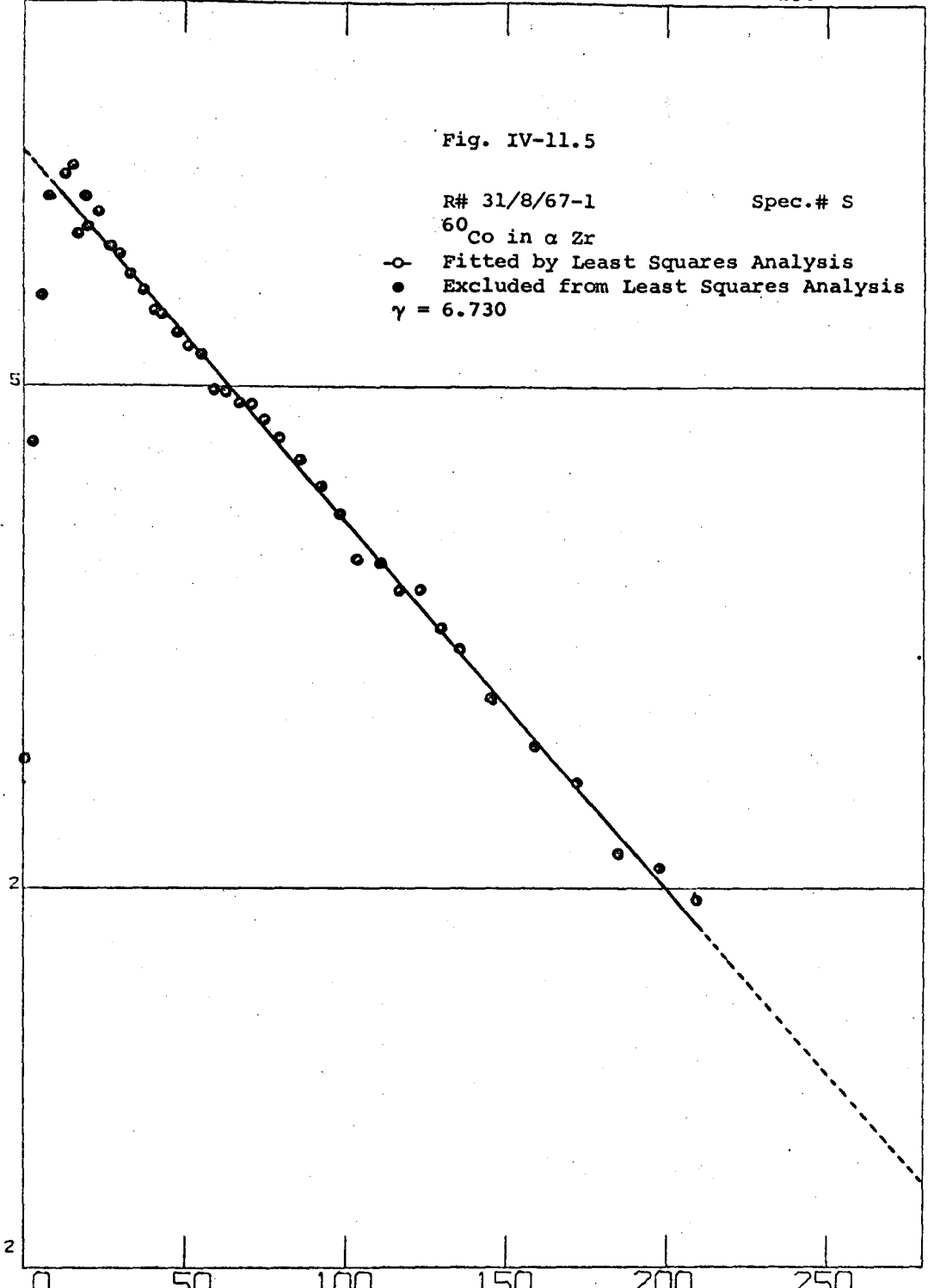
Spec.# S

⁶⁰Co in α Zr

-o- Fitted by Least Squares Analysis

● Excluded from Least Squares Analysis

γ = 6.730



5

2

10²

(PENETRATION)^{1/2} IN CM^{1/2} X 10⁻³

IV-11.6

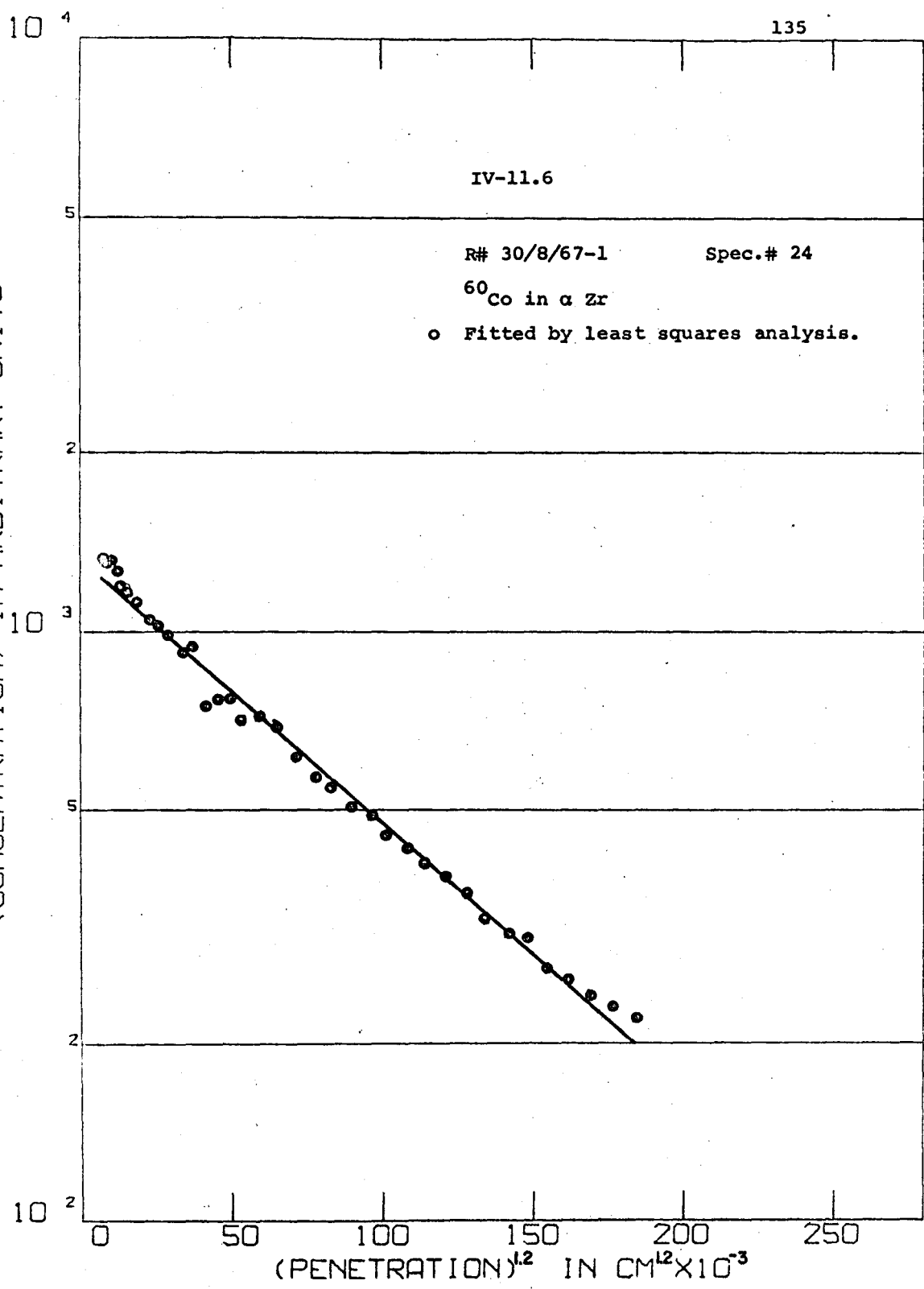
R# 30/8/67-1

Spec.# 24

⁶⁰Co in α Zr

○ Fitted by least squares analysis.

(CONCENTRATION) IN ARBITRARY UNITS



V-1 THE SHAPE OF THE CONCENTRATION PROFILES

Most of the concentration profiles observed in this study accurately follow the relationship of equation II-1.1 i.e.

$$C(x,t) = S_0 (\pi Dt)^{-\frac{1}{2}} \exp(-x^2/4Dt)$$

over the entire range. Unambiguous values of D can be extracted from such curves. Included amongst these are all of the results obtained for the diffusion of both ^{95}Zr and ^{60}Co in the dilute zirconium cobalt alloys, as well as the higher temperature results for ^{60}Co in β Zr. For the lower temperature β phase studies, however, and for all of the α phase studies, the curves show distinct departures from linearity in a plot of $\log C$ vs x^2 . In the β phase these take a characteristic and reproducible form, a rather pronounced example being that shown in figure IV-6.4 for R# 20/7/67-1. The initial high point followed by a sharp dip and the subsequent rise to start a normal portion of the curve will be discussed later.

Less surprising is the positive curvature in the $\log C$ vs x^2 plots at the deeper penetrations. This is characteristic of systems in which a significant fraction of the total diffusant is being transported along grain boundaries.

Several models have been discussed in the literature which take account of the possibility of fast diffusion from the surface, down grain boundaries and thence laterally

into the grains. The treatment by Suzuoka⁽³⁹⁾ follows the experimental boundary conditions of this study most closely. He considers the case of a thin film of diffusant being placed on a material in which grain boundaries of mean spacing $2b$ and thickness $2a$ are perpendicular to the surface. D_b is the diffusion coefficient characteristic of the grain boundary and D_v that of the bulk material. The average concentration \bar{C} of the diffusant in a slab at depths between x and $x + dx$ is then given by

$$\bar{C}(x, t) = C_1 + b^{-1} \bar{C}_2 \quad \text{V-1.1}$$

where $C_1 = S_0 (\pi Dt)^{-\frac{1}{2}} \exp(-x^2/4D_v t)$

is the contribution from the normal bulk diffusion alone and \bar{C}_2 that from the effect of the grain boundaries. \bar{C}_2 is a complex function of x , t , D_v , D_b , a and b . Its characteristic shape is shown in fig. V-1.1. Near the surface it has a net negative contribution since it acts as an effective sink in drawing off the diffusant from the neighbouring regions of the grains. In the deeper penetrations it can become dominant, in which case the relation between \bar{C} and x assumes the form

$$\log \bar{C} \propto x^{\frac{6}{5}} \quad \text{V-1.2}$$

The slope $\gamma = -\partial \log \bar{C} / \partial x^{\frac{6}{5}}$ is then related to $\alpha D_b / D_v$ and D_v . The intercept of the linear curve increases as the grain size decreases.

The relation given by equation V-1.1 yields

$$\log \bar{C} = \log C_1 + \log \left[1 + \frac{\bar{C}_2}{nC_1} \right] \quad \text{V-1.3}$$

Suzuoka has calculated the contribution from the second term as a function of $\eta = x/\sqrt{D_v t}$, assuming the grain size is such that $b = 20\sqrt{D_v t}$. Under these conditions he finds the contribution to be small up to $\eta \approx 3$ for a wide range of values of the parameter

$$\beta = 2a(D_b/D_v - 1) / \sqrt{D_v t} \quad V-1.4$$

that enters into the expression for \bar{C}_2 . Diffusion coefficients calculated from the slope of the initial portion of a $\log \bar{C}$ vs x^2 plot, on the assumption that only C_1 contributes to \bar{C} are then too large by about 5%.

In general, the deviations from linearity in the $\log \bar{C}$ vs x^2 curves shown in figs. IV-6.2 to 6.16 are relatively small, and in all but two cases the point for $\eta = 3$, as indicated by the arrows, fall within the linear region. The fact that curvature has not been reported previously is undoubtedly due to the smaller penetration regions analysed. The results of R# 20/7/67-1 are particularly interesting. The two specimens, #31 and O.R.N.L., were annealed together. The initial slopes agree within 4%, in spite of the fact that the curvature in the O.R.N.L. specimen is very much more marked than that of #31. What makes this so unexpected, however, is the fact that the O.R.N.L. specimen was cut from an α phase pseudo-single crystal. There was a very marked substructure present in the specimen as seen from the back reflection Laue film of fig. IV-2.1(c). It is difficult to say if this was the cause for the observation.

It seems reasonable to conclude, however, that the values of D_v obtained from the curves at the lower temperatures, will be affected by the grain boundary diffusion to at least + 5%.

Another source of positive curvature in the $\log \bar{C}$ vs x^2 plots has been considered in Appendix II. It takes into account the possibility that the boundary conditions leading to the expression for C_1 could have been violated. Normally, it is assumed that the ratio $L/\sqrt{Dt} \sim \infty$ where L is the specimen length; the large D 's in this system could result in some reflection of the diffusant from the surface at $x = L$, leading to the observed curvature. However, as shown in Appendix II, the effect is negligibly small.

The second anomaly in the shape of the penetration profile is rather more interesting. Its general form was first observed by the author some time ago during a cursory study of the diffusion of copper in lead single crystals⁽⁷⁸⁾. In the present case the effect appears to be confined to those specimens exhibiting the type of non-linearity discussed above, and to the α phase results. It is not seen in any of the alloy studies for either ^{95}Zr or ^{60}Co in the higher temperature β Zr runs. When it was present, the high initial point, followed by a sharp dip and subsequent rise, formed a smooth curve. This can be seen in the linear plot of \bar{C} vs x of Figure V-1.2. The model proposed to account for it is as follows.

During the annealing, the distribution has the normal Gaussian character of equation II-1.1. As the specimen is cooled, however, the concentration of solute at the surface exceeds the solubility limit and a thin layer of a solute-rich phase forms. This produces a high concentration in the first layer removed, followed by a few slices in which the diffusant has "back-diffused" to the surface. The process continues until the temperature is low enough

to immobilize the atoms.

One would expect the effect in systems in which the diffusion coefficient of a solute of low solubility is high. The excess diffusant in the initial slice should, of course, just balance that removed from the "dip region". That this occurs is clearly shown in figure V-1.2 in which the solid curve is that calculated from the linear portion of the $\log \bar{c}$ vs x^2 plot.

A more quantitative analysis can be made by considering the problem as one of desorption from the specimen into the precipitate. The total material M_0 passing the boundary between the phases at x_0 is then

$$M_0 = - \int_0^t J dt \quad \text{V-1.5}$$

This leads to

$$\frac{M_0}{C_0} = \sqrt{\frac{Dt}{\pi}} \quad \text{V-1.6}$$

where C_0 is the initial concentration prior to the quench, and t the effective time during which diffusion occurs.

The amount M_0 observed can be accounted for if $D \approx 5 \times 10^{-7}$ cm^2/sec and $t \approx 6$ seconds.

It remains to account for the absence of the effect in the other runs. Apart from those concerned with ^{95}Zr diffusion, in which no effect was seen, nor expected from the foregoing, there are the ^{60}Co runs in both the alloys and the high temperature anneals. The lack of the effect in the alloys is consistent with the model, of course, since the content of inactive cobalt was enough to swamp any effect from the extremely small quantity of tracer. Moreover, the degree of supersaturation would be uniform

throughout the specimen and hence no redistribution would be expected.

The absence of the effect for ^{60}Co diffusion in the higher temperature runs is not so readily understood. Discussion of this point will be deferred until the more general development of a model to account for other, related observations is complete.

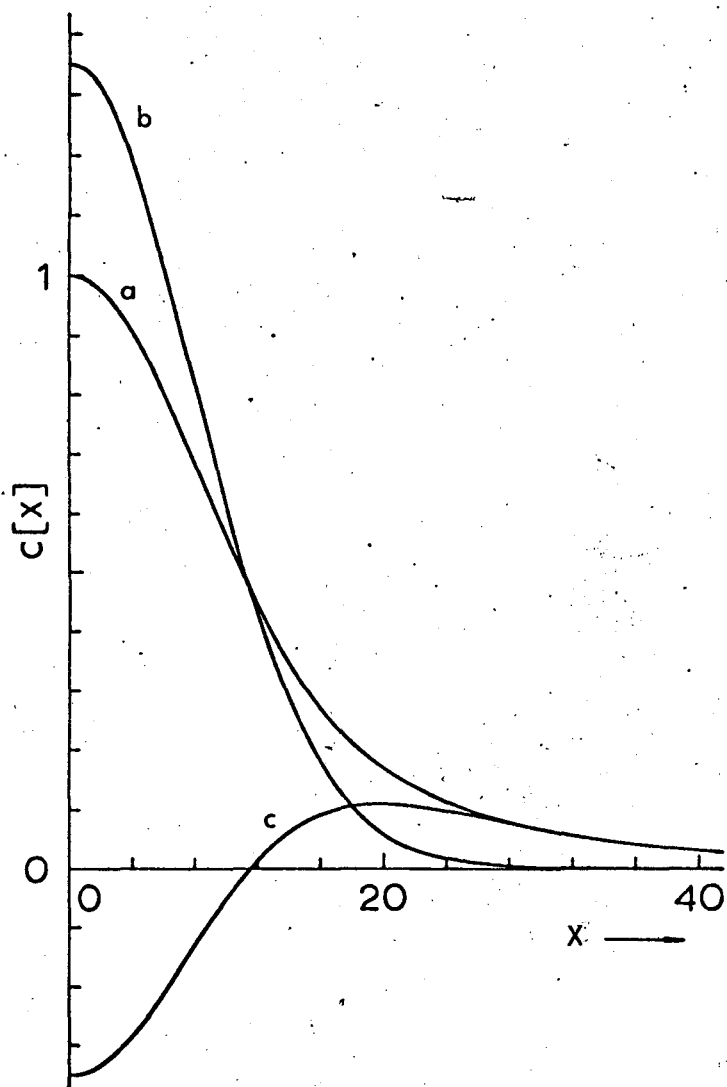


Fig. V-1.1

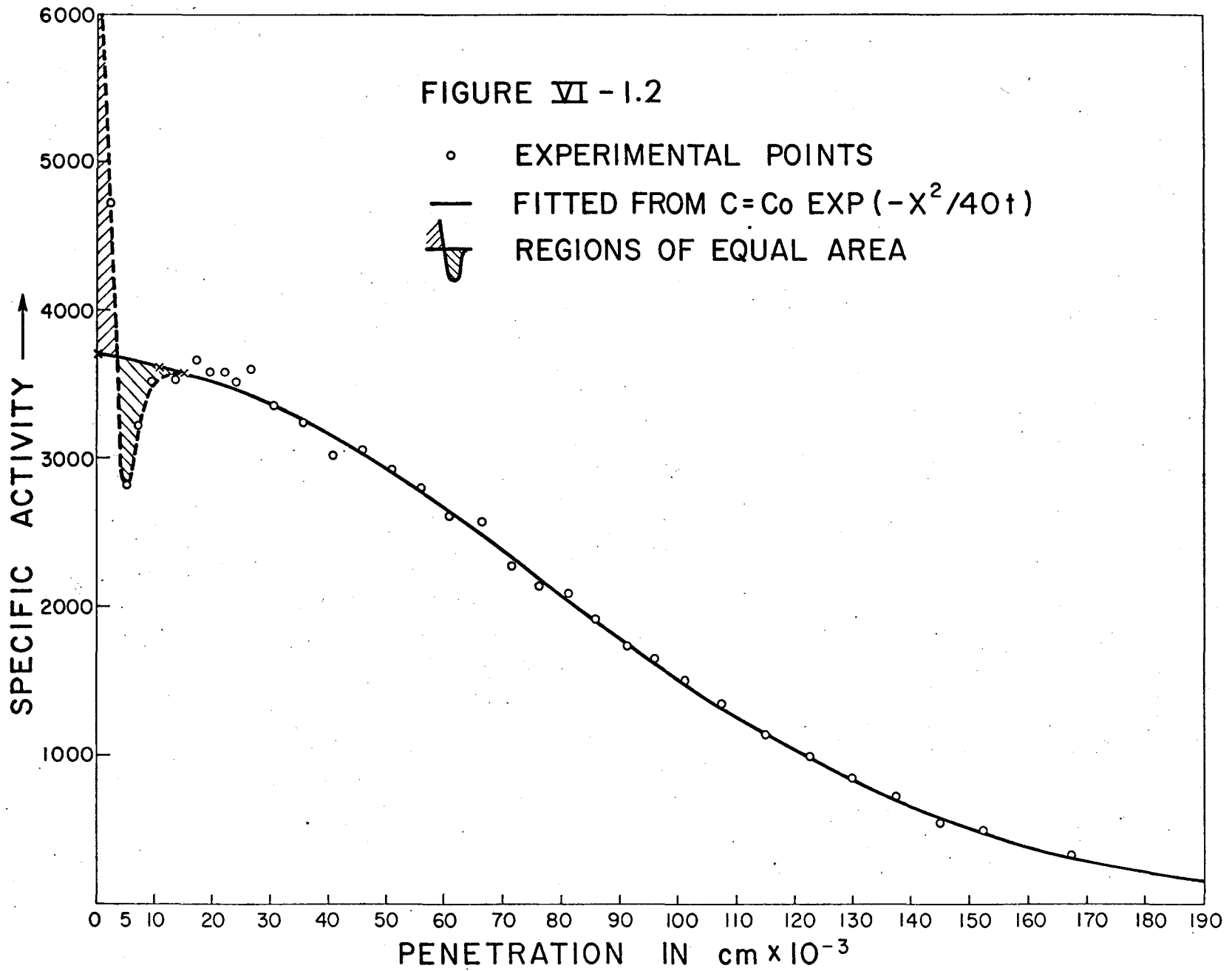
Decomposition of a concentration profile,
according to Suzuoka⁽³⁹⁾.

(a) \bar{c}

(b) c_1

(c) $\frac{1}{b} \bar{c}_2$

FIGURE VI - 1.2



The one feature common to all of the mechanisms proposed to account for the diffusion behaviour of the b.c.c. structures of Zr, Ti and U is that in one way or another, the vacancy mechanism is invoked. In the case of the one mechanism hypothesis the unusually fast diffusion and low D_0 and Q values are attributed to low values of H_V^m or H_V^f or both, although the details may differ from one model to another. In the two mechanism hypotheses the vacancy mechanism is assumed to be dominant at high temperatures with D_0 and Q values close to those of the normal systems, while different suggestions have been put forward regarding the second mechanism that is assumed to dominate at the lower temperatures. In an attempt to infer which of these two categories is most consistent with all of the experimental facts, one important point must be borne in mind. That is, that if a single vacancy mechanism occurs at the lower temperatures, it is only the magnitudes of the activation enthalpies that are unusual; the model must be consistent with any effects that are essentially phenomenological in their origin. We propose to examine this point by considering the implications of the results of the alloy experiments. The temperature at which these measurements were made was deliberately chosen in the range in which the differences between the two proposals would be maximized. Our method shall be to assume the single vacancy mechanism is operative, derive a relationship between measurable

parameters based on this assumption, and show that the present results are inconsistent with it. Alternative models will then be considered.

V - 3 THE EQUILIBRIUM DISTRIBUTION OF FREE AND ASSOCIATED VACANCIES IN A DILUTE B.C.C. ALLOY

Lidiard⁽¹⁸⁾ has discussed the effect of solutes on the diffusion of solvent atoms in a dilute f.c.c. alloy, assuming a vacancy mechanism. In order to adapt his method to a b.c.c. alloy, we require to know the number of free vacancies and associated vacancy-solute pairs in the alloy.

Reference to figure V-3.1 indicates a significant difference between the jump sequences of a vacancy in the vicinity of an impurity in f.c.c. compared to b.c.c. alloys. In the former, there are solvent atoms in the near neighbor coordination shell of an impurity that are also near neighbor to an associated vacancy. Thus the vacancy can exchange with such solvent atoms and remain associated with the solute.

This cannot occur in the b.c.c. atom. Any solvent-vacancy exchange in the latter moves an associated vacancy to a second, third or fifth near neighbor shell.

In the following it will be assumed that vacancy-solute interactions are appreciable in both the first and the second near neighbor shells but are negligible at larger distances. We shall follow the method of Lidiard⁽¹⁸⁾ in calculating the Gibbs free energy of the system, in a somewhat more general way. The resulting equations yield the Lidiard expressions when the same simplifying approximations are applied to f.c.c. systems.

Let N = the total number of solvent atoms

N_i = the total number of solute (impurity) atoms

P_k = the fraction of solute atoms that have an associated vacancy in the k th coordination shell, for $k = 1, 2$

n_v = the number of free, i.e. unassociated vacancies

g_v = change in Gibbs free energy less the configurational entropy per free vacancy added to the alloy

$(g_v + \Delta g_k)$ = ditto per vacancy added to the k th coordination shell of an impurity

g_i = ditto per added solute atom

N_s = total number of lattice sites

$$= N + n_v + 2N_i P_1 + 2N_i P_2 + N_i (1 - [P_1 + P_2])$$

$$= N + n_v + N_i + N_i P_1 + N_i P_2 \quad \text{V-3.1}$$

We require to determine the equilibrium numbers of $N_i P_1$, $N_i P_2$ and n_v .

In analogy with the treatment in Appendix AI-1,

$$G(T, P, N, N_i, N_i P_1, N_i P_2, n_v) = G_0(T, P, N) + N_i g_i + N_i P_1 (g_v + \Delta g_1) + N_i P_2 (g_v + \Delta g_2) + n_v g_v - kT \ln \Omega \quad \text{V-3.2}$$

where

$$\Omega = \Omega_{N_i P_1} \cdot \Omega_{N_i P_2} \cdot \Omega_{N_i (1 - [P_1 + P_2])} \cdot \Omega_v \quad \text{V-3.3}$$

The problem of calculating the number of distinguishable arrangements of the defects is treated by the method developed in AI-1. Each time a defect of species m is added to the lattice, α_m sites are excluded from that species and γ_m from subsequent species. If the defect is

not centrally symmetric, such as for associated pairs, there will be β_m distinguishable orientations per pair added. Finally, of course, the indistinguishable permutations amongst the species m must be accounted for.

The number of distinguishable arrangements of the m^{th} species over the N_m sites available to it is

$$\Omega_m = \frac{(\beta_m)^m}{m!} \prod_{s=0}^{m-1} (N_m - \alpha_m s) \quad \text{V-3.4}$$

$$= \frac{(\alpha_m \beta_m)^m \left(\frac{N_m}{\alpha_m} \right)!}{\left[\frac{N_m}{\alpha_m} - m \right]! m!} \quad \text{V-3.5}$$

Using Stirling's approximation, we obtain, after some manipulation:

$$-\ln \Omega_m = m \ln \left(\frac{m}{\beta_m N_m} \right) + \frac{N_m}{\alpha_m} \left(1 - \frac{\alpha_m m}{N_m} \right) \ln \left(1 - \frac{\alpha_m m}{N_m} \right) \quad \text{V-3.6}$$

As in Appendix AI-1, the equilibrium condition for each component r of the system is determined by setting

$$\mu(r_j) = \left(\frac{\partial G}{\partial r_j} \right)_{N, T, P, r_{k \neq j}} = 0 \quad \text{V-3.7}$$

From V-3.6 we obtain

$$-\frac{\partial \ln \Omega_m}{\partial r_j} = \frac{\partial m}{\partial r_j} \ln \left[\frac{m}{\beta_m (N_m - \alpha_m m)} \right] + \frac{1}{\alpha_m} \frac{\partial N_m}{\partial r_j} \ln \left(1 - \frac{\alpha_m m}{N_m} \right) \quad \text{V-3.8}$$

so that V-3.2 gives:

$$\prod_m \left(\frac{m}{\beta_m (N_m - \alpha_m)} \right)^{\frac{\partial m}{\partial r_j}} \left(1 - \frac{\alpha_m}{N_m} \right)^{\frac{1}{\alpha_m} \frac{\partial N_m}{\partial r_j}} = \exp(-g(r_j)/kT)$$

V-3.9

Equation V-3.9 is then the generalization of AI-1.

We identify the species m and the components r as:

$$\begin{aligned} m_1 &= N_i P & r_1 &= N_i P \\ m_2 &= N_i (1-P) & r_2 &= n_v \\ m_3 &= n_v \end{aligned}$$

In his model, Lidiard⁽¹⁸⁾ set

$$\begin{aligned} \alpha_1 &= 2 & \beta_1 &= Z & \gamma_1 &= 2 \\ \alpha_2 &= 1 & \beta_2 &= 1 & \gamma_2 &= Z+1 \\ \alpha_3 &= 1 & \beta_3 &= 1 & & \end{aligned}$$

and

$$\begin{aligned} N_1 &= N_s = N + N_i + N_i P + n_v \\ N_2 &= N_s - 2 N_i P \\ N_3 &= N_s - 2 N_i P - (Z+1) N_i (1-P) \end{aligned}$$

We construct the table

	$\partial/\partial r_1$	$\partial/\partial r_2$	$(1/\alpha)\partial/\partial r_1$	$(1/\alpha)\partial/\partial r_2$
m_1	1	0		
m_2	-1	0		
m_3	0	1		
N_1	1	1	1/2	1/2
N_2	-1	1	-1	1
N_3	Z	1	Z	1

Substituting the appropriate values into V-3.9 gives the relation for $r_1 = N_i P$:

$$\frac{N_i P}{Z N_i (1-P)} \left[1 - \frac{2N_i P}{N_s} \right]^{\frac{1}{2}} \left[1 - \frac{n_v}{N_s - 2N_i P - N_i (1-P)} \right]^Z = \exp-(g+\Delta g/kT)$$

V-3.10

Then setting $2N_i P/N_s$, $n_v/N_s - 2N_i P - N_i (1-P)$, $P \ll 1$

we obtain

$$N_i P = N_i Z \exp -(g + \Delta g/kT)$$

V-3.11

which is the result obtained by Lidiard. Similarly, for $r_2 = n_v$, we obtain

$$\frac{n_v}{N_s - N_i P - Z N_i (1-P)} = \exp -g/kT$$

V-3.12

Equation V-3.12 may be written as

$$C_v \simeq (1 - Z C_i) \exp(-g/kT)$$

V-3.13

where $C_v = n_v/N_s$, $C_i = N_i/N_s$, and we neglect $(Z-1)C_i P$.

Equation V-3.9 can be applied to the slightly more complex system of a dilute b.c.c. alloy in a straightforward way. We retain the same level of approximation as Lidiard, and use the following:

$$\begin{array}{lll} m_1 = N_i P_1 & \alpha_1 = 2 & \beta_1 = Z_1 \\ m_2 = N_i P_2 & \alpha_2 = 2 & \beta_2 = Z_2 \\ m_3 = N_i [1 - (P_1 + P_2)] & \alpha_3 = 1 & \beta_3 = 1 \\ m_4 = n_v & \alpha_4 = 1 & \beta_4 = 1 \end{array}$$

$$\begin{aligned}
 r_1 &= N_i P_1 & \gamma_1 &= 2 \\
 r_2 &= N_i P_2 & \gamma_2 &= 2 \\
 r_3 &= n_v & \gamma_3 &= z_1 + z_2 + 1
 \end{aligned}$$

$$N_1 = N_s = N + N_i + N_i P_1 + N_i P_2 + n_v$$

$$N_2 = N_s - \gamma_1 N_i P_1$$

$$N_3 = N_s - \gamma_1 N_i P_1 - \gamma_2 N_i P_2$$

$$N_4 = N_s - \gamma_1 N_i P_1 - \gamma_2 N_i P_2 - \gamma_3 N_i \left[1 - [P_1 + P_2] \right]$$

Then we again construct a table:

	$\partial/\partial r_1$	$\partial/\partial r_2$	$\partial/\partial r_3$	$(1/\alpha)\partial/\partial r_1$	$(1/\alpha)\partial/\partial r_2$	$(1/\alpha)\partial/\partial r_3$
m_1	1	0	0			
m_2	0	1	0			
m_3	-1	-1	0			
m_4	0	0	1			
N_1	1	1	1	1/2	1/2	1/2
N_2	-1	1	1	-1/2	1/2	1/2
N_3	-1	-1	1	-1	-1	1
N_4	(z_1+z_2)	(z_1+z_2)	1	(z_1+z_2)	(z_1+z_2)	1

Substituting for the appropriate parameters in equation V-3.9 we obtain to first order in C_i

$$N_i P_1 = N_i Z_1 \exp-(g + \Delta g_1/kT) \quad \text{V-3.14}$$

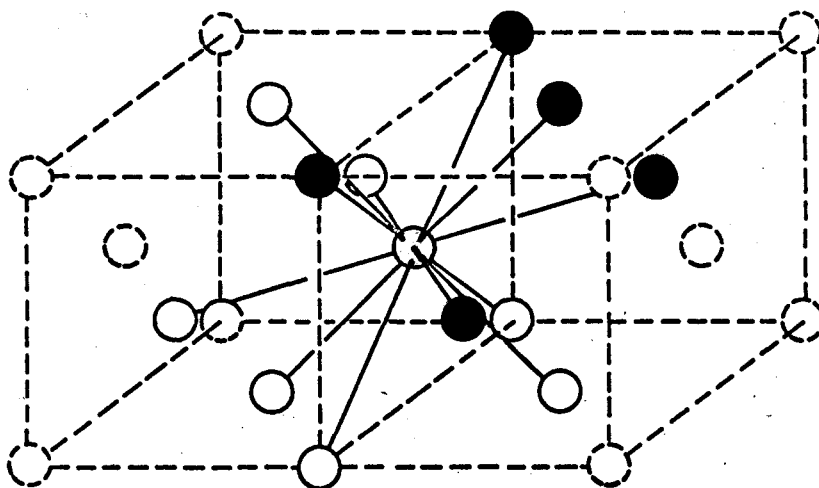
$$N_i P_2 = N_i Z_2 \exp-(g + \Delta g_2/kT) \quad \text{V-3.15}$$

$$\frac{n_v}{N_s - N_i (P_1 + P_2) - (Z_1 + Z_2) N_i [1 - (P_1 + P_2)]} = \exp - g/kT \quad \text{V-3.16}$$

or

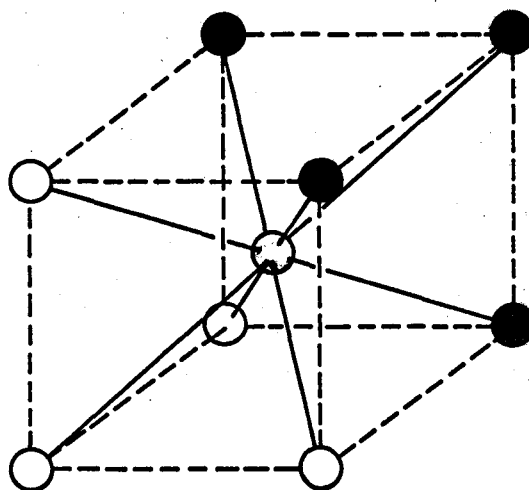
$$c_v \simeq [1 - (Z_1 + Z_2) c_i] \exp - g/kT \quad \text{V-3.17}$$

These results will be used as a basis for the discussion of the influence of solutes on the diffusion of solvent atoms in a dilute b.c.c. alloy, following the method developed by Lidiard⁽¹⁸⁾ for f.c.c. systems.



FACE CENTERED CUBIC

- IMPURITY
- ASSOCIATED VACANCY
- COMMON NEAR NEIGHBOR SITES



BODY CENTERED CUBIC

- IMPURITY
- ASSOCIATED VACANCY
- SITES IN FIRST NN SHELL OF VACANCY BUT SECOND NN SHELL OF IMPURITY

V-4 THE AVERAGE SOLVENT JUMP FREQUENCY IN DILUTE
B.C.C. ALLOYS

As discussed qualitatively in Chapter I-7, the addition of solute impurities to a crystal can influence the solvent-vacancy exchange frequencies. We aim to obtain the average solvent jump frequency in a dilute b.c.c. alloy, consistent with the model adopted in V-3, by following the method for f.c.c. alloys as outlined by Lidiard⁽¹⁸⁾. The method is to consider all distinguishable jump types of the solvent possible, sum them and average over the total number of solvent atoms. The expression for Γ so obtained is then used for the diffusion coefficient, assuming that the correlation factor of the solvent can be approximated by that of the pure crystal. The various types of vacancy-solvent exchange frequencies are, of course, just those that enter the expression for the impurity correlation factor f_i . Our ultimate aim, then, is to relate the latter to the observed change in the solvent diffusion coefficient due to the solute additions.

The distinguishable solvent-vacancy exchanges are as follows:

- W_{00} - from one disassociated site to another.
- W_{02} - " a " " " a second n.n.
- W_{01} - " " " " " " first " .
- W_{20} - " " second n.n. to a disassociated site.
- W_{10} - " " first " " " " " .
- W_{12} - " " " " " " second n.n.
- W_{21} - " " second " " " first " .

The number of first n.n. (near neighbour) vacancy-solute pairs is $N_i P_1$. From figure V-3.1 it is clear that each such pair can contribute $(3W_{12} + 4W_{10})$ jumps/sec to the total solvent jumps so that the total number of solvent jumps per second is

$$N_i P_1 (3W_{12} + 4W_{10}) \quad \text{V-4.1}$$

Similarly, the number from second n.n. vacancy-solute pairs is

$$N_i P_2 (4W_{21} + 4W_{20}) \quad \text{V-4.2}$$

The number of solute atoms that have no associated vacancies in either the first or the second n.n. shells is

$$N_i [1 - (P_1 + P_2)] \quad \text{V-4.3}$$

The probability that a given site in the crystal is occupied by such an atom is

$$\frac{1}{N_s} \cdot N_i [1 - (P_1 + P_2)] = C_i [1 - (P_1 + P_2)] \quad \text{V-4.4}$$

Similarly, the probability that a given site is occupied by a free vacancy is n_v/N_s . From figure V-4.1(b) we see that there are 20 sites from which a disassociated vacancy can move into a first n.n. site of an impurity in one jump (excluding, of course, second n.n. sites to the impurity). Similarly, figure V-4.1(c) shows there are 24 sites from which a disassociated vacancy can move to an associated site in the second n.n. shell of the impurity. The number of free vacancies that are separated by one jump from an associated position of the first kind is then

$$\left(20 C_i [1 - (P_1 + P_2)] \frac{n_v}{N_s} \right) N_s \quad \text{V-4.5}$$

Each such vacancy has a choice of Z_1 near neighbouring solvent atoms with which to exchange. Altogether there are $20 Z_1 C_i [1 - (P_1 + P_2)] n_v$ possible types of vacancy-solvent exchanges from this group. Reference to figure V-4.1(d) shows that from the 20 positions about the impurity, there are 32 distinct W_{01} jumps, the remaining 128 being W_{00} types. Thus the total solvent-vacancy exchanges per second are

$$Z_1 C_i [1 - (P_1 + P_2)] n_v [4W_{01} + 16W_{00}]^* \quad \text{V-4.6}$$

Similarly, from the vacancies separated by one jump from second n.n. sites, there are

$$Z_1 C_i [1 - (P_1 + P_2)] n_v [3W_{02} + 21W_{00}] \quad \text{V-4.7}$$

The remaining $n_v - 44 C_i [1 - (P_1 + P_2)] n_v$ free vacancies contribute

$$Z_1 n_v \left(1 - 44 C_i [1 - (P_1 + P_2)] \right) W_{00} \quad \text{V-4.9}$$

Collecting the terms from V-4.1, 4.2, 4.6, 4.7 and 4.9 and re-arranging, we obtain as the total number of vacancy-solvent exchanges per second:

$$\Gamma \cdot N = N_i P_1 \left\{ W_{10} \left(4 + 4 \frac{P_2}{P_1} \frac{W_{20}}{W_{10}} \right) + W_{12} \left(3 + 4 \frac{P_2}{P_1} \frac{W_{21}}{W_{12}} \right) \right\} \\ + Z_1 n_v W_{00} \left[1 + C_i [1 - (P_1 + P_2)] \left(\frac{4W_{01} + 3W_{02}}{W_{00}} - 7 \right) \right] \quad \text{V-4.10}$$

* where we have used $Z_1 = 8$

Since the aim is to relate Γ to the impurity correlation factor f_i , the same level of approximation used by Manning⁽⁷⁹⁾ in his treatment of the latter will be applied to the vacancy-solvent exchange frequencies appearing in V-4.10. This provides a considerable degree of simplification.

Since only solvent atoms are involved, it is assumed that all pre-exponential factors in the W_{ij} 's are equal; that is

$$W_{ij} = A \exp - g_{ij}/kT \quad \text{V-4.11}$$

where g_{ij} is the change in free energy associated with the exchange of a vacancy at site i with a solvent atom at site j . It can be seen from the schematic diagram in fig. V-4.2 that the differences Δg_1 and Δg_2 , between the formation free energies of the associated vacancies and the unassociated vacancies are related to their free energies of motion. In particular,*

$$g_{21} = g_{12} + (\Delta g_1 - \Delta g_2) \quad \text{V-4.12}$$

$$g_{10} = g_{01} - \Delta g_1 \quad \text{V-4.13}$$

$$g_{20} = g_{02} - \Delta g_2 \quad \text{V-4.14}$$

so that $W_{21} = W_{12} \exp (\Delta g_2 - \Delta g_1/kT) \quad \text{V-4.15}$

$$W_{10} = W_{01} \exp (\Delta g_1/kT) \quad \text{V-4.16}$$

$$W_{20} = W_{02} \exp (\Delta g_2/kT) \quad \text{V-4.17}$$

The remaining approximation is to assume

$$g_{01} = g_{02} \quad \text{V-4.18}$$

so that $W_{01} = W_{02} \quad \text{V-4.19}$

* Note that the zero point is taken as that of a dis-associated vacancy at a lattice point. Thus $\Delta g < 0$.

With these relations and those developed in V-3 for P_1 , P_2 and n_v , we have

$$4 \frac{P_2}{P_1} \frac{W_{20}}{W_{10}} = 4 \frac{P_2}{P_1} \frac{W_{21}}{W_{12}} = 3 \quad \text{V-4.20}$$

using $Z_2 = 6$, $Z_1 = 8$

$$\text{and } \left(\frac{4W_{01} + 3W_{02}}{W_{00}} - 7 \right) = 7 \left(\frac{W_{01}}{W_{00}} - 1 \right) \quad \text{V-4.21}$$

Dividing both sides of V-4.10 by N_s , using the relations in V-4.20 and 4.21 above and substituting for n_v/N_s from V-3, we obtain

$$\begin{aligned} \Gamma \frac{N}{N_s} &= Z_1 \exp(-g/kt) C_i \exp(-\Delta g_1/kT) \left[\frac{6W_{12} + 7W_{10}}{W_{00}} \right] W_{00} \\ &+ Z_1 \exp(-g/kT) W_{00} \left[1 + 7C_i \left[1 - (P_1 + P_2) \right] \left(\frac{W_{01}}{W_{00}} - 1 \right) \right] (1 - 14 C_i) \end{aligned} \quad \text{V-4.22}$$

From the second term

$$\begin{aligned} \left[1 + 7 C_i \left[1 - (P_1 + P_2) \right] \left(\frac{W_{01}}{W_{00}} - 1 \right) \right] (1 - 14 C_i) &\approx 1 - 21 C_i \\ &+ 7 C_i \frac{W_{01}}{W_{00}} + O C_i^2 \end{aligned} \quad \text{V-4.23}$$

for $1 \gg P_1 + P_2$.

Substituting V-4.23 into 4.22 and using

$$W_{01} = W_{10} \exp(-\Delta g_1/kT)$$

we obtain

$$\Gamma = \frac{N_s}{N} \left\{ Z_1 \exp(-g/kT) W_{00} \left[1 - 21 C_i + C_i \exp(-\Delta g_1/kT) \left(\frac{6W_{12} + 14W_{10}}{W_{00}} \right) \right] \right\}$$

$$\Gamma = Z_1 \exp(-g/kT) W_{00} \left[1 - 20 C_i + C_i \exp(-\Delta g_1/kT) 6 \left(\frac{W_{12} + \frac{7}{3} W_{10}}{W_{00}} \right) \right]$$

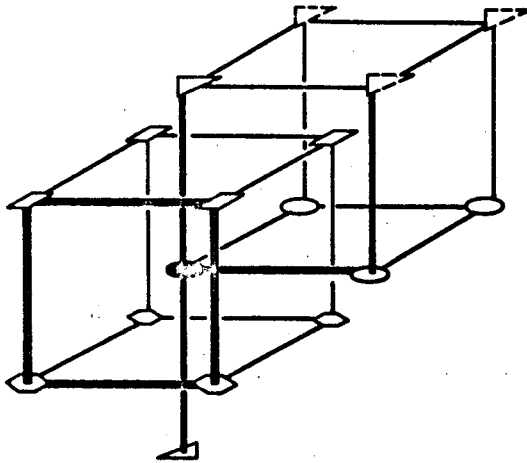
V-4.24

where we used $\frac{N_s}{N} \approx 1 + C_i$

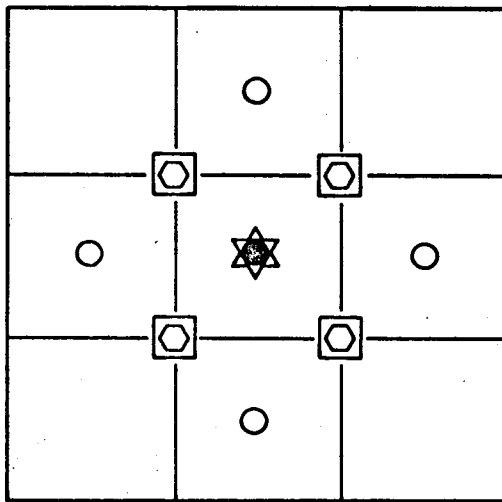
Γ is the average solvent jump frequency in the dilute alloy.

FIGURE V-4.1

VACANCY-SOLVENT EXCHANGES IN A B.C.C. LATTICE CONTAINING IMPURITIES

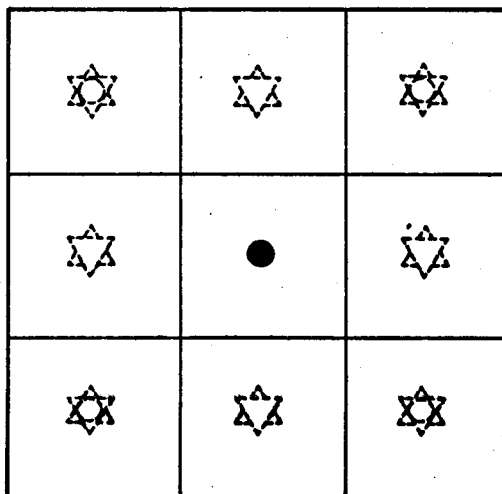


THE BODY-CENTERED CUBIC LATTICE, SHOWING AN IMPURITY ATOM AND ITS NEIGHBORING SITES



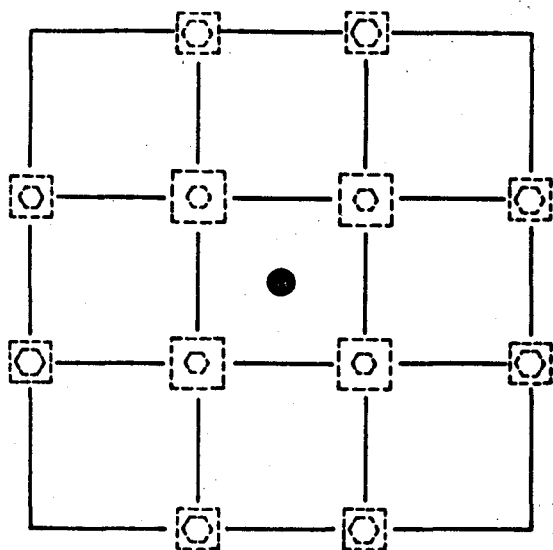
- IMPURITY ATOM
- ○ FIRST NEAR NEIGHBOR SITES
- △ ▽ ○ SECOND NEAR NEIGHBOR SITES

FIG V-4.1(A)



- IMPURITY ATOM
- △ ▽ ○ THE 20 SITES FROM WHICH A VACANCY CAN MOVE TO A FIRST NEAR NEIGHBOR SITE IN ONE JUMP. SECOND NEAR NEIGHBOR SITES ARE EXCLUDED.

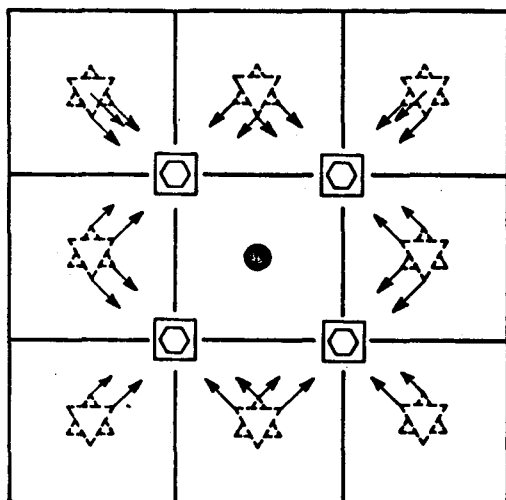
FIG V-4.1(B)



● IMPURITY ATOM

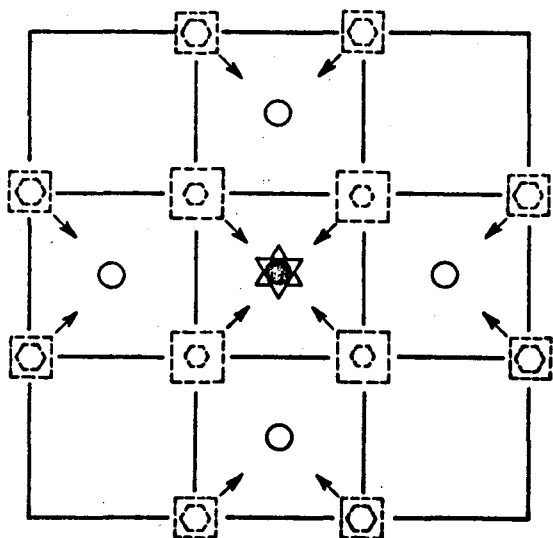
□ □ ○ ○ THE 24 SITES FROM WHICH A VACANCY CAN MOVE TO A SECOND NEAR NEIGHBOR SITE IN ONE JUMP. FIRST NEAR NEIGHBOR SITES ARE EXCLUDED.

FIG V-4.1(C)



THE 32 DISTINCTIVE WAYS IN WHICH A VACANCY CAN MOVE TO A FIRST NEIGHBOR SITE IN ONE JUMP,

FIG V-4.1(D)



THE 24 DISTINCTIVE WAYS IN WHICH A VACANCY CAN MOVE TO A SECOND NEAR NEIGHBOR SITE IN ONE JUMP.

FIG V-4.1(E)

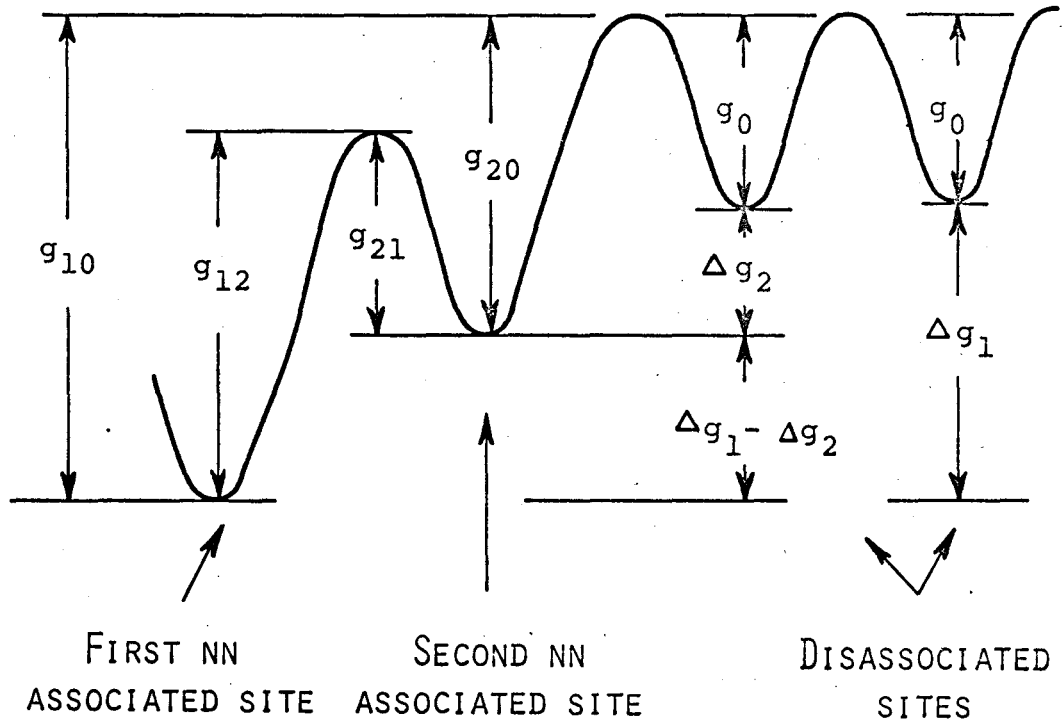


FIGURE V-4.2

SCHEMATIC DIAGRAM TO SHOW RELATIONS BETWEEN VACANCY-SOLUTE BINDING FREE ENERGIES Δg_1 , Δg_2 AND VACANCY-SOLVENT MOTION FREE ENERGIES g_{ij} ASSUMED IN THE MODEL OF THE TEXT.

V-5 THE SOLUTE CORRELATION FACTOR IN A DILUTE B.C.C. ALLOY

In sections I-4 and I-5 it was shown that the self diffusion coefficient could be written as

$$D_s(o) = \frac{a^2}{6} \Gamma_o f_o$$

$$= \frac{a^2}{6} Z_1 \exp(-g/kT) W_{oo} f_o \quad \text{V-5.1}$$

If we assume, with Lidiard⁽¹⁸⁾, that the solvent correlation factor f_o is only "weakly perturbed" by the presence of the impurities, we may write from V-4.24 and V-5.1

$$D_s(C_i) = D_s(o) \left[1 + bC_i \right] \quad \text{V-5.2}$$

where

$$b = -20 + 6 \frac{(W_{12} + \frac{7}{3} W_{10})}{W_{oo}} \exp(-\Delta g_1/kT) \quad \text{V-5.3}$$

We require to relate b and other measurable parameters to the impurity correlation factor, calculated on the same model as used in the foregoing. * We shall therefore adopt the form of f_i as developed by Manning⁽⁷⁹⁾ and modified by LeClaire⁽⁸⁰⁾ to account for the effect of returning vacancies.

Transforming his notation to our own gives

* Peterson and Rothman⁽⁵¹⁾ have considered this problem. However, they make several unnecessary approximations and their final result appears to be in error.

$$f_i = \frac{W_{12} + \frac{3}{2} W_{10} + \frac{1}{2} \left(\frac{W_{12} W_{20}}{2W_{21} + W_{20}} \right)}{W_2 + W_{12} + \frac{3}{2} W_{10} + \frac{1}{2} \left(\frac{W_{12} W_{20}}{2W_{21} + W_{20}} \right)} \quad \text{V-5.4}$$

where W_2 is the vacancy-solute exchange frequency.
Consider the term

$$\frac{W_{12} W_{20}}{2W_{21} + W_{20}}$$

From equations V-4.15, 4.17 and 4.19

$$\begin{aligned} \frac{W_{20}}{2W_{21} + W_{20}} &= \frac{W_{02} \exp(\Delta g_2/kT)}{2W_{12} \exp(\Delta g_2 - \Delta g_1/kT) + W_{02} \exp(\Delta g_2/kT)} \\ &= \frac{W_{10}}{2W_{12} + W_{10}} \end{aligned} \quad \text{V-5.5}$$

where we have used $W_{02} \exp \Delta g_1/kT = W_{10}$ by virtue of V-4.19 and V-4.16. Thus equation V-5.4 becomes

$$f_i = \frac{W_{12} + \frac{3}{2} W_{10} + \frac{1}{2} \left(\frac{W_{12} W_{10}}{2W_{12} + W_{10}} \right)}{W_2 + W_{12} + \frac{3}{2} W_{10} + \frac{1}{2} \left(\frac{W_{12} W_{10}}{2W_{12} + W_{10}} \right)} \quad \text{V-5.6}$$

Equation I-5.3 permits us to write for the tracer diffusion coefficient of the impurity in the pure solvent

$$D_i(o) = \frac{a^2}{6} Z_1 \exp(-g/kT) W_2 f_i \exp(-\Delta g_1/kT) \quad \text{V-5.7}$$

which, when combined with V-5.1 and V-5.6 gives

$$\left(\frac{f_o}{1-f_i}\right)\left(\frac{D_i(o)}{D_s(o)}\right)\exp \Delta g_1/kT = \frac{W_{12}}{W_{oo}} \left[1 + \frac{R}{2} \left(3 + \frac{1}{R+2}\right)\right] \quad V-5.8$$

where $R = W_{10}/W_{12}$.

But from V-5.3

$$\left(\frac{b+20}{6}\right)\exp \Delta g_1/kT = \frac{W_{12}}{W_{oo}} \left[1 + \frac{7}{3} R\right] \quad V-5.9$$

so that

$$\left(\frac{b+20}{6}\right)\left(\frac{1-f_i}{f_o}\right)\left(\frac{D_s(o)}{D_i(o)}\right) = \frac{1 + \frac{7}{3} R}{1 + \frac{R}{2} \left(3 + \frac{1}{R+2}\right)} = \Psi \quad V-5.10$$

Then

$$f_i = 1 - \frac{6 \Psi f_o D_i(o)}{(b+20) D_s(o)} \quad V-5.11$$

Equation V-5.11 cannot be evaluated further without an explicit knowledge of R and hence Ψ . However, two limiting cases can be considered. In the first, the vacancies are assumed to be tightly bound to the impurity so that

$$W_{10} \ll W_{12}$$

$$\text{and } R \rightarrow 0$$

Then $\Psi = 1$ and

$$f_i (R=0) = 1 - \frac{6 f_o}{(b+20)} \left(\frac{D_i(o)}{D_s(o)}\right) \quad V-5.12$$

In the second limiting case, the vacancies are not bound at all, so that

$$W_{10} = W_{12}$$

$$\text{and } R \rightarrow 1$$

$$\text{Then } \Psi = \frac{5}{4}$$

$$\text{and } f_i (R=1) = 1 - \frac{7.5 f_o}{(b+20)} \left(\frac{D_i(o)}{D_s(o)} \right) \quad \text{V-5.13}$$

Values of $R > 1$ can be excluded since they would imply a repulsive interaction between the impurity and vacancy. This is contrary to the evidence given by the enhancement of the zirconium diffusion rate by the addition of cobalt.

A check on the self consistency of the expression for f_i can be made by comparing it with f_o as $D_i(o)/D_s(o) \rightarrow 1$ and $b \rightarrow 0$.

The known value of $f = 8/11 = 0.7272$ as determined by Compaan and Haven⁽⁶⁾. Then, using V-5.13, since $R = 1$ for self diffusion, we obtain

$$\begin{aligned} f_i \left[R=1, D_i/D_s = 1, b = 0 \right] &= 1 - \frac{15}{2 \times 20} \cdot \frac{8}{11} \\ &= \frac{8}{11} \end{aligned} \quad \text{V-5.14}$$

A further check is made by noting that from V-5.3, $b = 0$ implies $\frac{20}{6} W_{00} = W_{12} + \frac{7}{3} W_{10}$

$$\text{for } W_{00} = W_{12} = W_{10} \text{ and } \Delta g_1 = 0 \quad \text{V-5.15}$$

We conclude that the development is correct and are in a position to apply it to the results obtained in the present study.

V-6. THE MECHANISM OF DIFFUSION IN B.C.C. Zr

The developments in the preceding sections indicate that small additions of the fast diffusing cobalt atoms should produce a linear increase in the diffusion coefficient of the solvent atoms in β Zr if the process is primarily associated with the simple vacancy mechanism. It is also shown that the solute correlation factor should be closely related to and derivable from measurements of this increase.

The expressions obtained in V-5.2, V-5.3 and V-5.11 have the same form as those developed by Lidiard for f.c.c. lattices. His equations have recently been applied by Rothman and Peterson⁽⁸¹⁾ to the results of their study of the diffusion of silver in dilute Ag-Zn alloys. They find a smooth linear increase in $D(\text{Ag})$ with increasing zinc concentration. The solute correlation factor they derive from these results agrees well with that obtained from their complementary isotope measurements, using the method outlined in I-6.

This kind of agreement in a system for which the vacancy mechanism has been well established is a reassuring indication of the general soundness of the model.

From figures V-6.1 and 6-2, however, it is evident that the results of the present investigation do not follow the expected behaviour. There is no enhancement of $D_s(\text{C})$, the diffusion coefficient of ^{95}Zr , in the alloy containing 0.4 at.% cobalt. If anything, there may be a small decrease between the pure reference material and the 0.4% alloy,

although the effect is within experimental error.

Between 0.4 and 1.6 % cobalt $D_s(C)$ does follow a linear increase and then appears to taper off at 2.0 at.% cobalt, the latter suggesting a saturation effect. The slope of the linear portion between 0.4 and 1.6% yields a value of

$$b = 94.3 \quad \text{V-6.1}$$

If we ignore for the moment the lack of increase in the initial range and use this value of b , along with the ratio

$$D_i(o)/D_s(o) = 384 \quad \text{V-6.2}$$

appropriate to the annealing temperature of 933°C, we find for the two limiting cases,

$$f_i (R=1) = -17.3 \quad \text{V-6.3}$$

$$f_i (R=0) = -13.6 \quad \text{V-6.4}$$

Both of these values, of course, are inconsistent with the physical requirement that

$$0 \leq f_i \leq 1 \quad \text{V-6.5}$$

From an examination of equation V-5.11, where

$$f_i = 1 - \frac{6 \Psi f_o}{(b+20)} \left(\frac{D_i(o)}{D_s(o)} \right)$$

it is clear that the large negative values of f_i are related to the very large ratio of $D_i(o)/D_s(o)$ which is not compensated by a proportionately large value of b . In fact, the measured ratio would require a value of $b \approx 2 \times 10^3$ to

produce a value of $f_i \approx 1/2$.

We conclude from these failures of the model that the results obtained are not consistent with a simple vacancy mechanism as assumed in arriving at equation V-5.11.

It remains to re-examine the results within the framework of the two mechanism hypothesis. We shall begin by assuming that one of the components is associated with the vacancy mechanism in which the parameters controlling the vacancy concentration and mobility are characteristic of "normal" systems. The second component will be assumed to arise from rapid diffusion along dislocations.

It was first pointed out by Hart⁽⁸²⁾ that if the atoms move along dislocation segments with a diffusivity D^d and through the bulk with a diffusivity D^v , then provided the segment length is small relative to the total diffusion length, the resulting concentration profiles will have a shape characteristic of normal bulk diffusion. For self diffusion, the observed coefficient can then be written as

$$D = (1 - g) D^v + g D^d \quad \text{V-6.6}$$

g is the average fraction of time spent by the diffusing atoms in the vicinity of the dislocations and can be taken as the fraction of lattice sites associated with those regions of rapid diffusion. Mortlock⁽⁸³⁾ suggested that if the diffusant is an impurity atom that tends to segregate to the dislocations, equation V-6.6 should be modified to read

$$D_i(o) = (1 - \kappa g) D_i^v + \kappa g D_i^d \quad \text{V-6.7}$$

where κ is the segregation coefficient. Thus the contribution of the second term in V-6.7 will be increasingly important as the degree of segregation increases. The

writer⁽⁷²⁾ noted that one of the features of the extensive studies of solute diffusion in β Ti, as summarized by Graham⁽⁵⁷⁾ is the large range covered by the diffusion coefficients of the solutes. The sequence in which they occur is

$$D_{Ni} \approx D_{Co} > D_{Fe} > D_{Mn} > D_{Cr} > D_{Nb} > D_{Mo} \quad V-6.8$$

On the other hand, the degree of solubility σ , which should be closely related to the segregation coefficient κ , lie in the order

$$\sigma_{Ni} \approx \sigma_{Co} < \sigma_{Fe} < \sigma_{Mn} < \sigma_{Cr} < \sigma_{Nb} < \sigma_{Mo} \quad V-6.9$$

A completely parallel set of relationships are found for solutes in γ U as well⁽⁷²⁾.

These points seem especially relevant to the present results in three respects. If both $D_i(o)$ and $D_s(o)$ are strongly influenced by dislocation effects, their observed ratio $D_i(o)/D_s(o)$ may bear little, if any, relation to the parameter b . On the other hand, if only that component of $D_i(o)$ associated with vacancies is assumed to influence the corresponding portion of $D_s(o)$, the ratio (D_i^v/D_s^v) could be quite consistent with the observed value of b . More specifically if we write

$$\frac{D_i^v}{D_s^v} = \frac{b + 20}{6 f_o \Psi} (1 - f_i) \quad V-6.10$$

$$\text{we find } D_i^v/D_s^v = 20.9 (1 - f_i) \quad \text{for } R = 1 \quad V-6.11$$

$$= 16.7 (1 - f_i) \quad \text{for } R = 0 \quad V-6.12$$

so that a value of

$$D_i^v/D_s^v \approx 10 \quad V-6.13$$

would correspond to $f_i \sim 1/2$.

Segregation of the cobalt atoms to dislocations and grain boundaries could be responsible for the absence of any significant increase in the diffusion of ^{95}Zr in the 0.4 at.% cobalt alloy by reducing the number of atoms dissolved in the matrix itself to a level too small to have any measureable effect on D_s^v .

Finally, we note that the decrease of the diffusion coefficient of ^{60}Co with increasing solute concentration in the alloy is again consistent with segregation effects. In this case, the saturation of the dislocations with inactive cobalt additions would reduce the free energy difference between the matrix and the regions of fast diffusion around the dislocations. This would reduce the average time spent by a ^{60}Co atom near the dislocations in the alloy relative to that in a cobalt free specimen.

These qualitative considerations that appear consistent with the dislocation hypothesis in the present investigation are supported by evidence from other studies.

For example, Peart and Tomlin⁽⁵⁵⁾ found that the coefficient of the normally slow diffusing solute ^{95}Nb in β Ti was increased by additions of fast diffusing iron atoms, whereas that of ^{59}Fe was decreased. Rothman and Peterson⁽⁵¹⁾ found that additions of up to 0.2 at.% cobalt produced a negligible effect on the diffusion of Uranium in γU at 822°C, in a manner very like that observed in β Zr. This is in sharp contrast to the behaviour in the Ag-Zn alloys reported by the same authors.

The unexpected effects of pressure on the diffusion of ^{59}Fe in pure β Ti and in Ti-Fe alloys as reported by Peart⁽⁵⁹⁾ can be accounted for on the basis of the foregoing as well. It will be recalled from chapter II-2, that

Peart observed a decrease in $D(^{59}\text{Fe})$ in the alloys with increasing pressure, but an increase in $D(^{59}\text{Fe})$ in the pure material, as shown in figure II-2.2. The latter effect could be due to an increased segregation of the tracer to the dislocations as a result of the applied pressure, with a consequent increase in the contribution from the second term in equation V-6.7. Conversely, in an alloy containing 10% iron, the dislocations would be saturated and only the normal vacancy component $(1 - \kappa g)D_i^v$ would be affected. D_i^v would then be expected to decrease with applied pressure, as observed.

It was pointed out in II-2 that Graham⁽⁶¹⁾ measured the correlation factor for self diffusion in γ Fe using the conventional isotope method and found $f_0(1450^\circ\text{C}) = 0.72$ in good agreement with the theoretical prediction for the vacancy mechanism. At 1121°C , however, the diffusion rates of ^{55}Fe and ^{59}Fe were indistinguishable. He noted that a significant amount of grain boundary diffusion occurred at this lower temperature. In applying the method to self diffusion in β Zr Graham found the diffusion rates were completely independent of mass at all the temperatures studied. Again, then, it may be inferred that if the relative disorder associated with grain boundaries is enough to overshadow a mass effect in γ Fe, so also could grain boundaries and/or dislocations do so in β Zr.

There have been at least two objections raised regarding the dislocation hypothesis. The most obvious is that a large dislocation density must be assumed to account for the value of g extracted from an analysis of the non-linear Arrhenius curves. While it was suggested by LeClaire⁽⁸⁴⁾

and the writer⁽⁷²⁾ that this could be due to the martensitic $\alpha \rightarrow \beta$ phase transformation, it has generally been regarded as highly unlikely that a significant density would remain at the high annealing temperatures involved.

The second basis for rejection is the lack of influence of the pre-annealing experiments reported by Kidson and McGurn⁽⁴⁴⁾ as outlined in II-2. The similar observation by Rothman concerning the diffusion of ^{60}Co in γU is also cited.

It is largely because of these objections that the dislocation hypothesis has not found general acceptance. These points make particularly interesting the results of the Laue X-ray studies described in IV-10.

Although the significance of some aspects of the observations are not understood, it seems very clear that the multiple diffraction spots recorded in figure IV-10.10(f) must be associated with polygonization. If we can surmise that this arises from dislocations produced during the transformation it must be concluded that they are essentially immobile at temperatures below 1300°C for times of the order of 3 hours. This, of course, would account for the lack of any effect from the pre-annealing treatment of 30 minutes at 1200°C reported by Kidson and McGurn.

In summary, then, there is a considerable body of indirect evidence from the diffusion measurements, as well as the more direct evidence from the X-ray observations to support the assumption that dislocations make a significant contribution to the diffusion coefficients. The points discussed in II-2 as well as the observed enhancement of D by cobalt additions suggest, on the other hand, that the vacancy mechanism is also important.

Having presented these arguments to justify the assumption that D and D_i are properly represented by V-6.7 and 6.8, we can now more carefully consider the quantitative implications of the alloy measurements.

It was pointed out in chapter II and indicated in figure II-2.1 that the self diffusion results in β Zr could be represented by

$$D(o) = 1.34 \exp(-65200/RT) + 8.5 \times 10^{-5} \exp(-27700/RT) \text{ cm}^2/\text{sec} \quad \text{V-6.14}$$

This representation, of course, is not unique, but was arrived at on the assumption that the vacancy component was "normal" and hence negligibly small at the lower temperatures. That is, it was pre-supposed that

$$(1 - g) D^v \ll gD^d \quad \text{V-6.15}$$

for $T < 1400^\circ\text{C}$.

We shall find, in the following, however, that some aspects of the alloy results cannot be accounted for in a straightforward way on this basis.

In writing equation V-6.10, it has been assumed that all of the observed increase in $D(C)$ is associated with the effect of the component D_i^v on D^v alone. That is

$$\Delta D(C) = (1 - g) \Delta D^v(C) \quad \text{V-6.16}$$

so that

$$\frac{\Delta D(C)}{D(o)} = (1 - g) \frac{\Delta D^v(C)}{D(o)} \quad \text{V-6.17}$$

$$\text{Let us define } \beta = D(o)/(1 - g)D^v(o) \quad \text{V-6.18}$$

Then V-6.17 becomes

$$\frac{\Delta D(C)}{D(o)} = \frac{1}{\beta} \frac{\Delta D^v(C)}{D^v(o)} \quad \text{V-6.19}$$

The value of β at the alloy annealing temperature obtained from the assumed decomposition of $D(o)$ in equation V-6.14 is

$$\beta(933^\circ\text{C}) = 358.$$

Since the observed $\Delta D(C)/D(o) \approx 1$ for $\Delta C \approx 1\%$ (in the range 0.4 to 1.6%), we see that equation V-6.19 requires

$$\frac{\Delta D^v(C)}{D^v(o)} = \beta = 358, \quad \text{V-6.20}$$

a value that is unrealistically large.

We can consider two alternatives. The first is to assume that both D^v and D^d in equation V-6.6 are affected by the cobalt additions. Then, using V-6.18 we can write

$$\frac{\Delta D(C)}{D(o)} = \frac{1}{\beta} \frac{\Delta D^v(C)}{D^v(o)} + \frac{\beta - 1}{\beta} \frac{\Delta D^d(C)}{D^d(o)} \quad \text{V-6.21}$$

$$\approx \frac{1}{358} \frac{\Delta D^v(C)}{D^v(o)} + \frac{\Delta D^d(C)}{D^d(o)} \quad \text{V-6.22}$$

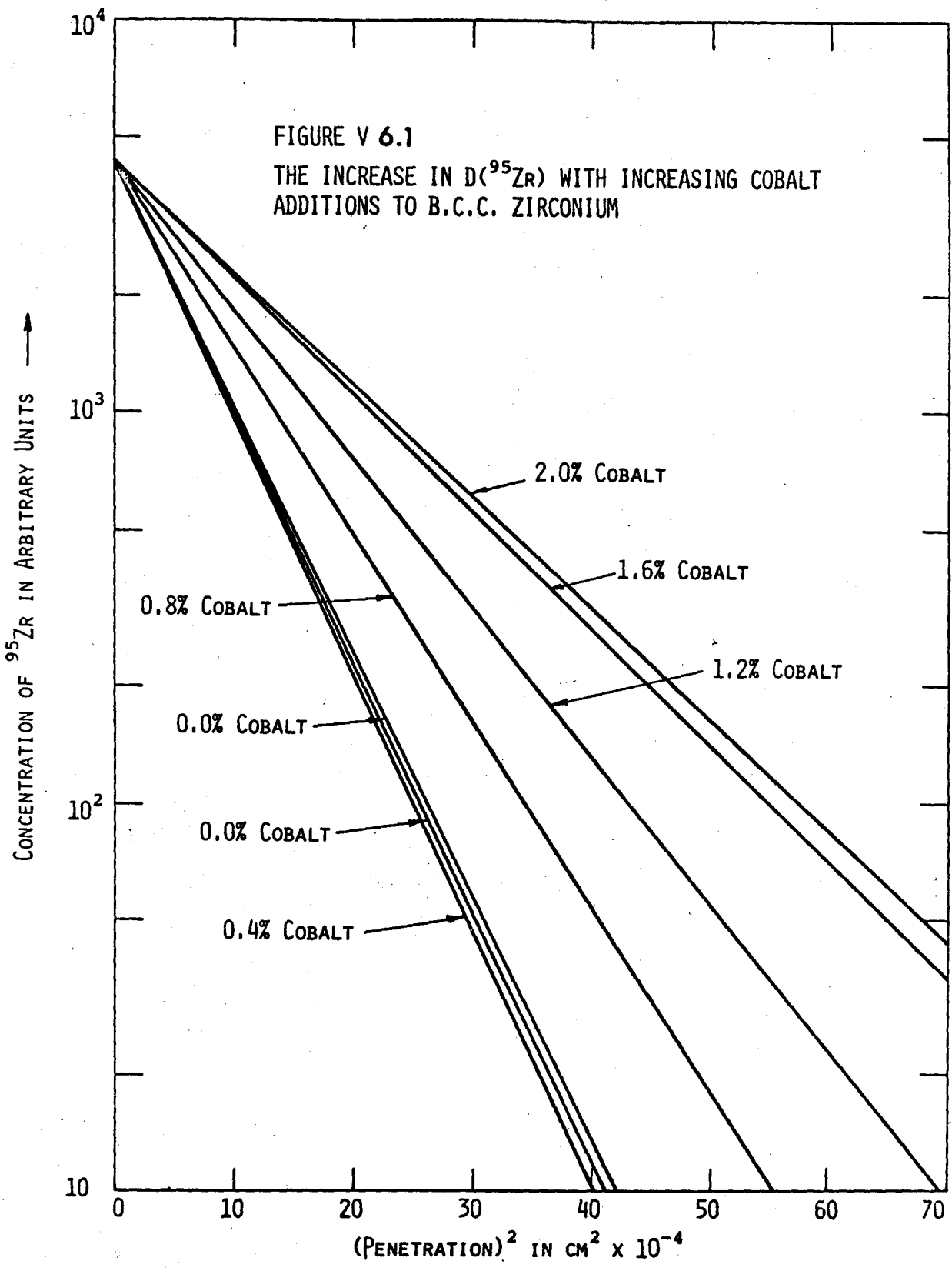
A reasonable value for $\Delta D^v(C)/D^v(o)$ now implies that essentially all of the observed increase in D is due to an increase in the dislocation component. This conclusion is not entirely unreasonable. If the total diffusion coefficient is dominated by the effect of dislocations at the lower temperatures, it may well be that the cobalt additions significantly enhance the solvent diffusion rate in the vicinity of the dislocations, giving rise to the observed $\Delta D(C)$. Of course, if such is the case, the measured parameter b does not have the significance assumed in sections V-4 and V-5.

The foregoing hypothesis does raise some difficulties, amongst which are the lack of any increase in D in the 0.4% alloy and the rather large cobalt concentration required to produce evidence of saturation.

The alternative way of accommodating the alloy results within the vacancy-dislocation hypothesis is to assume that the contribution of the vacancy mechanism is much larger than indicated in equation V-6.14.

While the proponents of the single mechanism effectively assume $\beta = 1$, we have already shown this to lead to a meaningless value of the deduced solute correlation factor. On the other hand, a value of $\beta \sim 5$ is not unreasonable with respect to the ratio $\Delta D(C)/D(o)$ and would still account for the difficulties associated with the correlation factor.

If this assumption is correct, of course, the points argued by the proponents of the one-mechanism school must be largely accepted since such a value of β requires much lower values of D_o^v and Q^v for self diffusion than implicit in the method of decomposition of the Arrhenius curve that led to equation V-6.14.



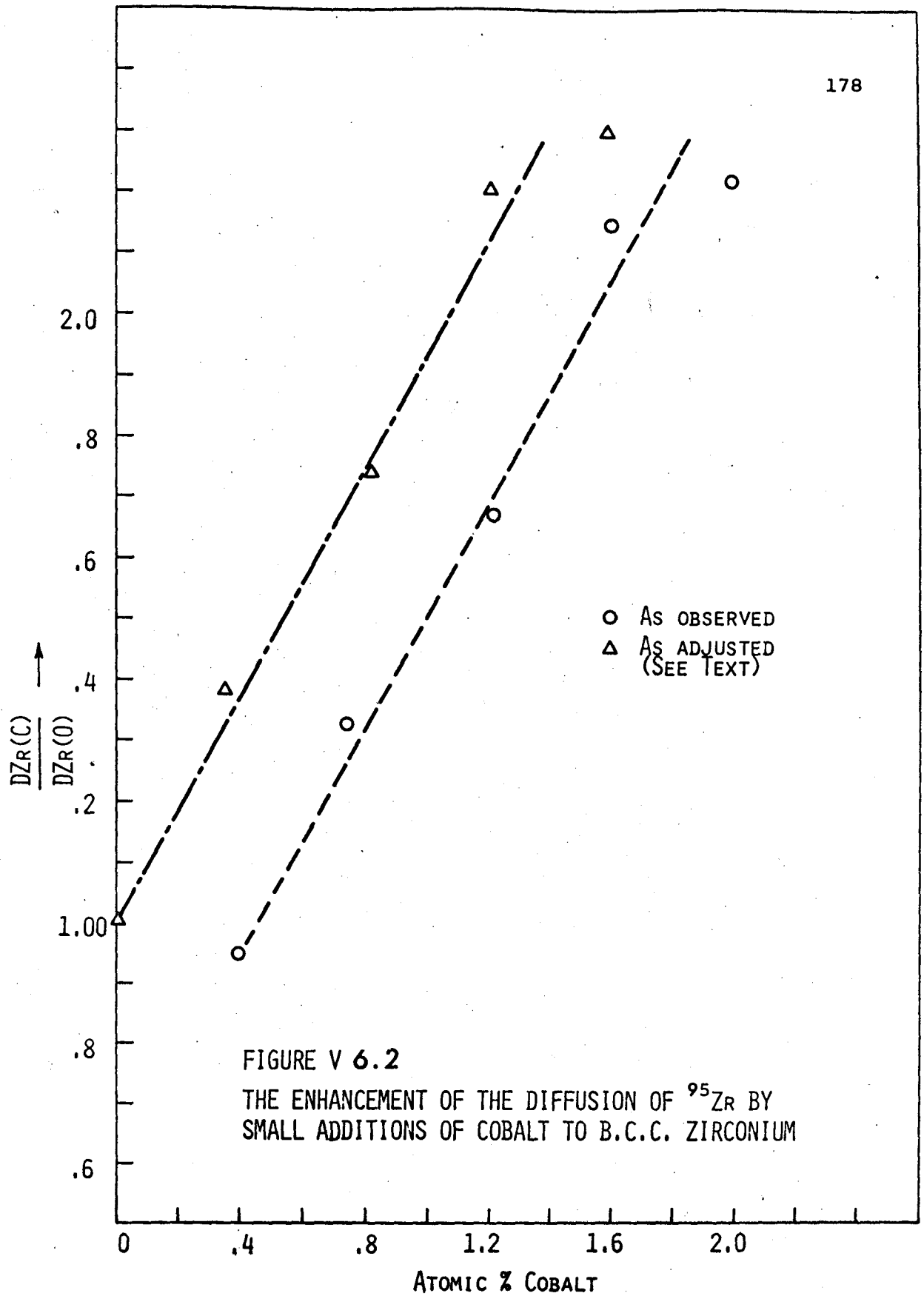
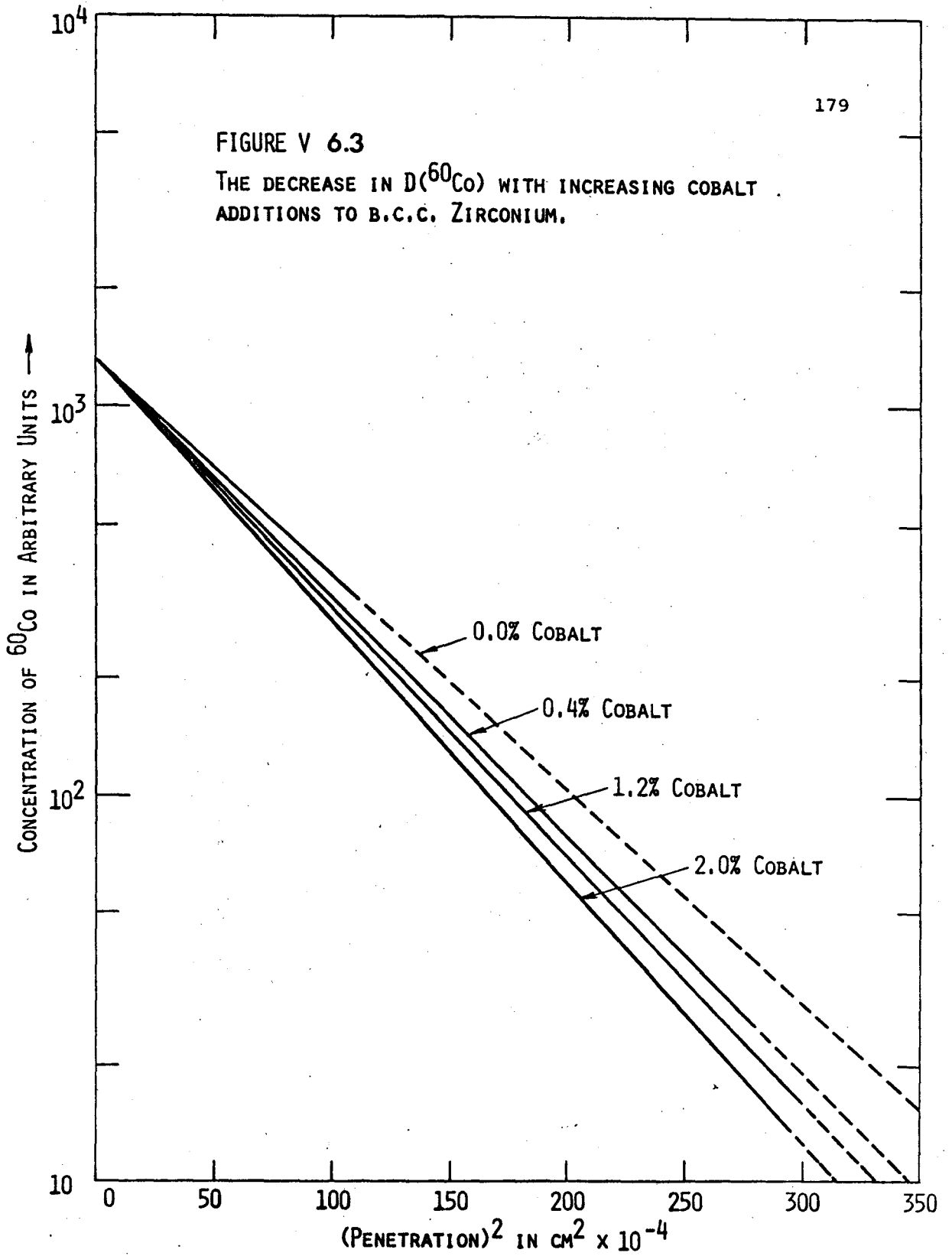


FIGURE V 6.3
THE DECREASE IN $D(^{60}\text{Co})$ WITH INCREASING COBALT
ADDITIONS TO B.C.C. ZIRCONIUM.



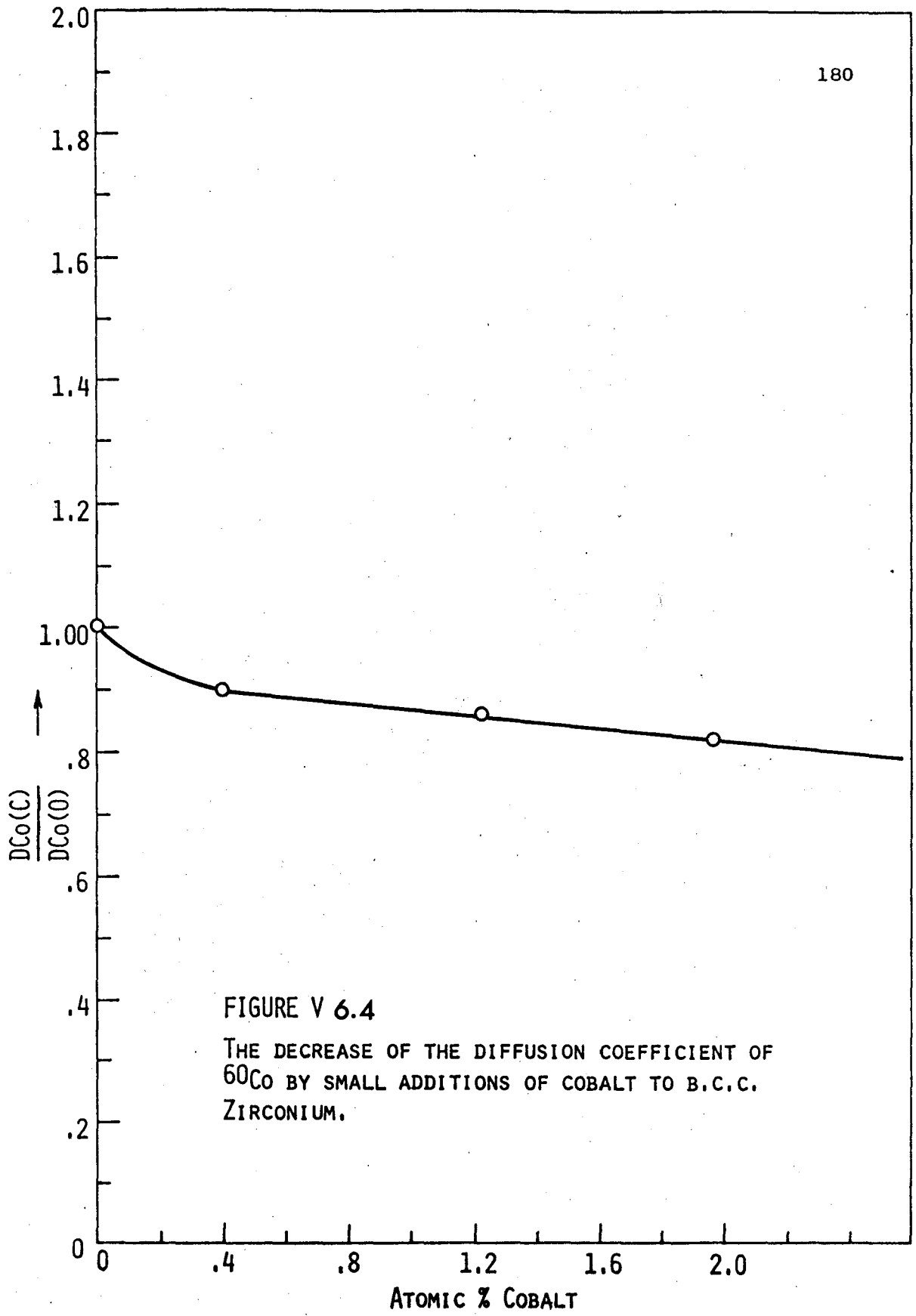


FIGURE V 6.4
THE DECREASE OF THE DIFFUSION COEFFICIENT OF ^{60}Co BY SMALL ADDITIONS OF COBALT TO B.C.C. ZIRCONIUM.

V-7 COBALT SEGREGATION IN β AND α ZIRCONIUM

Some estimate of the segregation coefficient κ for cobalt in β Zr may be inferred from these results if equations V-6.7 and V-6.8 are assumed to be valid. From the latter, we can write

$$\frac{D_i - (1 - \kappa g) D_i^v}{D - (1 - g) D^v} = \frac{\kappa g D_i^d}{g D^d} \quad \text{V-7.1}$$

and using $\beta = D/D^v$, V-7.1 becomes

$$\beta \left(\frac{D_i}{D} \right) - (1 - \kappa g) \left(\frac{D_i^v}{D^v} \right) = \kappa \left(\frac{D_i^d}{D^d} \right) (\beta - (1 - g)) \quad \text{V-7.2}$$

whence

$$\kappa \left(\frac{D_i^d}{D^d} \right) = \frac{\beta \left(\frac{D_i}{D} \right) - \left(\frac{D_i^v}{D^v} \right)}{(\beta - 1 + g) \left(1 - \frac{D_i^v}{D_i^d} \right)} \quad \text{V-7.3}$$

Since even the maximum value of g used in the models described in V-6 satisfy $g \ll 1$, and since it is very reasonable to put $(D_i^v/D_i^d) \ll 1$, equation V-7.3 can be approximated by

$$\kappa \left(\frac{D_i^d}{D^d} \right) = \left(\frac{D_i}{D} \right) + \frac{1}{\beta - 1} \left(\frac{D_i}{D} - \frac{D_i^v}{D^v} \right) \quad \text{V-7.4}$$

Inserting the measured value of $(D_i/D) = 384$ and the assumed

value of $(D_i^v/D^v) \approx 10$ into V-7.4, we obtain

$$\kappa \left(\frac{D_i^d}{D^d} \right) \approx 384 + \frac{374}{\beta-1} \quad \text{V-7.5}$$

V-7.5 reflects the fact that as the assumed values of β increase, the component D^d of self diffusion increases, making the L.H.S. of V-7.5 decrease. The minimum value of the latter, however, is 384. If, for the moment, we assume

$$(D_i^d/D^d) = 1 \quad \text{V-7.6}$$

then

$$\kappa(933^\circ\text{C}) \geq 384 \quad \text{V-7.7}$$

Again, if we assume (86)

$$\kappa \approx \exp Q_k/RT \quad \text{V-7.8}$$

we find

$$Q_k \geq 14 \text{ kcal/mole}$$

$$\approx 0.6 \text{ eV}$$

This large binding energy thus inferred would be reduced to about 8.6 kcal/mole if either the ratio in V-7.6 or a pre-exponential factor in V-7.7 were assumed to be 10 instead of unity.

The rather remarkable results from the diffusion runs in the α phase provide clear evidence for a high degree of segregation in this structure. Even those crystals having only low angle polygonized structures comparable to that indicated in fig. IV-2.1(b) show that grain boundary diffusion dominates in this system.

The inclusion of a segregation coefficient in the analysis of grain boundary diffusion, while not considered explicitly by Suzuoka⁽³⁹⁾ or others, serves only to modify the effective width of the grain boundary. That κ is large in α Zr relative to β Zr is consistent with the markedly lower solubility of cobalt in the former. It is particularly unfortunate that the grain boundary effects so dominate the concentration profiles, that the self-consistent method proposed by Suzuoka cannot be used to extract both D (bulk) and D (grain boundary) for the C.P.H. structure.

Returning to the β phase results, we note that the binding energy of the impurity to the dislocations will reduce the measured activation energy associated with D_i^d , since

$$D_i^d = D_{i0}^d \exp-(Q_i^d - Q_\kappa/RT) \quad \text{V-7.9}$$

In β Ti, the differences between the self and solute diffusion coefficients cannot be ascribed to differences in activation energies alone since there is no clear pattern of increasing slope in the same sequence as decreasing solute diffusion coefficient at a given temperature. This implies that the pre-exponential terms in either D_i^d or D_i^v , or both, must also contribute to the D 's of the impurities.

The diffusion rate of ^{60}Co in β Zr is remarkably fast. The Arrhenius curve, shown in Fig. IV-6.17, is accurately linear from 863°C up to 1600°C, but shows some indication of a positive curvature above that temperature. In this respect the results are more similar to those reported by the Reading University Group⁽⁵⁷⁾ for solute diffusion in β Ti and to those obtained by Peterson and Rothman⁽⁵¹⁾ for γU than they are to the results of studies of self diffusion and solute diffusion in β Zr, as reported by Lundy et al⁽⁵⁷⁾. We conclude that this difference is significant, and that it supports the two mechanism hypothesis since the linear region of the Arrhenius curves occur in the lower temperature range of the fast diffusing solutes. If $\kappa D_i^d \gg (1 - \kappa g) D_i^v$, as suggested in Chapter V, the influence of the vacancy component may be too small to affect the linearity of the Arrhenius plot. Conversely, for self diffusion and diffusion of the slower solutes, D^v becomes increasingly important and hence gives rise to curvature over the whole temperature range.

The physically unreasonable result for the impurity correlation factor deduced from a model based on the vacancy mechanism alone affords a sensitive test between the One and Two-Mechanism hypotheses. Since no argument based on the magnitudes or temperature dependences of the atom-vacancy exchange frequencies alone can account for what is essentially a phenomenological result, we conclude that the basic premise of a vacancy mechanism acting alone is incorrect. It remains a fact, nevertheless, that the quantitative

analysis of the results obtained here are not easily accommodated within the assumption of a normally behaving vacancy component D^V coupled with a very large contribution from dislocations unless one is prepared to accept the rather ad hoc assumption that essentially all of the observed enhancement of the solvent diffusion by cobalt additions can be attributed to effects associated with the dislocation component. While this is by no means an unreasonable view, the alternative assumption that the vacancy component is, in fact, very large, as advocated by the single mechanism proponents, can equally well account for the results*.

In summary, then, while the single mechanism, based on vacancy diffusion, has been shown to be an inadequate model, and while considerable evidence in support of the assumption of a large contribution from diffusion along dislocations has been advanced, there remain unanswered intriguing and challenging questions concerning the diffusion process in this interesting material.

* Such a situation would, of course, confirm the basic tenet of Voltaire's "Candide".

APPENDIX I

AI-1 THE EQUILIBRIUM NUMBER OF SINGLE VACANCIES IN A PURE METAL

In order to establish the method to be applied in section V-3 to a crystal containing solute atoms, free vacancies and associated solute-vacancy pairs, the simpler case of single vacancies in a pure metal will be developed here. We begin by imposing slightly more exacting restrictions than normally assumed and then indicate the approximation used in arriving at the expression quoted in I-7.

- Let N = total number of atoms
- n_v = " " " vacancies
- g = increase per vacancy added of the Gibbs free energy less the configurational entropy
- T = absolute temperature
- P = pressure

We choose as our standard state, the perfect lattice, containing no vacancies, at T and P , and let the associated Gibbs free energy be $G(N, T, P)$. Then for n_v small we may write⁽⁶⁹⁾

$$G(n_v, N, T, P) = G(N, T, P) + n_v g - k T \ln \Omega \quad \text{AI-1.1}$$

where $k \ln \Omega$ is the configurational entropy associated with the vacancies and Ω is the total number of distinguishable

arrangements of the n_v vacancies on the $N + n_v$ lattice sites. In calculating the latter we impose the restriction that no two vacancies can be near neighbours since these would constitute higher order defects.

If $N_s = N + n_v$, there are N_s ways of placing the first vacancy on the lattice, $N_s - \alpha$ of placing the second, $N_s - 2\alpha$ of placing the third, and so on, where α is the number of sites excluded per added vacancy. In the present treatment, we set $\alpha = Z + 1$, where Z is the first near neighbour coordination number.

Then the total number of distinguishable arrangement of vacancies is

$$\Omega = \frac{1}{n_v!} \prod_{k=0}^{n_v-1} [N_s - k\alpha] \quad \text{AI-1.2}$$

where we have divided by $n_v!$ to take into account the indistinguishable permutations among the vacancies.

Equation AI-1.2 can be rearranged to give*

$$\Omega = \frac{\alpha^{n_v} \left(\frac{N_s}{\alpha}\right)!}{\left[\frac{N_s}{\alpha} - n_v\right]! n_v!} \quad \text{AI-1.3}$$

* This implicitly assumes, of course, that (N_s/α) is integral. If not, then $N_s/\alpha = I + \delta$, where I is an integer and δ is of the order of $1/N_s$ since $N_s \gg \alpha$.

Using Stirlings approximation for $\ln x! \approx x \ln x - x$ we obtain

$$\begin{aligned} \ln \Omega &= n_v \ln \alpha + (N_s/\alpha) \ln (N_s/\alpha) - (N_s/\alpha) \\ &\quad - \left[\left(\frac{N_s}{\alpha} - n_v \right) \ln \left(\frac{N_s}{\alpha} - n_v \right) - \left(\frac{N_s}{\alpha} - n_v \right) \right] \\ &\quad - n_v \ln n_v + n_v \end{aligned}$$

which can be written as

$$\ln \Omega = - \left[n_v \ln \left(\frac{n_v}{N_s} \right) - \frac{N_s}{\alpha} \left(1 - \frac{\alpha n_v}{N_s} \right) \ln \left(1 - \frac{\alpha n_v}{N_s} \right) \right] \quad \text{AI-1.4}$$

The condition for equilibrium is

$$\mu_v = \frac{\partial}{\partial n_v} \left\{ G_o(N, T, P) + n_v g - kT \ln \Omega \right\}_{N, T, P} = 0 \quad \text{AI-1.5}$$

From AI-1.4:

$$\frac{\partial \ln \Omega}{\partial n_v} = - \ln \left(\frac{n_v}{N_s - \alpha n_v} \right) \left(1 - \frac{\alpha n_v}{N_s} \right)^{\frac{1}{\alpha}} \quad \text{AI-1.6}$$

so that

$$\left(\frac{n_v}{N_s - \alpha n_v} \right) \left(1 - \frac{\alpha n_v}{N_s} \right)^{\frac{1}{\alpha}} = \exp - g/kT \quad \text{AI-1.7}$$

The usual approximation is to set $\alpha = 1$, whence AI-1.7 becomes

$$\frac{n_v}{N_s} = \exp - g/kT$$

APPENDIX II THE EFFECT OF FINITE SPECIMENS

The boundary value problem, leading to equation II-1.1 is

$$\frac{\partial C(x,t)}{\partial t} = D \frac{\partial^2 C(x,t)}{\partial x^2} \quad \text{AII-1.1}$$

$$C(x,0) = 0, \quad x > 0 \quad \text{AII-1.2}$$

$$\lim_{x \rightarrow \infty} C(x,t) = 0 \quad \text{for all } t. \quad \text{AII-1.3}$$

$$\int_0^{\infty} C(x,t) dx = S_0 \quad \text{for all } t. \quad \text{AII-1.4}$$

If the specimen is of finite length L , and the surfaces at $0, L$ are perfectly reflecting, we replace AII-1.3 and AII-1.4 by

$$\left(\frac{\partial C(x,t)}{\partial x} \right)_{x=L} = 0 \quad \text{for all } t. \quad \text{AII-1.5}$$

$$\left(\frac{\partial C(x,t)}{\partial x} \right)_{x=0} = 0 \quad \text{for } t > 0 \quad \text{AII-1.6}$$

$$\int_0^L C(x,t) dx = S_0 \quad \text{for all } t. \quad \text{AII-1.7}$$

The solution can be obtained by Laplace Transform or Fourier Expansion methods*

* The author is indebted to Dr. S. Kushneriuk of the Theoretical Physics Division, CRNL, for advice and confirmation of the solution obtained.

and is of the form

$$C(x, t) = C_1 \left[1 + \sum_{m=1}^{\infty} \exp -\frac{mL}{Dt} (L-x) + \exp -\frac{mL}{Dt} (L+x) \right] \quad \text{AII-1.8}$$

$$\text{where } C_1 = \frac{S_0}{\sqrt{\pi Dt}} \exp - (x^2/4Dt) \quad \text{AII-1.9}$$

Putting $x = \beta L$, AII-1.8 becomes

$$\frac{C(x, t) - C_1}{C_1} = \sum_{m=1}^{\infty} \left(\exp -\frac{mL^2}{Dt} (1 - \beta) + \exp -\frac{mL^2}{Dt} (1 + \beta) \right) \quad \text{AII-1.10}$$

For $L = 0.635 \text{ cm}$, $Dt = 5 \times 10^{-3} \text{ cm}^2$, $\beta = 9 \times 10^{-2}$, we find

$$\frac{C - C_1}{C_1} \approx e^{-7} + e^{-9} + O\{e^{-14}\} \quad \text{AII-1.11}$$

and conclude that the error involved in using equation II-1.1 is negligible.

The effect of diffusion along grain boundaries was considered in chapter V-1, wherein it was concluded that a maximum error of about +5% at $T \leq 1200^\circ\text{C}$ could arise from taking the diffusion coefficient from the linear portion of the $\ln C$ vs x^2 plot.

From equation II-1.1 we see that

$$D = D(t, C, x) \quad \text{AIII-1.1}$$

so that errors in any of these variables can produce errors in D . We shall briefly consider these in turn. Some will be assumed to be random, others are well defined so that corrections can be made.

The very rapid diffusion rates at the higher temperatures made it necessary to use rather short annealing times. At 1700°C , for example, the time at the annealing temperature was only 7 minutes. For this reason, the contribution of the diffusion taking place during the heating and cooling periods was significant. The method of correction for this is straightforward. We begin by establishing an approximate Arrhenius curve for the diffusion coefficients, using the uncorrected annealing time. Then, from the measured time-temperature record, we can plot the diffusion coefficient as a function of time, i.e. $D(t)$. If the diffusion annealing temperature is T_0 , we require to determine t_e so that

$$D(T_0) \cdot t_e = \int_0^t D[T(t)] dt \quad \text{AIII-1.2}$$

Thus t_e can be used to obtain a more accurate value of $D(T_0)$, and if necessary the process repeated. In the present work, two attributes of the high temperature annealing furnace made these corrections particularly simple. The first was the very rapid heating rate, from room temperature to 1600°C in about 75 seconds. The second was that cooling curves of all the runs were virtually indistinguishable over the relevant temperature ranges. The relative error in time at 1700°C was 9.48%; this decreased to 1.6% at 1440°C .

The concentration C was measured in terms of the specific activity, by the method outlined in IV-5. Random statistical fluctuations in the radioactivity decrease as $1/\sqrt{n}$, where n is the total counts recorded. By taking $n \sim 10^4$, this kept such fluctuations to about $\pm 1\%$. The effects of variations in instrumental stability and background were reduced by measuring the latter between counts, and referring all counts to a standard, also counted frequently. A further uncertainty in the specific activity was associated with the accuracy of weight determinations. If W_0 is the true weight $W' = W_0 + \delta W$ the incorrectly measured weight, then

$$\frac{C' - C}{C} = - \frac{\delta W}{W_0 + \delta W} \quad \text{AIII-1.3}$$

where $C' = \text{Total Activity}/W'$.

The individual slice weights were of the order of 10 mgms, the uncertainty of the scales used was $\pm 20 \mu\text{gms}$ so that the relative uncertainty in $C \simeq \pm 0.2\%$.

None of the foregoing affects are cumulative.

They tend to produce scatter in the concentration profiles, but no systematic error in the slope.

A more serious result of error in weight determination arises in the calculation of penetration depths, since here they are cumulative. In IV-4 we pointed out that the mid-point position x_j , of the j^{th} slice was determined from the slice thickness t_k by:

$$x_j = \sum_{k=1}^{j-1} t_k + \frac{1}{2}t_j \quad \text{AIII-1.4}$$

Each slice thickness is calculated from the relation

$$t_k = \frac{W_k}{\rho A}, \text{ where } \rho \text{ is the density and } A \text{ the specimen area.}$$

Thus

$$t'_k = \frac{W_k}{\rho A} + \frac{\delta W_k}{\rho A}$$

$$\text{and } x'_j = \left(\sum_{k=1}^{j-1} \frac{W_k}{\rho A} + \frac{W_j}{2\rho A} \right) + \left(\sum_{k=1}^{j-1} \frac{\delta W_k}{\rho A} + \frac{\delta W_j}{2\rho A} \right)$$

$$= x_j + f(x) \quad \text{AIII-1.5}$$

The effect of x' on the measured diffusion coefficient D' is obtained by noting that

$$\frac{1}{4D't} = - \frac{\partial \log C}{\partial (x')^2}$$

$$= \frac{\partial \left(\frac{x_o^2}{4Dt} + \text{const} \right)}{\partial (x')^2}$$

$$\text{Then } \frac{D'}{D} = \frac{(x_o + f(x))}{x_o} \frac{dx'}{dx_o} = 1 + \frac{f(x)}{x_o} \text{ for } \frac{dx'}{dx_o} \sim 1.$$

Thus the error in taking the slope of the $\log C$ vs $(x')^2$

curve is a function of x' . From AIII-1.5:

$$\frac{D' - D}{D} \approx \sum_{k=1}^{j-1} \left(\frac{\delta W_k}{W_k} \right) \quad \text{AIII-1.6}$$

If the errors in W_k are random, AIII-1.6 will be reduced by taking many points. If they are systematic, the $\log C$ vs x'^2 plot will exhibit a positive or negative curvature, dependent on the sign of δW . The absence of any curvature other than in those exhibiting grain boundary effects suggests no significant systematic error occurred. If we take all δW 's to be (20 μgm) we obtain, for a representative run, using the slice thicknesses given on p. 75,

$$\sum_{k=1}^{40} \frac{\delta W}{W_k} \approx \frac{18 \times 20 \times 10^{-6}}{10 \times 10^{-3}}$$

so that the maximum error in D' , for all δW 's positive, and the slope taken at the last slice is about 3.6%.

In the same way, an error in the measurement of the specimen diameter d gives rise to an error in the area A , and we find

$$\frac{\Delta D}{D} = \frac{A^2 - (A')^2}{(A')^2} \approx \frac{-4(\delta d/d)}{1 + 4(\delta d/d)} \quad \text{AIII-1.7}$$

$$\approx \pm 1 \%$$

for the values used here.

If all errors are additive, we find the maximum uncertainty to be $\frac{\Delta D}{D} = +10\%$ at the lower temperatures, and

$\frac{\Delta D}{D} = \pm 5\%$ at the higher temperatures.

This analysis, of course, does not take account of systematic errors.

Uncertainties in the D_0 and Q values are affected by the non-linearity of the Arrhenius curve. Apart from that, the largest contribution comes from an uncertainty in the temperature measurements and the D 's.

Writing

$$Q = -R \frac{\Delta \log D}{\Delta \left(\frac{1}{T}\right)} \quad \text{AIII-1.8}$$

and considering uncertainties arising from the D 's alone, we have

$$\begin{aligned} Q' &= \frac{-R}{\Delta(1/T)} \log D_1' / D_2' \\ &= \frac{-R}{\Delta(1/T)} \log \frac{D_1}{D_2} \left[\frac{1 + \Delta D_1/D_1}{1 + \Delta D_2/D_2} \right] \end{aligned}$$

so that

$$\frac{Q' - Q}{Q} = \frac{\log \left(\frac{1 + \Delta D_1/D_1}{1 + \Delta D_2/D_2} \right)}{\log D_1/D_2} \quad \text{AIII-1.9}$$

If, of course, $\Delta D_1/D_1 = \Delta D_2/D_2$, there is no error in Q since the correct and incorrect plots would be parallel.

If we take, as the maximum case:

$$\frac{\Delta D_1}{D_1} = \pm 5\%, \quad \frac{\Delta D_2}{D_2} = \pm 10\%, \quad D_1 = 10^{-5}, \quad D_2 = 10^{-7}, \quad \text{we find}$$

$$\frac{Q' - Q}{Q} \leq \pm 3\%$$

Similarly, if we consider errors from temperatures alone

$$\frac{Q' - Q}{Q} = \left(\frac{\frac{1}{T_1} - \frac{1}{T_2}}{\frac{1}{T_1} - \frac{1}{T_2}} - 1 \right) \quad \text{AIII-1.10}$$

The thermocouples were checked using the gold point melting technique and found accurate to 1°C. Differences between the two thermocouples at 1700°C amounted to 5°C. If then we use

$$T_1' = T_1 \pm 1$$

$$T_2' = T_2 \pm 5$$

We find

$$\frac{Q' - Q}{Q} \leq \pm 1.4\% \quad \text{for } T_1 = 1500^\circ\text{C},$$

$$T_2 = 900^\circ\text{C}.$$

The maximum error in Q then, is $\leq 4.4\%$.

If now we take D at the midpoint of the $(1/T)$ range measured, and write

$$D_o' = D \exp(Q \pm \Delta Q/RT)$$

we find

$$\frac{D_o' - D_o}{D_o} = \pm 85\%$$

REFERENCES

1. Fick, A., Ann. Phys. Lpz. $\overline{170}$ (1855), p. 59.
2. Chandrasekhar, S., Rev. Mod. Phys. $\overline{15}$ (1943), p. 1.
3. LeClaire, A.D. and Lidiard, A.B., Phil. Mag. $\overline{1}$ (1956), p. 518.
4. Bardeen, J. and Herring, C., Imperfections in Nearly Perfect Crystals, (New York: Wiley), p. 261.
5. Shewmon, P.G., Diffusion in Solids (Toronto: McGraw-Hill), p. 103.
6. Compaan, K. and Haven, Y., Trans. Far. Soc., $\overline{52}$ (1956) p. 786.
7. Peterson, N.L., Phys. Rev. $\overline{136}$, (1964) p. A568.
8. Manning, J.R., Phys. Rev. $\overline{136}$, (1964) p.A1758.
9. Mullen, J.G., Phys. Rev. $\overline{124}$, (1961) p. 1723.
10. Howard, R.E., Phys. Rev. $\overline{144}$, (1966) p. 650.
11. Barr, L.W. and LeClaire, A.D., Proc. Brit. Cer. Soc. $\overline{1}$, (1964) p. 109.
12. Vineyard, G.H., Jour. Phys. Chem. Solids $\overline{3}$, (1957) p. 121.
13. Schoen, A.H., Phys. Rev. Letters, $\overline{1}$, (1958) p. 524.
14. Tharmalingham, K. and Lidiard, A.B., Phil. Mag. $\overline{4}$, (1959) p. 899.
15. Wert, C., Phys. Rev. $\overline{79}$, (1950) p. 601.
16. Mullen, J.G., Phys. Rev. $\overline{121}$, (1961) p. 1649.

17. LeClaire, A.D., Phil. Mag. 14, (1966) p. 1271.
18. Lidiard, A.B., Phil. Mag. 59, (1960) p. 1171.
19. Hoffman, R.E., Turnbull, D. and Hart, Acta Met. 5, (1957) p. 74.
20. Reiss, H., Phys. Rev. 113, (1959) p. 1445.
21. Howard, R.E. and Manning, J.R., Phys. Rev. 154, (1967) p. 561.
22. Crank, J., The Mathematics of Diffusion (Oxford: Clarendon) p. 9.
23. Kuper, A., Letaw, H., Slifkin, L., Sonder, E. and Tomizuka, C.T., Phys. Rev. 96, (1954) p. 1224.
24. Peart, R.F., Diffusion in Body-Centered & Cubic Metals (ASM) (1965) p. 235.
25. Lundy, T.S., Federer, J.I., Pawel, R.E. and Winslow, F.R., Diffusion in Body-Centered & Cubic Metals (ASM) (1965) p. 35.
26. Slifkin, L., Lazarus, D. and Tomizuka, T., Jour. Appl. Phys. 23 (1952) p. 1032.
27. Peterson, N.L., Phys. Rev., 136(2A) (1964) p. A568.
28. Kidson, G.V. and Ross, R., Proc. 1st UNESCO Int. Conf., Radioisotopes in Sci. Res. (1958) p. 185.
29. Pawel, R.E. and Lundy, T.S., Jour. Phys. Chem. Solids 26, (1965) p. 937.
30. Shewmon, P.G., Trans. Met. Soc. AIME 206 (1956) p. 918.
31. Askill, J., Diffusion in Body-Centered Cubic Metals (ASM) (1965) p. 253.

32. Wajda, E.S., Shirn, G.A., Huntington, H.B., *Acta Met.* 3 (1955) p. 39.
33. Mead, H.W. and Birchenall, C.E., *Trans. Met. Soc. AIME* 206 (1956) p. 1336.
34. Suzuoka, T., *Trans. Jap. Inst. Metals*, 2 (1961) p. 25
35. Shewmon, P.G., *Diffusion in Solids* (Toronto: McGraw-Hill) p. 170.
36. Zener, C., *Imperfections in Nearly Perfect Crystals*, (New York: Wiley) (1952) p. 289.
37. Baurte, J. and Koehler, J., *Phys. Rev.* 107 (1957) p. 1493.
38. Simmons, S. and Balluffi, R., *Phys. Rev.* 117 (1960) p. 52.
39. Adda, Y. and Kirianenko, A., *Compt. Rend.* 247 (1958) p. 744.
40. Bochvar, A.A., Kuzenefsova, V.G. and Sergeev, V.S., *A/Conf. 15/P/2306* (1958).
41. Rothman, S., Lloyd, L. and Harkness, A., *Trans. AIME* 218 (1960) p. 605.
42. Mortlock, A. and Tomlin, D., *Phil. Mag.* 4 (1959) p. 628.
43. Paxton, H. and Gondolf, E., *Arch. Eisenhüttenw.*, 30 (1959) p. 55.
44. Kidson, G.V. and McGurn, J.F., *Can. Jour. Phys.* 39 (1961) p. 1147.
45. Kuczynski, G.C., *Jour. Appl. Phys.* 21 (1950) p. 632.
46. Barnes, R.S., *AERE-R3162* (1959).
47. Ells, C.E. and Evans, W., *Trans. AIME*, 227 (1963) p. 438.

48. Lundy, T.S. and Federer, J.I., ORNL-3339 (1962).
49. Murdock, J.F., Lundy, T.S. and Stansbury, E.E., Acta Met. $\overline{12}$ (1964) p. 1033.
50. Adda, Y., Mairy, C. and Andrev, J.L., Comm. aux Jour. D'Automme, C.E.A. (1959).
51. Peterson, N.L. and Rothman, S.J., ANL-6568 (1965).
52. Tomlin, D.H. (1963) private communication.
53. Hagel, W., Trans. AIME, $\overline{224}$ (1962) p. 430.
54. Gibbs, G.B., Graham, D. and Tomlin, D.H., Phil. Mag. $\overline{8}$ (1963) p. 1269.
55. Peart, R.F. and Tomlin, D.H., Acta Met. $\overline{10}$ (1962) p. 123.
56. Rothman, S.J. and Peterson, N.L., Diffusion in Body-Centered Cubic Metals (ASM) (1965) p. 183.
57. Wheeler, J.A. and Winslow, F.R., Editors, Diffusion in Body-Centered Cubic Metals (ASM) (1965).
58. Askill, J., Phys. Stat. Sol. $\overline{16}$ (1966) p.k63.
59. Peart, R.F., Phys. Stat. Sol. $\overline{20}$ (1967) p. 545.
60. Lazarus, D. and Nachtrieb, N.H., Solids Under Pressure (New York: McGraw-Hill) (1963) p. 43.
61. Graham, D., (1967) Private communication.
62. Graham, D., Bull. Amer. Phys. Soc. $\overline{11}$ (1966) p. 331 (BH 16).
63. Dienes, G.J., Acta Met. $\overline{13}$ (1965) p. 433.
64. Dienes, G.J., Acta Met. $\overline{13}$ (1965) p. 1215.
65. Gibbs, G.B., Acta Met. $\overline{13}$ (1965) p. 926.

67. Aaronson, H.I., Shewmon, P.G., Acta Met. $\overline{15}$ (1967) p. 385.
68. Lazarus, D., Phys. Rev. $\overline{93}$ (1954) p. 973.
69. Zener, C., Phys. Rev. $\overline{71}$ (1947) p. 847.
70. Fisher, E.S. and Renken, C.J., Phys. Rev. $\overline{1352A}$ (1964) p. A482.
71. Kidson, G.V., Can. Jour. Phys. $\overline{41}$ (1963) p. 1563.
72. Kidson, G.V., Diffusion in Body-Centered-Cubic Metals (ASM) (1965) p. 329.
73. Gruzin, P.L., AEC-tr-2924 (1955) p. 343.
74. Gibbs, G.B., RD/B/N.380 (1965).
75. Askill, J. and Gibbs, G.B., Phys. Stat. Sol. $\overline{11}$ (1965) p. 557.
76. Walker, D.A.S., AECL Internal Report No. Cl-227 (1965).
77. Kidson, G.V., Electrochem. Tech. $\overline{4}$ (1966) p. 193.
78. Kidson, G.V., Unpublished work.
79. Manning, J.R., Phys. Rev. $\overline{116}$ (1959) p. 819.
80. LeClaire, A.D., Private Communication referred to in reference 51.
81. Peterson, N.L. and Rothman, S.J., Phys. Rev. $\overline{154}$ (1967) p. 552.
82. Hart, E.W., Acta Met. $\overline{5}$ (1957) p. 597.
83. Mortlock, A., Acta Met. $\overline{8}$ (1960) p. 132.
84. LeClaire, A.D., International Symp. on High Temp. Tech., Asilomev, California (1963).

85. Howard, R.E. and Lidiard, A.B., Reports on Prog. in Phys. (1964).
86. Swalin, R.A., Thermodynamics of Solids, John Wiley & Sons, Inc. (1962) p. 236.